

CRANFIELD UNIVERSITY

Mohamed Essid El-Alej

Monitoring Sand Particle Concentration in Multiphase Flow Using
Acoustic Emission Technology

SCHOOL OF ENGINEERING

PhD THESIS

Academic Year: 2013 -2014

Supervisor: Professor David Mba

January, 2014

CRANFIELD UNIVERSITY

SCHOOL OF ENGINEERING

PhD THESIS

Academic Year 2013 -2014

Mohamed Essid El-Alej

Monitoring Sand Particle Concentration in Multiphase Flow Using
Acoustic Emission Technology

Supervisor: Professor David Mba

January, 2014

Doctor of Philosophy

© Cranfield University 2014. All rights reserved. No part of this
publication may be reproduced without the written permission of the
copyright owner.

ABSTRACT

Multiphase flow is the simultaneous flow of two or several phases through a system such as a pipe. This common phenomenon can be found in the petroleum and chemical engineering industrial fields. Transport of sand particles in multiphase production has attracted considerable attention given sand production is a common problem especially to the oil and gas industry. The sand production causes loss of pipe wall thickness which can lead to expensive failures and loss of production time. Build-up of sand in the system can result in blockage and further hamper production. Monitoring of multiphase flow is a process that has been established over several decades.

This thesis reports an assessment of the application of Acoustic Emission (AE) technology as an alternative online technique to monitoring of sand particles under multiphase flow conditions in a horizontal pipe. The research was conducted on a purpose built test rig with the purpose of establishing a relation between AE activity and sand concentration under different multiphase flow conditions.

The investigation consisted of five experimental tests. The initial experiment was performed to provide a basis for the application of AE technology to detect sand particle impact prior to performing tests in multiphase flow conditions. Further investigations are reported on two phase air-sand, water-sand and air-water-sand three-phase flows in a horizontal pipe for different superficial gas velocities (V_{SG}), superficial liquid velocities (V_{SL}) and sand concentrations (SC).

The experimental findings clearly showed a correlation exists between AE energy levels and multiphase flow parameters, such as superficial liquid velocity (V_{SL}), superficial gas velocity (V_{SG}), sand concentration and sand minimum transport condition (MTC).

Keywords:

Multiphase flow, acoustic emission, pipeline monitoring, sand monitoring and sand minimum transport condition (MTC).

ACKNOWLEDGEMENTS

Firstly, all the praises to ALLAH for the strengths and his blessing that enabled me in completing this thesis.

Secondly, I would like to express my sincerest gratitude and appreciation to my supervisor Prof. David Mba for his patience, unconditional support and valuable guidance throughout the duration of this study.

I also would like to extend my gratefulness and gratitude to Dr. Tinghu Yan, Dr. Abdulmajid Addali and Dr Mohamed Elforjani for their continuous advice in helping me bring this work to completion.

Many thanks to the Process Systems Engineering Laboratory team for their technical support and assistance.

My deepest gratitude goes to my beloved family for their endless love, prayers and encouragement.

Finally, I would like to thank my sponsor (Cranfield University) for granting me a scholarship to do my PhD programme. Also, I would like to express my thanks to the staff members of the department of Power and Propulsion, responsible for direct oversight of my research.

PUBLICATIONS

Journal Publications

- M El-Alej, D Mba, T Yan and S Hassen, Investigation on sand particle impingement on steel pipe in two-phase flow using acoustic emission technology, *The Journal of Applied Mechanics and Material*, vol. 315, 2013, pp. 540-544, (ISSN 1660-9336), ISBN-13: 978-3-03785-635-2, 3rd International Conference on Mechanical and Manufacturing Engineering (ICME2012), 20-21 November 2012, UTHM, Malaysia, Code 96646.
- M El-Alej, D Mba and T Yan, Identification of minimum transport condition for sand in two-phase flow using acoustic emission technology, *Journal of Applied Acoustics*, vol. 74, Issue 11, (2013), 1266–1270.
- M El-Alej, D Mba and T Yan, Monitoring sand particle concentration in two phase flow using acoustic emission, *Proceedings of the Institution of Mechanical Engineers, Part E: Journal of Process Mechanical Engineering*, doi:10.1177/0954408913485066 (2013).
- M El-Alej and D Mba, Monitoring the presence of droplets in a horizontal pipe with Acoustic Emission technology, *Journal of Applied Acoustics*, (Accepted on February, 2014).
- M Alssayh, A Addali, D Mba and M El-Alej, Slug velocity measurement using acoustic emission technology, *Proceedings of the Institution of Mechanical Engineers, Part E: Journal of Process Mechanical Engineering*, (Accepted on March, 2014).

Conference Publications

- M El-Alej, D Mba and T Yan, Monitoring sand particles in two-phase flow with acoustic emission (AE), 15th International Conference on Applied Mechanics (AMME15), 28-30 May 2012, Cairo, Egypt.
- M El-Alej, D Mba, T Yan and M Elforjani, Monitoring sand transport characteristics in multiphase flow in horizontal pipelines using acoustic

emission technology, World Academy of Science Engineering and Technology (WASET), 20-21 June 2013, Istanbul, Turkey.

- M El-Alej, D Mba and H Young, Assessment of the Application of Acoustic Emission Technology for Monitoring the Presence of Sand Under Multiphase Flow Condition, The 8th International Symposium on Measurement Techniques for Multiphase Flows, December 13-15, 2013, Guangzhou, China.

TABLE OF CONTENTS

<i>ABSTRACT</i>	i
<i>ACKNOWLEDGEMENTS</i>	ii
<i>PUBLICATIONS</i>	iii
LIST OF FIGURES.....	ix
LIST OF TABLES	xiii
LIST OF EQUATIONS.....	xiv
NOMENCLATURE	xv
<i>Chapter one</i>	1
1 Introduction.....	1
1.1 Background and Motivation	1
1.2 Project Scope	2
1.3 Thesis Outline.....	3
1.4 Scientific Contribution	3
1.5 Publications	4
1.5.1 Journal Publications	4
1.5.2 Conference Publications	4
<i>Chapter two</i>	6
2 Fundamentals of Multiphase Flow.....	6
2.1 Multiphase Flow.....	6
2.1.1 Multiphase Flow Parameters.....	7
2.1.2 Gas-Liquid Two-Phase Flow	9
2.1.2.1 Gas-Liquid Flow Regimes in Horizontal Pipes.....	10
2.1.2.2 Gas-Liquid Flow Regimes in Vertical Pipes	11
2.1.3 Liquid-Liquid Flow in Horizontal Pipes.....	13
2.1.4 Gas-Solid Flow in Horizontal Pipes	14
2.1.5 Solid - Liquid Flow in Horizontal Pipes	15
2.1.6 Two-Phase Flow Regimes in Inclined Pipes	17
2.1.7 Three-Phase Flow.....	18
2.1.7.1 Gas–Liquid-Solid Flow Regimes in Horizontal pipes	20
2.2 Conclusions	21
<i>Chapter three</i>	22
3 Review of Multiphase Flow Measurement Techniques	22
3.1 Non-Invasive Techniques	22
3.1.1 Differential Pressure (DP)	22
3.1.2 Electric Impedance Meters.....	24
3.1.3 Ultrasound Technique	25
3.1.3.1 Doppler Flow-Meter	26
3.1.3.2 Transit-Time Flow-Meters	26
3.1.4 Particle Image Velocimetry (PIV)	28
3.1.5 Electrical Resistance Tomography (ERT) Technique.....	30

3.1.6 Acoustic Emission Technique (AE)	31
3.2 Invasive Techniques	32
3.2.1 Needle Probes	32
3.2.1.1 Electric Impedance Probes	32
3.2.1.2 Optical Probes	33
3.3 Acoustic Sand Detectors.....	34
3.3.1 Intrusive Sand Detectors	35
3.3.1.1 Roxar Intrusive Ultrasonic (RIU) Probe.....	36
3.3.1.2 Jorin Visual Particle Analyser (ViPA)	37
3.3.2 Non-Intrusive Detectors.....	38
3.3.2.1 Clamp-On DSP-06 Particle Monitor	40
3.3.3 Combining Acoustic and Erosion-Based Sand Probes	42
3.4 Viability and Drawbacks of Techniques	43
3.5 Conclusions	46
<i>Chapter four</i>	47
4 Sand Deposition and Erosion/Corrosion in Horizontal Pipes.....	47
4.1 Sand Deposition	47
4.2 Erosion and Corrosion	48
4.3 Forces Acting on a Particle	49
4.3.1 Gravitational Force	49
4.3.2 Buoyancy Force	49
4.3.3 Drag Force	50
4.3.4 Lift Force	50
4.4 Motion of Particles in Fluids	51
4.5 Previous Work	52
4.5.1 Conductivity Ring	52
4.5.2 Ultrasound Technique	53
4.5.3 Particle Image Velocimetry (PIV)	54
4.5.4 Digital Image Analysis	54
4.5.5 Acoustic Emission (AE) Technique	55
4.5.6 Acoustic Non-Intrusive Sand Monitor and Intrusive Erosion Sand Measurement Detectors Techniques	56
4.5.7 Mechanistic Model	57
4.6 Conclusions	58
<i>Chapter five</i>	59
5 Acoustic Emission (AE)	59
5.1 Definition of Acoustic Emission (AE).....	60
5.2 Mechanism of Acoustic Emission.....	60
5.2.1 Kaiser Effect.....	61
5.2.2 Felicity Effect.....	62
5.3 Acoustic Emission System.....	62
5.3.1 Acoustic Emission Sensors/Transducers	63

5.3.2 Acoustic Emission Preamplifier	64
5.3.3 Data Acquisition (DAQ) Board.....	65
5.4 Mounting Conditions for AE Sensors	65
5.5 Acoustic Emission Signals	66
5.6 AE Wave Propagation Modes.....	66
5.7 AE Sensor Calibration and Attenuation Test.....	68
5.8 Acoustic Emission Measurements	71
5.8.1 Hit Driven Data Measurements	71
5.8.2 Time Driven Data Measurement	72
5.9 Location of AE Sources	73
5.10 Energy Measurement.....	74
5.11 Sources of Acoustic Emission in Process Industries.....	75
5.11.1 AE Generated from Bubbles	75
5.11.2 AE Generated from Solid Particle Impacts	77
5.11.3 AE Generated from Turbulent Flow.....	77
5.12 Advantages and Disadvantages of AE Technology	78
5.13 Applications of AE Technology	79
5.14 Methods for Acoustic Emission Signal Analysis.....	80
5.15 Conclusion	82
<i>Chapter six</i>	83
6 Experimental Investigation and Methodology	83
6.1 Initial Test-Rig Design and Layout	83
6.1.1 Instrumentations and Experimental Setup.....	84
6.1.2 Experimental Procedure.....	86
6.1.3 Results of Monitoring.....	87
6.2 Multiphase Flow Test-Rig Design and Layout.....	89
6.2.1 Monitoring sand transport characteristics in multiphase flow (air-water-sand flow).....	93
6.2.1.1 Experimental Procedure	94
6.2.1.2 Results of Monitoring	95
6.2.2 Identification of Minimum Transport Condition (MTC) for Sand in Sand-Water Two-Phase Flow	97
6.2.2.1 Results of Monitoring	98
6.2.3 Monitoring Sand Particle Characteristics in Air-Sand Two-Phase Flow	100
6.2.3.1 Results of Monitoring	101
6.2.4 Monitoring the Presence of Droplets in a Horizontal Pipe	103
6.2.4.1 Results of Monitoring	104
6.3 Conclusion	105
<i>Chapter seven</i>	106
7 Analysis and Discussion.....	106
7.1 Sand Particle Impact Test.....	106

7.2 Two-Phase Flow Test	110
7.3 Monitoring Sand Transport Characteristics in Multiphase Flow in Horizontal Pipelines	115
7.3.1 Sand Transport Characteristic in Segregated Flow	116
7.3.1.1 Sand Transport Characteristic in Stratified Flow	116
7.3.1.2 Sand Transport Characteristic in Stratified- Wavy Flow.....	117
7.3.2 Sand Transport Characteristic in Intermittent Flow	119
7.3.2.1 Sand Transport Characteristic in Plug Flow	119
7.3.2.2 Sand Transport Characteristic in Slug Flow.....	120
7.3.3 The effect of AE sensor location on AE Energy	123
7.3.4 The effect of VSL, VSG and Sand Concentration on AE Energy ...	125
7.4 Identification of Minimum Transport Condition (MTC) for Sand in Two- Phase.....	127
7.5 Monitoring the Presence of Droplet in a Horizontal Pipe.....	132
<i>Chapter eight</i>	140
8 Conclusion and Recommendations for Future Work.....	140
8.1 Conclusions	140
8.2 Recommendations for future work	142
Appendix A	155
Appendix B	156
Appendix C	165

LIST OF FIGURES

Figure 2-1: Classifications of multiphase flows.....	9
Figure 2-2: Gas-liquid two-phase flow regimes in horizontal pipes.....	11
Figure 2-3: Gas-Liquid two-phase flow regime in vertical pipes	13
Figure 2-4: Flow patterns in equal density oil-water mixture flows	14
Figure 2-5: Gas-solid flow regimes in a horizontal pipe.....	15
Figure 2-6: Solid-Liquid flow (slurry flow) in horizontal pipes.....	16
Figure 2-7: Two-phase flow in inclined pipes; (a) Single – phase liquid, (b) Slug flow at low gas velocities, (c) Slug flow at medium gas velocities, (d) Pulsating roll waves at high gas velocities, (e) Liquid blowout	17
Figure 2-8: Pipe inclination VS liquid holdup-fraction where positive angles indicate uphill flow (λ is input liquid fraction).....	18
Figure 2-9: Three-phase gas-oil-water in horizontal pipes.	20
Figure 2-10: Gas-liquid–solid flow patterns in horizontal pipes.....	20
Figure 3-1: Derivation of the basic DP meter equation.....	23
Figure 3-2: Configuration of electrodes for electrical conductivity probes: (a) two full rings, (b) half rings.....	25
Figure 3-3: Operating principle of Doppler flow meter	26
Figure 3-4: Operation of transit-time flow meter	27
Figure 3-5: Schematic layout of PIV equipment	29
Figure 3-6: Double-frame images for PIV computation.....	29
Figure 3-7: Structure of a typical electrical resistance tomography system.....	30
Figure 3-8: Operating schematic of the conductivity probe	33
Figure 3-9: Principle of operation of De Lasa optical probe.....	34
Figure 3-10: Operating principle of ISE probe in flow-line	36
Figure 3-11: Principle of operation of RIU probe	37
Figure 3-12: Principle operation of Jorin ViPA.....	38
Figure 3-13: Acoustic sand detector located on flow line	39
Figure 3-14: Acoustic sand detection principle of operation	41
Figure 3-15: Combination of acoustic and erosion-based sand probes.....	42

Figure 4-1: Solids deposition as a function of average flow velocity.....	48
Figure 5-1: Principle of Acoustic Emission process.....	61
Figure 5-2: Kaiser and Felicity effects	62
Figure 5-3: Typical Acoustic Emission system	62
Figure 5-4: Acoustic Emission sensors	63
Figure 5-5: Basic construction of an AE sensor.....	64
Figure 5-6: Burst signals compared to continuous Acoustic emissions	66
Figure 5-7: Typical P-, S - and surface waves.....	67
Figure 5-8: Example of wideband AE sensor calibration certificate.....	69
Figure 5-9: Hsu-Nielsen source.....	71
Figure 5-10: AE signals measurement parameters	72
Figure 5-11: Typical AE waveforms.....	73
Figure 5-12: Acoustic Emission source location	73
Figure 5-13: Zone location method to monitor leakage in the pipe.....	74
Figure 5-14: Schematic of the bubbles generated in slug flow in a horizontal pipe	76
Figure 5-15: Solid particles in horizontal pipe.....	77
Figure 5-16: Original signal and wavelet analysis of an AE event.....	81
Figure 6-1: Schematic diagram of initial experimental test	84
Figure 6-2: Initial experimental test	85
Figure 6-3: AE Energy vs drop height for different size of sand particles	87
Figure 6-4: Example of AE transient signal from sand particle impact dropped from 20 cm	88
Figure 6-5: Example of AE transient signal from sand particle impact dropped from 60 cm	88
Figure 6-6: Schematic diagram of three-phase flow test facility	89
Figure 6-7: Multiphase flow test facility.....	90
Figure 6-8: Water-Sand mixture feeder unit	91
Figure 6-9: Data acquisition system (channels box).....	92
Figure 6-10: Distribution of sand particle diameters in Congleton HST50 sand.....	94
Figure 6-11: Test section for three-phase flow	95

Figure 6-12: AE Energy VS Superficial Gas Velocity (V_{SG}) for Different Sand Concentration and fixed Superficial Liquid Velocity (V_{SL}) of 0.2 ms^{-1}	96
Figure 6-13 Test section for two-phase flow.....	98
Figure 6-14: Schematic diagram of two-phase flow test facility	101
Figure 6-15: Test section of air-sand two-phase flow facility	101
Figure 6-16: AE energy levels as a function of V_{SG} for a range of sand injection rates	102
Figure 6-17: Test section of two-phase flow	103
Figure 7-1: Time domain (top) and time frequency (bottom) plots for single sand Particle of $500 \mu\text{m}$ in diameter dropped onto a 1.5 mm thickness steel plate from a height of 20 cm	107
Figure 7-2: Time domain (top) and time frequency (bottom) plots for single sand particle of $500 \mu\text{m}$ in diameter dropped onto a 1.5 mm thickness steel plate from a height of 60 cm	108
Figure 7-3: AE Energy vs drop height for different size of sand particles	109
Figure 7-4 Time domain (top) and Time Frequency domain (bottom) plots for sands of 0.2 g impacting on a steel pipe with V_{SG} of 11 ms^{-1}	111
Figure 7-5: Time domain (top) and Time Frequency domain (bottom) plots for sand mass of 0.2 g impacting on a steel pipe with V_{SG} of 11 ms^{-1} (0 to $300 \mu\text{sec}$)	111
Figure 7-6: Time domain (top) and Time Frequency domain (bottom) plots for sands of 1.0 g impacting on a steel pipe with V_{SG} of 11 ms^{-1}	112
Figure 7-7: AE energy levels VS V_{SG} for a range of sand injections	113
Figure 7-8: AE energy levels plotted against V_{SG} for a range of sand injections	114
Figure 7-9: Schematic of sand behaviour in stratified flow regime	116
Figure 7-10: AE energy levels plotted against sand concentration (stratified flow)	117
Figure 7-11: Schematic of sand behaviour in stratified wavy flow regime	118
Figure 7-12: AE energy levels plotted against sand concentration (stratified wavy flow)	118
Figure 7-13: Schematic of sand behaviour in plug flow regime	119
Figure 7-14: AE energy levels plotted against sand concentration (plug flow)	120
Figure 7-15: Schematic of sand behaviour in slug flow regime	121

Figure 7-16: AE energy levels plotted against sand concentration (slug flow)	122
Figure 7-17 AE energy levels plotted against sand concentration for different flow regimes	123
Figure 7-18: AE energy levels plotted against sand concentration for stratified & stratified-wavy flows (top & bottom sensors)	124
Figure 7-19: AE energy levels plotted against sand concentration for slug & plug flows (top & bottom sensors)	125
Figure 7-20: AE-Energy levels against a range of superficial gas velocity (V _{SG}) for different sand concentration and constant V _{SL} of 0.2 m/s	126
Figure 7-21: AE-Energy levels against a range of superficial gas velocity (V _{SG}) & superficial liquid velocity (V _{SL}) and constant sand concentration of 300lb/1000bbl	127
Figure 7-22: Sand flow pattern in water flow for sand concentration of 600lb/1000bbl and C _v of 6.46E-04 at V _{SL} ranges of between 0.1 ms ⁻¹ to 1.2 ms ⁻¹	129
Figure 7-23: AE-Energy plotted against V _{SL} for a range of Sand Concentration	130
Figure 7-24: V _{MTC} (m/s) VS sand concentration (lb/1000bbl)	131
Figure 7-25: AE-Energy variation with increasing total droplet volume and V _{SG} captured by bottom sensor	133
Figure 7-26: AE-Energy variation with increasing total droplet volume and V _{SG} captured by top sensor	134
Figure 7-27: AE-Energy variation with increasing total droplet volume and V _{SG} captured by top & bottom sensors (water-sand droplets)	134
Figure 7-28: AE-Energy variation with increasing total droplet volume and V _{SG} captured by bottom & top sensors (water droplets)	135
Figure 7-29: Wavelet analysis of AE signal for 5 ml of water-droplet at V _{SG} 9 ms ⁻¹ captured by bottom sensor	136
Figure 7-30: Wavelet analysis of AE signal for 5 ml of water-sand droplets at V _{SG} 9 ms ⁻¹ captured by bottom sensor	137
Figure 7-31: Wavelet analysis of AE signal for 5 ml of water-sand-droplets at V _{SG} 10 ms ⁻¹ captured by bottom sensor	138
Figure 7-32: Wavelet analysis of AE signal for 5 ml of water-only at V _{SG} 11 ms ⁻¹ captured by top sensor	139
Figure 7-33: Wavelet analysis of AE signal for 5 ml of water-only droplets at V _{SG} 11 ms ⁻¹ captured by bottom sensor (The red represents maximum energy)	139

LIST OF TABLES

Table 3-1: Viability and drawbacks of a number of multiphase measurement techniques.....	44
Table 6-1: Sand weight of different sand concentrations used in test	94
Table 6-2: AE-Energy levels as a function of sand concentration for different flow regimes	97
Table 6-3: AE-Energy against VSL for a range of sand concentration	99
Table 6-4: Sand minimum transport velocity (VMTC) for a range of sand concentrations.....	100
Table 6-5: Experimental measurements AE – Energy for air-sand two-phase flow.....	102
Table 6-6: AE-Energy as a function of V_{SG} for a range of droplet volumes (water & water-sand droplets) captured at bottom sensor.....	104
Table 6-7: AE-Energy as a function of V_{SG} for a range of droplet volumes (water & water-sand droplets) captured at top sensor.....	105
Table 7-1: AE energy change in % for different sand sizes for a fixed drop height	109
Table 7-2: AE energy change in % for constant sand quantities and varying V_{SG}	115

LIST OF EQUATIONS

(2-1).....	7
(2-2).....	8
(2-3).....	8
(2-4).....	8
(3-1).....	23
(3-2).....	23
(3-3).....	24
(3-4).....	27
(3-5).....	27
(3-6).....	39
(3-7).....	41
(4-1).....	48
(4-2).....	49
(4-3).....	50
(4-4).....	50
(4-5).....	50
(4-6).....	51
(5-1).....	69
(5-2).....	69
(5-3).....	70
(5-4).....	70
(5-5).....	70
(5-6).....	70
(5-7).....	75
(6-1).....	86
(6-2).....	93

NOMENCLATURE

Roman symbols

A	Cross-sectional area of the pipe (m^2)
Q	Volumetric flow rate
E_L	Liquid hold-up
V_1 & V_2	Mean velocity (m/s)
P_1 & P_2	Line pressure (barg)
f	Frequency (kHz)
T	Integration process for the whole event duration
V	Mean bulk velocity (m/s)
v(t)	Time dependent voltage provided by AE transducer (sec)
R	Constant of system electric impedance (k Ω)
g	Gravity acceleration constant (9.81 m/s ²)
H	Drop height (cm)
M	Mass of the sand particle in kg
SE	Signal Energy (Joule)
C_V	Sand Volume Fraction
ER	Erosion Rate
u	Particle Velocity (m/s)
F_{GP}	Gravitational force on a particle (m/s ²)
d	Spherical diameter (cm)

D	Pipe Diameter (cm)
F_{wp}	Buoyancy force on particle (N)
F_D	Drag force (N)
A_t	Attenuation
r	transmission distance
f	signal frequency (kHz)
SA	The amplitude of a given signal (mV)
V_{max}	The maximum amplitude of a given signal (mV)
V_s	Signal voltage (mV)

Greek symbols

λ	Input liquid fraction
Θ	Angle (degree)
π	Pi (3.14)
μ	Fluid viscosity
γ	Shear rate
ρ	Density (kg/m ³)
ρ_P	Density of the particle (kg/m ³)
β	Medium Coefficient

Acronyms

VSL	Superficial Liquid Velocity (ms ⁻¹)
-----	---

Vsg	Superficial Gas Velocity (ms^{-1})
GVF	Gas Void Fraction
DP	Differential pressure flow meters
PIV	Particle Image Velocimetry
ERT	Electrical Resistance Tomography Technique
T1 & T2	Transducers
AE	Acoustic Emission
NDT	Non-destructive test
PAC	Physical Acoustic Corporation
HDT	Hit Definition Time
HLT	Hit Lockout Time
PDT	Peak Definition Time
SC	Sand Concentration (lb/1000bbl)
QoS	Quantity of Sand (g)
MTC	Sand Minimum Transport Condition
VMTC	Sand Minimum Transport Velocity (ms^{-1})
DAQ	Data Acquisition Board
WD	Wideband
RMS	Root Mean Square
FFT	Fast Fourier Transform
WT	Wavelet Transform

1 Introduction

1.1 Background and Motivation

Multiphase flow is the simultaneous flow of two or several phases through a system such as a pipe [1]. Multiphase flow can be classified according to the phases present in the flow. Two – phase flow is the simplest case of multiphase flow, and may be grouped according to the phases involved as (1) gas-liquid mixture, (2) gas-solid mixture, (3) liquid-solid mixture, and (4) two-immiscible-liquids mixture. Two-phase flow can appear in different configurations, called flow regimes or flow patterns. These regimes are; separated flow, intermittent flow and dispersed flow. A mixture of gas, oil and water is the most commonly encountered three phase flow, but solid in the form of sand particles may also be present in some cases. Description of flow in the pipe at different conditions is known as mapping of flow patterns.

Sand production is a common problem especially in the oil and gas industry. Build-up of sand in the system can result into blockage and loss of pipe wall thickness, which can lead to expensive failures and loss of production time [2]. The damage caused by the sand particles depends upon factors such as the pipe material, particle velocity and the incident angle of the eroding particles [3]. It is therefore of great interest to accurately detect the presence of sand and determine the amount of produced sand to allow oil/gas production rate to be maximised while maintaining sand-free production.

Monitoring of multiphase flow is a process that has been established over several decades using multiphase flow measurement technology. A number of different measurement techniques are available in the market. These differ in terms of design, functions and capabilities, and employ a great diversity of measurement principles. Multiphase measurement techniques are classified mainly as non-invasive and invasive. Non-invasive techniques are the ones which can be used externally (outside the pipe), to measure parameters such as pressure drop, and liquid and/or gas holdup. They are characterised by the ease with which they can be modified to

extend their useful life, which minimises replacement costs. They may also be used to provide field checks or verification of fixed meter performance (e.g. conductivity probes and ultrasonic techniques).

Invasive techniques require the instrument intrude into the flow and these are used in applications when non-invasive technique are difficult to install or too expensive. Invasive techniques are mainly used for measuring high gas hold-up. Heat transfer and needle probes are examples of these types of probes. However, such techniques have many limitations. For instance, the accuracy of conductivity rings and ultrasonic techniques are significantly affected by the variation of gas void fraction (GVF) (the accuracy decreases with the increase in GVF). Thus, in order to overcome such limitations, this research has investigated Acoustic Emission (AE) based sensing technology as a non-invasive tool monitoring of sand particles in multiphase flow in horizontal pipes.

1.2 Project Scope

In the past, pipelines were used until they failed and were then repaired. However, run-to-failure is costly mainly due to loss of production time and is no longer an acceptable option. Thus, this research investigates the AE technique as a powerful tool for monitoring and characterising sand particles in multiphase flows within horizontal pipes. Such technology may offer:

- Monitoring of sand transport and deposition characteristics under different air-sand and air-water-sand multiphase flow conditions in horizontal pipes;
- Identification of the minimum sand transport condition (MTC) based on different sand volume fractions;
- Establishment of a correlation between AE energy generated by particle impacts and size of sand particles, sand concentration, superficial liquid velocity, V_{SL} , superficial gas velocity, V_{SG} , and slug velocity, V_s ;
- Detection and monitoring of moving water and water-sand droplets in a horizontal flow loop.

To achieve the final goal of this research study, an experimental test rig was employed and final results have been discussed and analysed.

1.3 Thesis Outline

This thesis includes eight chapters:

Chapter 2 presents an overview of multiphase flow that summarises the definitions and types of multiphase flow regimes in horizontal and vertical pipes and the multiphase flow parameters related to this study.

Chapter 3 summarises the multiphase flow measurement techniques that are available in the market in terms of principle, functions and capabilities.

Chapter 4 presents a brief overview of sand deposition and erosion/corrosion in horizontal pipes and ends by reviewing several previous measurement techniques used for multiphase flow.

Chapter 5 discusses Acoustic Emission (AE) technology, including the definition of AE, AE mechanism, AE systems, types of AE signals, AE wave propagation modes, AE measurements, location of AE sources and advantages and disadvantages of AE.

Chapter 6 presents the two-phase and three-phase flow test rigs. This includes test rig design, laboratory experiments, results and observations.

Chapter 7 discusses and analysis the results presented in previous chapters.

Chapter 8 presents the conclusions from the main findings and suggests recommendations for future research.

1.4 Scientific Contribution

The work addresses the potential of monitoring and assessing sand concentration in multiphase flow in horizontal pipes using Acoustic Emission (AE) technology. The work makes a significant contribution to the knowledge concerning the application of AE technology in terms of establishing a correlation between AE-energy levels and multiphase flow parameters, such as V_{SL} , V_{SG} and sand concentration. To date this

investigation is the first known attempt at applying AE technology to identifying the MTC and monitoring droplets in horizontal pipes.

1.5 Publications

Findings of this research have been published in three journals and presented at four conferences.

1.5.1 Journal Publications

- M El-Alej, D Mba, T Yan and S Hassen, Investigation on sand particle impingement on steel pipe in two-phase flow using acoustic emission technology, *The Journal of Applied Mechanics and Material*, vol. 315, 2013, pp. 540-544, (ISSN 1660-9336), ISBN-13: 978-3-03785-635-2, 3rd International Conference on Mechanical and Manufacturing Engineering (ICME2012), 20-21 November 2012, UTHM, Malaysia, Code 96646.
- M El-Alej, D Mba and T Yan, Identification of minimum transport condition for sand in two-phase flow using acoustic emission technology, *Journal of Applied Acoustics*, vol. 74, Issue 11, (2013), 1266–1270.
- M El-Alej, D Mba and T Yan, Monitoring sand particle concentration in two phase flow using acoustic emission, *Proceedings of the Institution of Mechanical Engineers, Part E: Journal of Process Mechanical Engineering*, doi:10.1177/0954408913485066 (2013).
- M El-Alej and D Mba, Monitoring the presence of droplets in a horizontal pipe with Acoustic Emission technology, *Journal of Applied Acoustics*, (Submitted on November, 2013).
- M Alssayh, A Addali, D Mba and M El-Alej, Slug velocity measurement using acoustic emission technology, *Proceedings of the Institution of Mechanical Engineers, Part E: Journal of Process Mechanical Engineering*, (Submitted on May, 2013).

1.5.2 Conference Publications

- M El-Alej, D Mba and T Yan, Monitoring sand particles in two-phase flow with acoustic emission (AE), 15th International Conference on Applied Mechanics (AMME15), 28-30 May 2012, Cairo, Egypt.

- M El-Alej, D Mba, T Yan and M Elforjani, Monitoring sand transport characteristics in multiphase flow in horizontal pipelines using acoustic emission technology, World Academy of Science Engineering and Technology (WASET), 20-21 June 2013, Istanbul, Turkey.
- M El-Alej, D Mba and H Young, Assessment of the Application of Acoustic Emission Technology for Monitoring the Presence of Sand Under Multiphase Flow Condition, The 8th International Symposium on Measurement Techniques for Multiphase Flows, December 13-15, 2013, Guangzhou, China.

2 Fundamentals of Multiphase Flow

This chapter commences by presenting various aspects of multiphase flows in pipelines, initially focusing on flow regimes that can occur in horizontal pipes as a result of changes in gas and liquid superficial velocities. A flow regime map is introduced to explain these regimes according to changes in the velocities.

Next, a selective background of current commercially available techniques that have been used to measure multiphase flow pipelines are discussed including their capabilities, limitations, accuracies, and applications.

2.1 Multiphase Flow

As a general definition, a multiphase flow is the simultaneous passage in a system of a stream composed of two or more phases [4]. The phases that can be present in a multiphase flow are:

1. Solids, which are normally in the form of relatively small particles. The solid phase is incompressible and has non-deformable interfaces with surrounding fluids.
2. Liquids, which are also relatively incompressible, but their interfaces with the other phases are deformable.
3. Gases, where the phase is compressible and deformable.

Multiphase flow can be classified according to the variation in the physical distribution of the phases in the flow by two-phase and three-phase flow regimes, see Figure 2-1 [16]. The most common class of multiphase flow are two-phase flows, which have been grouped into four categories as:

1. Gas-liquid flow, which are probably the most important form of multiphase flow and is widely found in industrial applications.
2. Liquid-liquid flow, such as emulsions of oil and water in pipelines.

3. Liquid-solid flow, which are widely encountered in hydraulic conveying of solid material.
4. Gas-solid flow, where solid particles are suspended in gases, which are of industrial importance in pneumatic conveying and fluidized beds.

Three-phase flows are also of practical significance, examples being;

1. Gas-liquid-solid flows, which occur when carrying out gas-liquid reactions in the presence of a particulate solid catalyst.
2. Gas-liquid-liquid flows, such as are found in condensation or evaporation of immiscible liquid mixtures.
3. Solid-liquid-liquid flows, such as sand mixed with oil and water in a pipeline.

2.1.1 Multiphase Flow Parameters

Gas and liquid superficial velocities, gas volume fraction and liquid hold-up significantly affect the behaviour of the flow [5]. These parameters are briefly described here.

Superficial liquid velocity (V_{SL})

The velocity can be calculated from the hold-up. The hold-up is the cross sectional area occupied by the liquid in the pipe carrying the wet gas flow [5]. A parameter called the superficial liquid velocity is often used as an intermediate step and as an input to many of the correlations. The superficial liquid velocity (V_{SL}) is defined as the individual volumetric flow rate (Q) divided by the cross-sectional area of the pipe (A). This is the velocity if the liquid were to fill the entire cross-section of the pipe.

$$V_{SL} = \frac{Q_L}{A} \quad (2-1)$$

Superficial gas velocity (V_{SG})

If the gas were to fill the entire cross-section of the pipe, the consequent velocity is called superficial gas velocity: again defined as the individual volumetric flow rate (Q) divided by the cross-sectional area of the pipe (A).

$$V_{SG} = \frac{Q_G}{A} \quad (2-2)$$

Gas Volume Fraction (GVF)

When there are multiple phases passing through a cross-section of the pipe, obviously each phase cannot cover more than a fraction of the area. If, for instance, a fourth of the cross-section is occupied by gas, this is known as the gas area fraction (or the volume fraction, since volume is directly proportional to area if the length of that volume is infinitely small), here gas fraction $\alpha_G = 0.25$.

In other words, the gas volume fraction is the ratio of volumetric flow of gas to the total volumetric flow rate:

$$GVF = \alpha_G = \frac{Q_G}{Q_L + Q_G} = \frac{V_{SG}}{V_{SG} + V_{SL}} \quad (2-3)$$

Liquid Hold-Up (E_L)

If the area not occupied by gas is occupied by liquid, the liquid fraction has to be $\alpha_L = 1 - 0.25 = 0.75$. Some authors choose to use a different name for liquid fraction and call it liquid holdup or simply holdup, while sticking to the fraction-terminology in case where the fluid is a gas.

Thus, the ratio of volumetric flow of liquid to the total volumetric flow rate is known as liquid hold-up, and determined by:

$$E_L = \alpha_L = \frac{Q_L}{Q_L + Q_G} \quad (2-4)$$

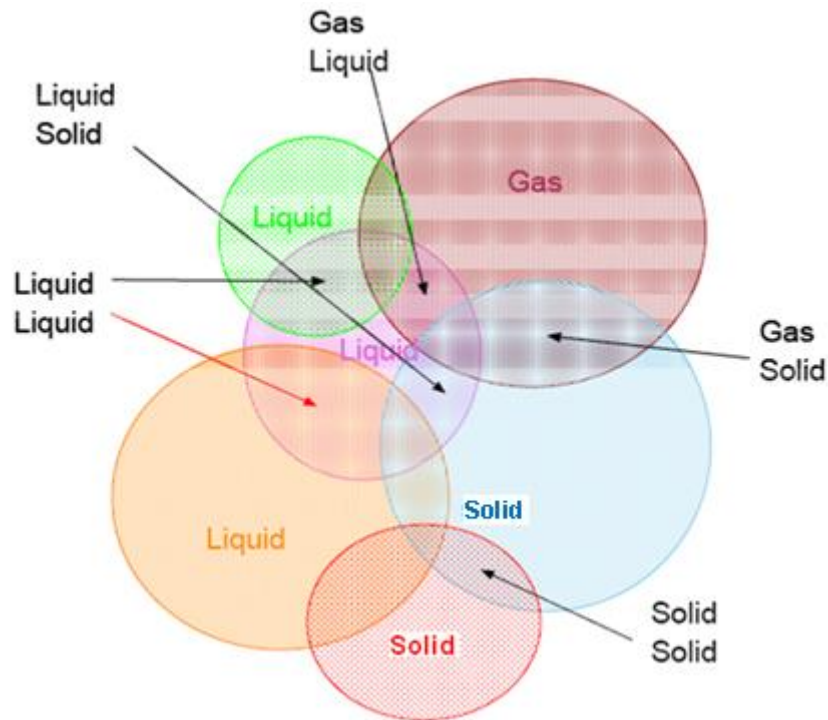


Figure 2-1: Classifications of multiphase flows [16]

Figure 2-1 presents a summary of the different types of multiphase combinations. Each of these types of flow will be discussed in the following sections, with particular reference to the nature of the flows (flow patterns/regimes).

2.1.2 Gas-Liquid Two-Phase Flow

Two-phase flow is the simplest case of multiphase flow, and arises when a mixture of gas and liquid simultaneously flow together in a pipeline. Two-phase flow may be defined as the interacting flow of a gas and liquid where the interfaces between the phases are influenced by their motion. The behaviour of two-phase flow is significantly affected by the physical parameters, such as relative viscosities, densities and velocities of the phases. In addition there is the influence of the geometry, size (diameter) and orientation of the pipe carrying the flow [5]. Consequently, gas-liquid two-phase flows can appear in different configurations, called flow regimes or flow patterns. These classifications are:

- **Separated flow** - a non-uniform phase distribution, such as stratified and annular flow.
- **Intermittent flow** - non-continuous with locally unsteady behaviour, such as elongated bubble, churn and slug flow.

- **Dispersed flow** - a uniform phase distribution, such as bubble flow and mist flow.

2.1.2.1 Gas-Liquid Flow Regimes in Horizontal Pipes

The transition from one flow regime to another is depends primarily on the change in gas-to liquid ratio [6]. However, gas – liquid mixtures flow in horizontal pipes is affected by gravitational forces. Gravity causes the less dense phase to migrate to the top of the pipe [5]. The various flow regimes for gas-liquid flow in a horizontal pipe range from bubble flow to annular mist flow are described below [5], see Figure 2-2.

- **Dispersed Bubble Flow** - When the mixture that flows in a horizontal pipe is almost all liquid (the ratio of liquid superficial velocity to gas superficial velocity is large), then the gas which represents a minor percentage of the mixture forms small dispersed bubbles which tend to migrate and concentrate in the upper part of the pipe due to their buoyancy.
- **Plug / Elongated Bubble Flow** – As the ratio of liquid superficial velocity to gas superficial velocity decreases, large bubbles of length comparable to the pipe diameter appear and occupy the top part of the pipe leading to an unsteady, intermittent flow. These bubbles are known as plug or elongated bubbles. The gas bubbles are separate from the continuous liquid flow along the bottom of the pipe.
- **Stratified Flow** - As the ratio of liquid to gas superficial velocities is further reduced, this leads to a flow in which there is a complete gravitational separation with the liquid on the bottom of the pipe and the gas on the top separated by an undistributed horizontal interface.
- **Stratified-Wavy Flow** - Increased gas velocity generates waves on the surface of the liquid due to the motion of the gas and gives rise to a wavy, stratified flow leading to droplet formation and entrainment of liquid into the gas.
- **Slug Flow** - Further increase in the gas velocity flow leads to the formation of large amplitude waves and pockets of liquid separated by large pockets of gas. These waves have a high crests reaching to the top of the pipe wall, and the gas flows in the form of slugs. This regime referred to as slug flow.

- **Annular Flow** - Further increase in gas flow rate, leads to the liquid forming a continuous annular film, thicker at the bottom than the top, around the perimeter of the pipe. The gas flows in the centre of the pipe and has no contact with the wall at these larger gas flow rates, save that the liquid film may contain some gas bubbles. In the same way, the gas phase may carry some liquid droplets and even liquid pockets.
- **Annular Mist Flow** - Further increase in gas flow rates may strip the liquid from the wall and it is entrained as small droplets in continuous gas flow. This type of flow is called annular mist flow.

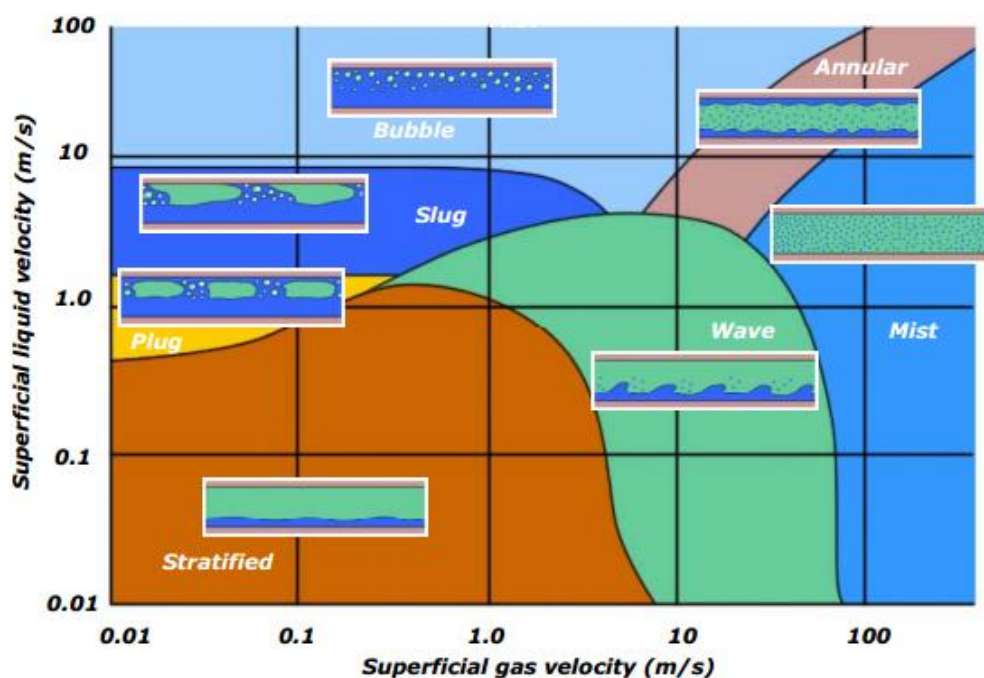


Figure 2-2: Gas-liquid two-phase flow regimes in horizontal pipes [5]

2.1.2.2 Gas-Liquid Flow Regimes in Vertical Pipes

The flow regimes for vertical gas-liquid flow in a pipe range from bubble flow to annular mist flow [5]. Stratified and stratified-wavy flows don't occur in this case due to direction of the action of the gravitational forces and the geometry of the pipe [7]. Five flow regimes for fully-developed vertical pipe have been identified, see Figure 2-3.

- **Bubble Flow** - The liquid paths are continuous and contain a dispersion of bubbles. The bubbles can vary widely in size and shape as a result of the

interactions between forces due to surface tension, viscosity, inertia and buoyancy, but they are almost spherical in shape and much smaller than the pipe diameter.

- **Slug / Plug Flow** – With increase in superficial gas velocity the bubbles coalesce and grow to a size comparable to the pipe diameter, leading to a large rise in velocity of the gas phase. With this flow regime, the bubble can rise in the centre of the pipe while the liquid film at the wall can fall downward. These types of flows are inherently intermittent and unsteady.
- **Churn Flow** – Further increase in the gas superficial velocity breaks down the slug flow bubbles and the bubbles begin to form into irregular shapes. The liquid tends to move up and down in the pipe in an oscillatory fashion, and leads to an unstable regime. This regime represents the transition between slug and annular flow. In small diameter pipes, churn flow may not develop at all and the flow passes directly from slug flow to annular flow.
- **Annular Flow** - When the gas velocity is sufficiently large it sweeps the liquid upwards and (as in horizontal flow) the liquid flows along the wall forming an annular irregular film, though droplets are entrained into the gas core.
- **Annular / Mist Flow** - Further increase in gas flow leads to a liquid flow confined to a liquid layer moving along the wall and droplets (mist) in the core. This flow is described as an annular mist regime. A continuous exchange between the liquid layer and the mist flow occurs by entrainment of droplets from the liquid layer and deposition of core droplets on the wall.

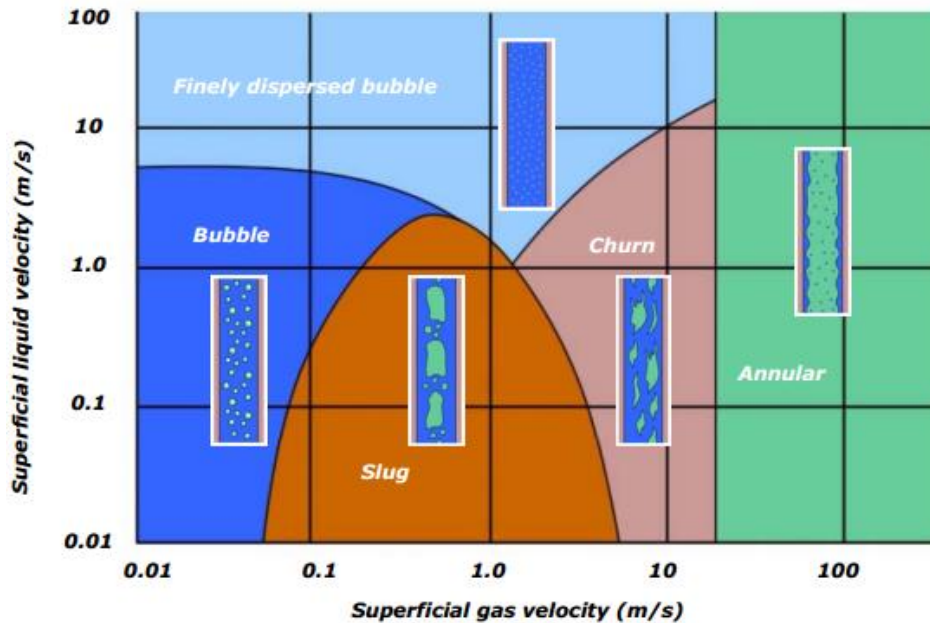


Figure 2-3: Gas-Liquid two-phase flow regime in vertical pipes [5]

2.1.3 Liquid-Liquid Flow in Horizontal Pipes

Compared to gas-liquid flows, liquid-liquid flow regimes are more complex (see Figure 2-4). For the case of oil-water flows, the oil and water will generally have different densities and the degree of difference will strongly affect the flow regime. In general, the regimes have somewhat the same characteristic forms for those for gas-liquid flows with dispersion increasing as the velocities increase. Depending on the fluid characteristics and the input flow rates, different kinds of dispersed flow can be detected depending on the size of droplets. Figure 2-4 illustrates possible flow regimes.

- **Water drops in oil** - Oil forms the continuous media and the water appears as drops suspended in the oil.
- **Oil in water annular flow** - An annular region of water is formed at the wall of the pipe around the core flow of oil.
- **Oil slugs in water** - The oil forms large pockets or slugs separated by annular water.
- **Oil bubbles in water** - The slugs reduce to large oil bubbles with a diameter similar to the pipe diameter.

- **Oil droplets in water** - Oil droplets are suspended in the water when the water flows as the continuous medium.

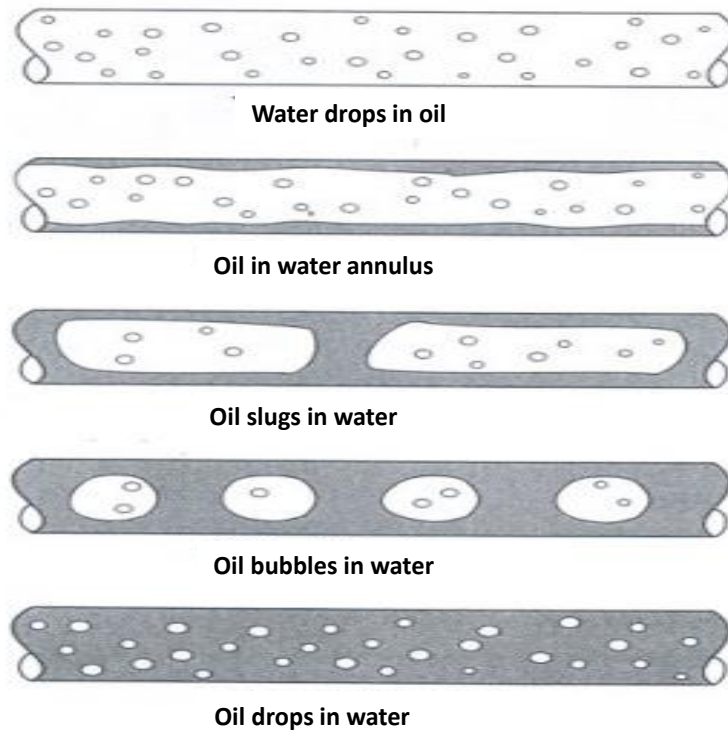


Figure 2-4: Flow patterns in equal density oil-water mixture flows [8]

2.1.4 Gas-Solid Flow in Horizontal Pipes

Gas-solid flows occur in numerous industrial processes and various natural phenomena. Industrial processes include pneumatic conveying of particulates as is commonly used in food, coal, and mineral powder processing. Fluidization is a common gas-solid flows operation with numerous important industrial applications such as catalytic cracking of intermediate hydrocarbons [9]. Natural phenomena include sand storms, moving sand dunes, aerodynamic ablation, and cosmic dust.

In gas-solid flows, flow regimes of both phases depend not only on the initial conditions and physical boundaries of the system but also on the mechanisms of momentum transfer or the interacting forces between the phases. These forces may be classified into three groups: (1) forces through the interface between the fluid and particles; (2) forces due to the interactions between particles; and (3) forces imposed by external fields [8]. Figure 2-5 illustrates some observed flow regimes of gas-solids in a horizontal pipe.

- **Homogeneous Flow** - Near the pipe entrance the solid particles retain their fluidized state with uniform density, and if the flow velocity is high enough, this state is maintained along the length of the pipe.
- **Dune Flow** - At lower velocities particles begin to settle in the pipe and form dunes.
- **Slug Flow** - As solids progressively settle in the pipe, the dunes flow, sometimes almost filling the pipe. Small ripples seem to travel along the top of the solid layer, and the lower portion appears to be practically stationary. Depending on the solids-gas ratio, intermittent flow of solids may occur in place of dune formation.
- **Packed Bed** - When loading of solids is increased, the dunes can flow as plugs which extend over the cross-section of the pipe. In which case, the gas flow can be represented as flow through a packed bed.

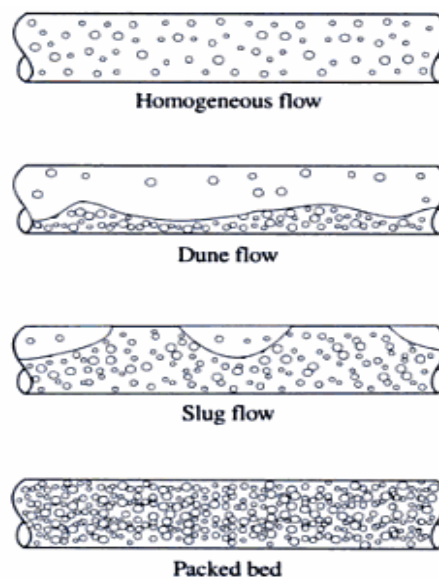


Figure 2-5: Gas-solid flow regimes in a horizontal pipe [8]

2.1.5 Solid - Liquid Flow in Horizontal Pipes

The flow of a mix of liquid and solid particle is known as slurry, the transport of slurries through pipelines is common in the chemical and other industries. The behaviour of the slurry is influenced by many variables, such as the characteristic

dimension of the pipe, the orientation of the pipe, solid concentration and the properties of the fluid/particle interface.

Four regimes of transport of solid-liquid mixtures through pipelines for a given liquid, sediment material, and pipe size have been qualitatively described, as shown in Figure 2-6. These are homogeneous flow, heterogeneous flow, saltation moving bed and saltation static bed flow [10].

- **Homogeneous Flow** – This occurred when size of solid particles being transported are so small, and the velocity of liquid is relatively high. Particles are fully suspended and uniformly distributed.
- **Heterogeneous Flow** - In this regime all the solid particles are in suspension, but not uniformly distributed. This can be attributed to the reduction in the liquid velocity, or due to the increase in the particles size.
- **Moving-Bed Flow (Saltation Flow)** - Further decrease in liquid velocity and flow may contain large particles which lead to the build-up of a backed-bed at the bottom of the pipe. Solid particles in moving-bed are moving in flow direction in three forms, sliding, rolling or saltation.

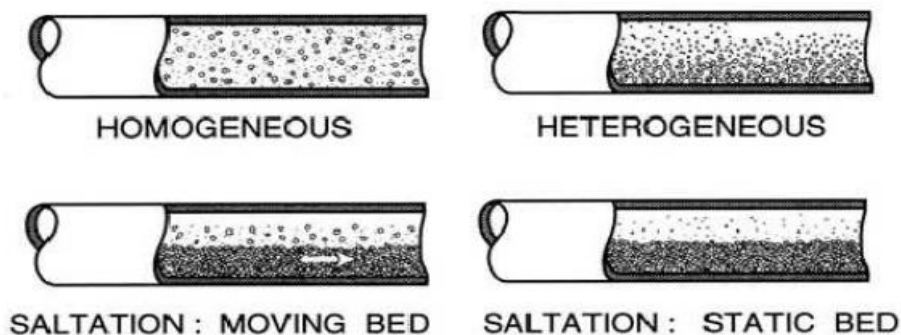


Figure 2-6: Solid-Liquid flow (slurry flow) in horizontal pipes [117]

The regime of flow that involves a moving bed (including saltation) might normally be avoided in practice because the occurrence of irregularities (ripples and dunes) on the moving bed usually causes a distinctive increase of head loss.

- **Stationary-Bed Flow (Saltation Flow)** - In this flow regime, particles deposited at the pipe bottom (form a bed) and they do not move. This can be attributed to the very low liquid velocity and large solid particles.

2.1.6 Two-Phase Flow Regimes in Inclined Pipes

It has been observed that the transition from one regime to another, such as from stratified flow to intermittent depends on the angle of inclination of the pipe to the vertical [11]. Slight upward inclination causes intermittent flow to take place over a wider range of flow conditions. Thus, different flow patterns could be obtained for multi-phase flow depending on the inclination of the pipe.

In inclined pipes, liquid holdup (the volume fraction of the pipe which is occupied by liquid) becomes an important factor. Since, the gas normally travels faster than the liquid, so it has been observed that the liquid holdup depends on the gas superficial velocity, the liquid holdup increased with the increase of the gas superficial velocity [11].

The schematic diagrams in Figure 2-7 illustrate how change of flow occurs with increase of gas superficial velocity. For example, for an inclination of 5° to the horizontal, the gas superficial velocity increases and the liquid flow is in a rolling state. When the angle of inclination of the pipe increases to 30° , the gas moves at a higher superficial velocity and large slugs of liquid flow develop.

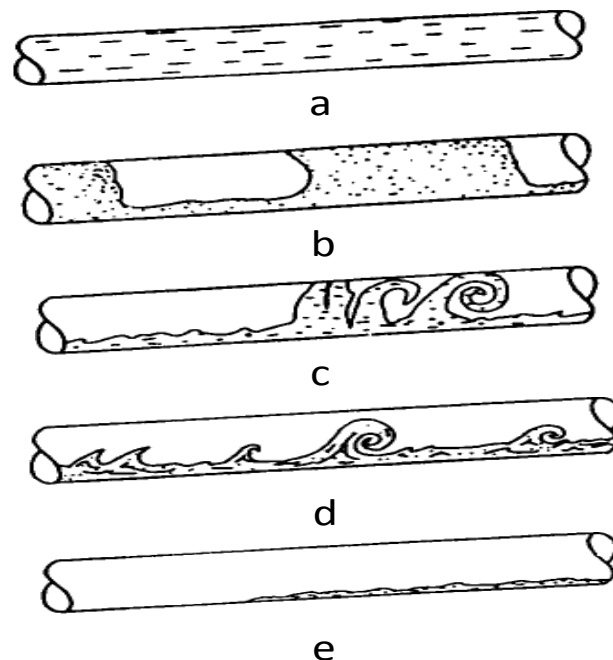


Figure 2-7: Two-phase flow in inclined pipes; (a) Single – phase liquid, (b) Slug flow at low gas velocities, (c) Slug flow at medium gas velocities, (d) Pulsating roll waves at high gas velocities, (e) Liquid blowout [12]

Figure 2-8 shows the relation between the pipe inclination and liquid holdup fraction. It can be seen that the holdup fraction is greatly influenced by the angle of inclination.

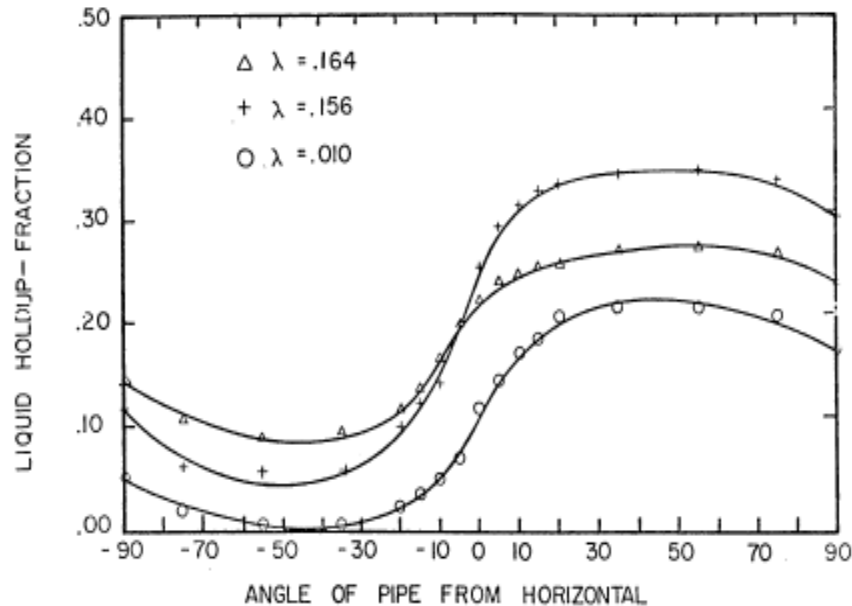


Figure 2-8: Pipe inclination VS liquid holdup-fraction where positive angles indicate uphill flow (λ is input liquid fraction) [12]

Curved pipes or bends provide a large degree of flexibility to gas – solid transport systems by allowing routing and distribution. Thus gas–solid flow in a pipe bend is of major interest because it contributes significantly not only to pressure drop effects but also to erosion problems that result from the directional impacts of the solids. A basic description of the flow of a suspension through bends is thus considered critical from the viewpoint of transport system design [9].

2.1.7 Three-Phase Flow

A mixture of gas, liquid and solid flowing simultaneously constitutes a three-phase flow, with a mixture of gas, oil and water the most commonly encountered, but the presence of solids such as sand or any other particles can occur. Thus, it is quite possible to have four–phase flow where build-up of the sand in the system can result in blockages unless transported out quickly. This may be achieved by maintaining high flow velocities but incurring higher energy costs.

Three-phase flows are not frequently encountered but some important systems which involve three-phase flow are:

- Air-Lift Pump - in which air is injected near the bottom of a pipe filled with a liquid-solid mixture, and the bubbles rise through the mix giving a pumping action. This has applications in well-drilling and pumping coal in shafts [13].
- Injection of air into slurries - the purpose of this process is to reduce drag. Experimental work by Heywood and Richardson [14] has shown that very significant reduction in pressure gradient can be achieved.

Most of the studies which have produced three-phase flow regime maps have been experimental, see the detailed description by Acikgoz [15], where flow classification is given regarding gas-liquid and liquid-liquid states. Ten flow regimes were identified for water and gas superficial velocities for a fixed oil superficial velocity. The difficulty for these maps is to represent the three-dimensional entry on a two-dimensional map, see Figure 2-9.

The superficial velocity of each phase is presented on each axis as a fraction of the total superficial velocities. A pure gas flow has the superficial velocity fraction defined as 1. For a pure liquid (oil-water) flow, the superficial gas velocity fraction is zero, which is shown as a straight line in the oil-water plane. In the same way, if the water is zero, then the operating point will be on a line in the gas-oil plane. When the oil contents zero the operation point will be on a line in the gas-water plane. Consequently, all operation points for three-phase flow lie on the triangle shown [16].

The illustrations (Figure 2-9) along the borders show some (though not all) of the two-phase flow regimes possible for gas-oil (left border), gas-water (right border), and oil-water (lower border) flows. When all phases are present simultaneously, many more different flow regimes become possible

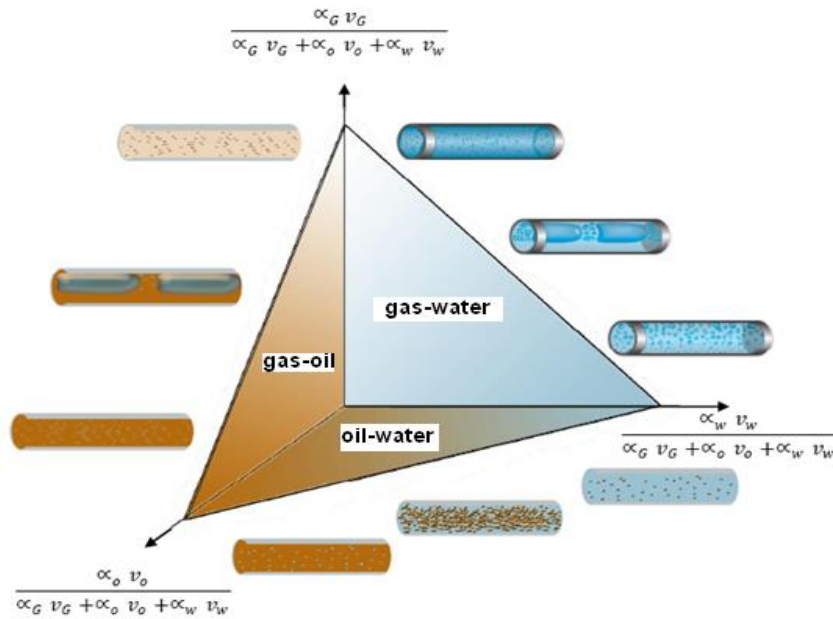


Figure 2-9: Three-phase gas-oil-water in horizontal pipes [16]

2.1.7.1 Gas-Liquid-Solid Flow Regimes in Horizontal pipes

Flow regime definition (also referred as flow pattern) for these three-phase flows totally depends on visual observation and varies with flow rates [17]. Figure 2-10, illustrates the gas-liquid-solid flow regimes in horizontal pipes and these are described below, the strong similarity with gas-liquid flows when the solids consist of fine particles and has a low superficial velocity should be noted.

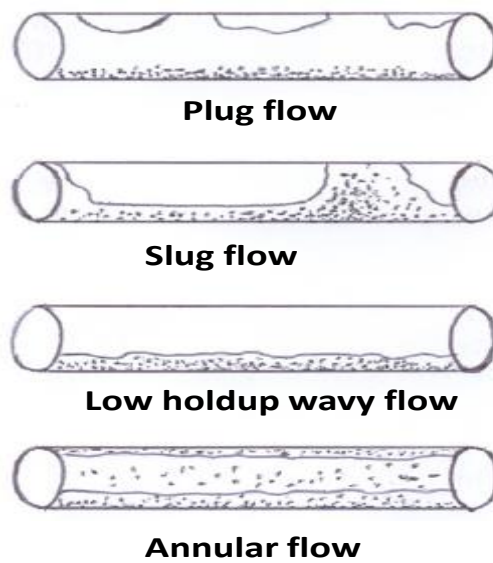


Figure 2-10: Gas-liquid-solid flow patterns in horizontal pipes [51]

- **Plug Flow** - Due to the difference in densities, the gas bubbles occupy the top part of the pipe, and are separated from the continuous liquid flow along the lower part of the pipe. The entire pipe cross-sectional area can be filled by plugs of liquid separated by small regions of gas. Flows of solid particles are little affected by the regions of gas. Increasing the quantity of gas increases the size of the gas regions.
- **Slug Flow** - Higher gas velocity (more gas flowing) generates regions of gas separated by regions full of liquid. At lower liquid velocity and higher gas velocity the gas tends to push the slugs of liquid downstream. During the passage of the film region, solids may settle and then be transported in the slug body which can cause difficulties in transport of solids. In the situation where the solid is not transported by slug or film the result is a bed formation.
- **Low Hold Up Wavy Flow** - In wet gas pipelines both gas and solid phases are separated from the liquid phase flowing along the pipe's bottom. Near to the gas-liquid interface, waves of different lengths and amplitude can appear. In this situation the film may contain on a high solid concentration or a wet solid bed.
- **Annular Flow** - At a high gas flow rate, liquid forms a continuous annular film without contact with the wall, the film is thinner at the top and thicker at the lower part of the pipe, and may contain some gas. The gas flows in the core of the pipe and may carry some liquid droplets. Solids are transported in both the liquid film and in the gas core. At high velocities there is the risk of a high erosion rate.

2.2 Conclusions

The basic fundamentals of multiphase flow such as flow regimes have been outlined. The focus of this chapter was on the multiphase flow in horizontal pipes with solid-phase is one of the main components. Multiphase flow can exist in different forms of flow regimes depending on different parameters such as flow rates, size of solid particles and difference in density of fluids. Two-phase flow is the most simple and common class of multiphase flow, whereas three-phase flow is much more complex.

3 Review of Multiphase Flow Measurement Techniques

There is need for multiphase flow measurement in the oil and gas production industry to provide continuous monitoring of multiphase flows in pipes. These technologies can be used to measure different parameters such as, velocities of individual multiphase flow components and sand concentration. Thus, these technologies can be utilized to improve performance, to extend useful life and minimize operation and maintenance costs. Multiphase flow meters from different manufacturers will invariably differ in their design, function and capabilities. A number of different meters are available in the market, employing a great diversity of measurement principles and solutions. Multiphase measurement techniques are divided into non-invasive and invasive as listed below;

3.1 Non-Invasive Techniques

Non-invasive techniques are meters that can be used external to the pipe, to investigate pressure drop, liquid and/or gas holdup. They are characterised by the ease with which they can be modified to extend their useful life and minimize replacement cost [5]. They also provide the possibility of field checking and verification of the performance of fixed meters. Some of the relevant techniques are listed below;

3.1.1 Differential Pressure (DP)

Differential pressure flow meters encompass a wide variety of types that includes; orifice meter, venturi meters, nozzles and pitot tubes. Indeed, the measurement of flow using differential pressure is still the most widely used method. DP meters are available in a wide variety of shapes and sizes. They can be used on liquid or gas applications. DP meters infer the flow-rate from the pressure drop across a restriction, and can be used to determine gas void fraction and liquid or solid holdup [18]. They consist of two basic parts, the

primary element which generates the pressure difference and a secondary element which senses the differential and transmits either an analogue or digital signal which is proportional to flow.

Differential pressure devices all make use of Bernoulli's equation. This equation relates the pressure to the velocity of a fluid of constant density flowing in a pipe. Consider flow through a restriction of arbitrary design shown in Figure 3-1. A fluid of density ρ flowing in pipe, area A_1 , has a mean velocity V_1 at a line pressure P_1 . It then flows through a restriction into a pipe of area A_2 , where the mean velocity increases to V_2 and the pressure falls to P_2 . By applying the Bernoulli's equation to sections 1 and 2, and relate the pressure drop to the mean flow velocity:

$$P_1 + \frac{1}{2}\rho V_1^2 = P_2 + \frac{1}{2}\rho V_2^2 + \text{Losses} \quad (3-1)$$

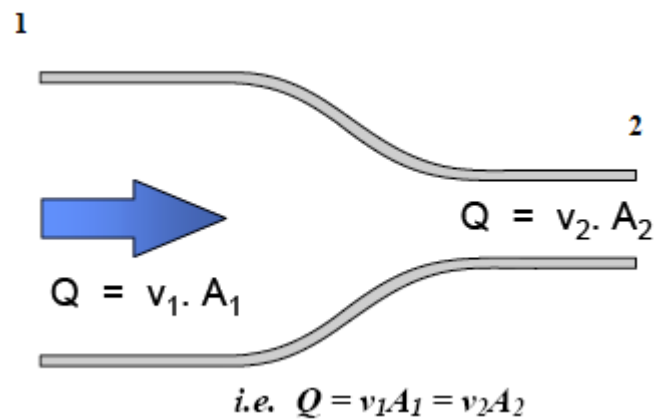


Figure 3-1: Derivation of the basic DP meter equation [18]

The continuity equation relates the velocity to the cross-sectional area for a fluid of constant density flowing in a pipe. This relation between sections 1 and 2 in Figure gives:

$$Q = A_1 V_1 = A_2 V_2 \quad (3-2)$$

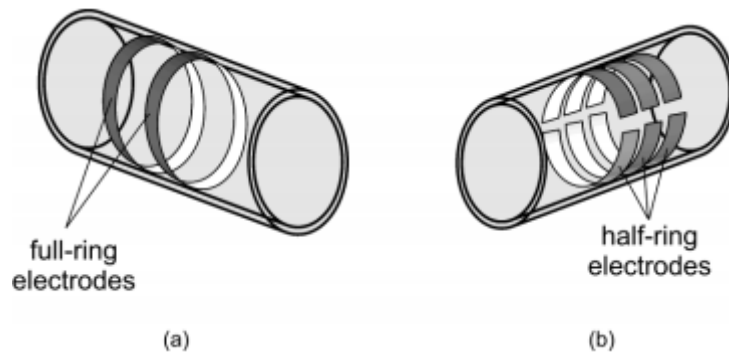
Defining the area ratio, m , as A_1/A_2 , and substituting Equation 3-2 into Equation 3-1, we obtain:

$$Q = \frac{A_2}{(1-m)^{1/2}} \left(\frac{2(P_1-P_2)}{\rho} \right)^{1/2} \quad (3-3)$$

The Venturi meter is the most common form of DP technology used in the oil and gas industry. This instrument has the capability of handling 25% more flow than other DP types such as the orifice plate. Also, Venturi meters are robust, resistant to erosion and corrosion, not significantly affected by entrained solid particles (e.g. sand), are highly insensitive to velocity profile effects and can have a low total pressure lost. Venturi meters have some disadvantages such as their construction and installation are expensive and accurate results are limited to clean instruments [19].

3.1.2 Electric Impedance Meters

The principle of the impedance meter is based on the dependence of the electrical impedance of a multiphase flow on the relative concentrations of the different phases. This meter is low cost and easy to construct [20]. The basic impedance void fraction meter consists of a number of concentric ring-type electrodes, powered by a high-frequency AC source and surrounding a non-conducting section of a pipe through which the fluid mixture is passing, see Figure 3-2. This method provides a time-dependent cross-sectional or annular average of void fraction with a high-frequency response [21]. However, because the outputs of impedance meters are very sensitive to the phase regime (i.e., whether it is bubbly, slug, or annular flow), they can be used only if the flow regime is known [22].



**Figure 3-2: Configuration of electrodes for electrical conductivity probes:
(a) two full rings, (b) half rings [21]**

A new measurement technique called electrical impedance spectroscopy has been developed to measure the solid concentration of slurry mixtures. In principle, this technique is based on the fact that the AC frequency responses of solids are different from those for the liquid phase. The operating frequency range of this instrument is 0.1 Hz to 1 MHz [23].

3.1.3 Ultrasound Technique

A key aspect of the ultrasound technique in comparison to the electromagnetic is its ability to work with almost any type of flowing liquid notwithstanding its electric conductivity. Ultrasound is a sound with an operating frequency range of 20 kHz to 1 GHz [24]. Ultrasonic meters include a number of different designs for measuring an average velocity in a flowing system. They are all based on an ultrasonic signal being affected by the fluid flow. There are two distinct types of ultrasonic meter. The first to appear was the Doppler type which is more of a flow monitor than a flow meter. The other type is the transit-time flow meter.

Many types of flow (e.g. mixtures of solid and liquid) may also cause attenuation of the ultrasound signal but this need not be a serious problem [25]. Ultrasound techniques have been successfully used to discriminate between different concentrations of Kaolin slurries [26].

3.1.3.1 Doppler Flow-Meter

The Doppler flow meter operates on the principle that if sound of a known frequency is reflected from a moving object, the frequency of the reflected beam is altered by an amount that is proportional to the speed of the moving object. Thus, if the process stream contains scatters such as sand particles or gas bubbles, then the velocity of these will be indicative of the stream velocity [26]. Figure 3-3 shows the principle of the Doppler flow-meter.

Clamp-on sensors for Doppler flow meters have a typical operating frequency of 0.640 MHz, whereas the operating frequency for wetted sensors is 1.2 MHz [19]. Typical applications of Doppler meters would include flows of sewage, solid-liquid mixtures, sludge and aerated liquids [26]. Doppler meters are sensitive to velocity profile effects.

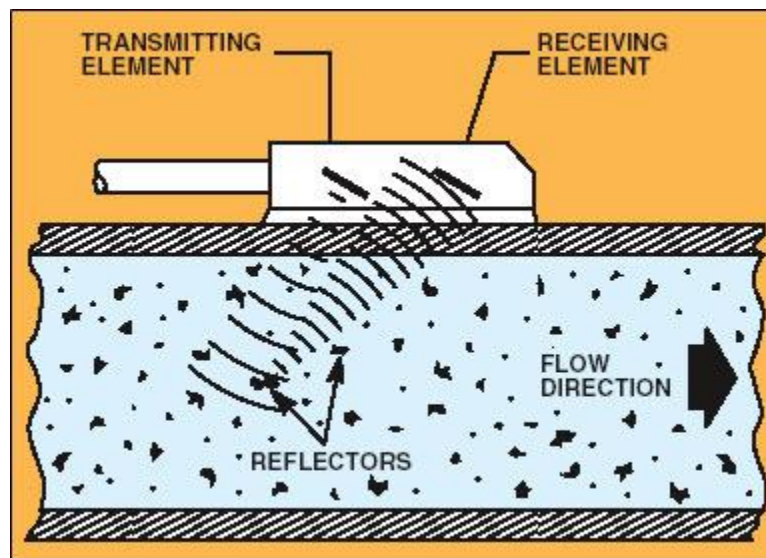


Figure 3-3: Operating principle of Doppler flow meter [19]

3.1.3.2 Transit-Time Flow-Meters

These types of meter rely on the measurement of time difference between ultrasonic waves that are transmitted in opposite directions through the flow [27]. Figure 3-4 demonstrates the operating principles when two ultrasonic pulses are used travelling in opposite directions. Transducer T1 is at the bottom of the pipe and transducer T2 is at the top.

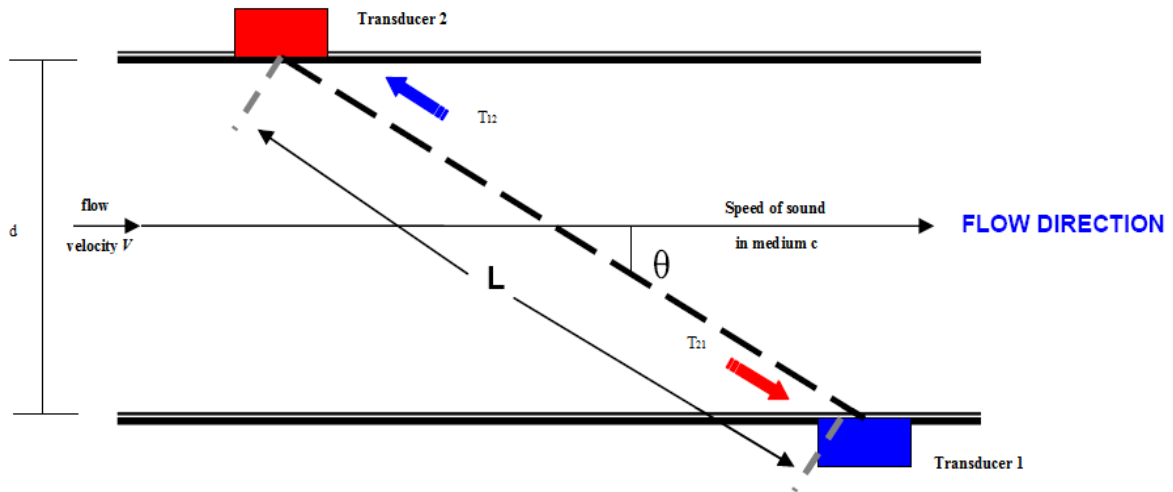


Figure 3-4: Operation of transit-time flow meter [27]

Two ultrasonic beams, each inclined at an angle Θ to the flow propagate through a fluid whose mean bulk velocity is V . The transit times required for a pulse to pass between the two locations (T_{12} and T_{21}) are given by

$$T_{12} = d / \sin \theta (C - V \cos \theta) \text{ and } T_{21} = d / \sin \theta (C + V \cos \theta) \quad (3-4)$$

By subtracting the two terms in Equation 3-4 gives a time difference of;

$$\Delta T = T_{12} - T_{21} = 2d \cot \theta \left(\frac{V}{C^2} \right) \quad (3-5)$$

They have been successfully applied to water flows, clean process liquids, liquefied gases and natural gas pipes. This technique is suitable for very low transit time measurement but not to measure fluid with high concentrations such as slurry flow [19].

Advantages of Ultrasonic Meters

- No pressure drop, since meters are same diameter as adjacent piping;
- High frequency pulse rate of output minimizes errors from effects of pulsation and fluctuating flow;
- Installation can be simple and inexpensive;

- High rangeability;
- No moving parts in contact with flowing fluid;
- Simple mechanical calibration easily checked without a throughput test.

Disadvantages of Ultrasonic Meters

- Sensitive to velocity profile;
- Power required for operation;
- Flow profile must be fully developed for an average velocity to be determined from a single path or reflection unit;
- High initial cost;
- Generally poor reputation in terms of long term stability.

3.1.4 Particle Image Velocimetry (PIV)

The Particle Image Velocimetry (PIV) technique records images of flow fields (e.g. gaseous and liquid mediums) and extracts velocity information out of these images [28].

The PIV technique measures the velocity of a fluid element indirectly by means of the measurement of the velocity of tracer particles within the flow. In most applications these tracer particles have been added before the commencement of the experiment and have well defined characteristics [29].

Figure 3-5 is a sketch the apparatus with typical layout. A PIV system typically consists of a laser with sheet optics, one or two digital cameras, and a computer with a timer unit to control the system and store the data. Velocity fields are measured in a planar 2D domain. The measurement plane is cut in the flow by a laser sheet and the measurement area in this plane is cropped by the field of view of the camera(s).

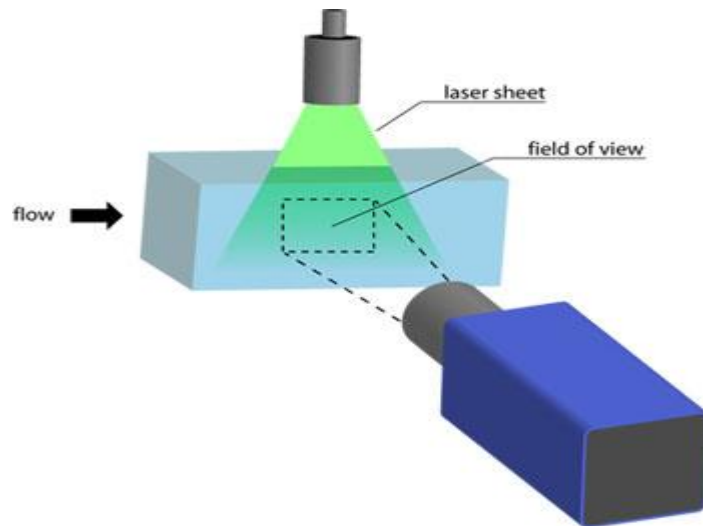


Figure 3-5: Schematic layout of PIV equipment [30]

The measurement commences with addition of small tracer particles to the flow. A plane (light sheet) within the flow is illuminated twice by means of a laser. It is assumed that the tracer particles move with local flow velocity between the two illuminations. The light scattered by the tracer particles is recorded via a high quality lens either on a single frame or on two separate frames on special cross-correlation digital cameras, see Figure 3-6. The output of the digital sensor is transferred to the memory of a computer directly.

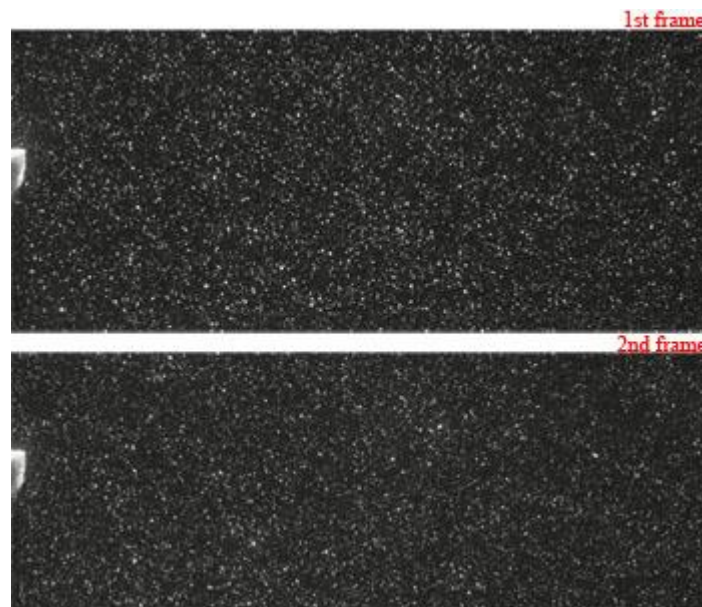


Figure 3-6: Double-frame images for PIV computation [30]

PIV is capable of providing excellent visualization. Typically, the number of points is between 2,000 and 20,000, and the flow pattern is captured for a very short instant in time. Typically, the accuracy is 0.2 – 2% of full scale, not quite as good as single-point methods such as laser-Doppler velocimetry, but still very usable for the computation of statistics and the evaluation of derivative quantities such as velocity [30].

3.1.5 Electrical Resistance Tomography (ERT) Technique

ERT is a technique developed to make cross-sectional images of an object [31]. This technique was effectively used in measuring flow that has a non-conducting fluid as its continuous phase [32]. In principle, the void fraction profile can be determined to a fine detail by having a source emitting a narrow beam of radiation and an opposing detector scanning across the cross-section. This yields a series of chordal average measurements. To obtain a distribution of the void fraction across a given cross-section, one would have to obtain a series of such scans at different angular orientations. The process of obtaining the voidage profile from such measurement is commonly referred to as tomography. Figure 3-7 is a schematic diagram of a typical electrical resistance tomography system.

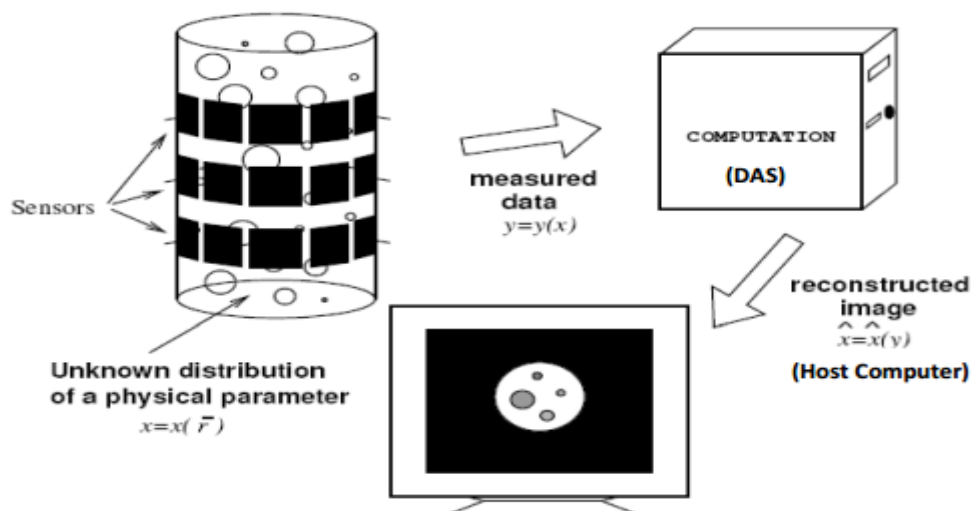


Figure 3-7: Structure of a typical electrical resistance tomography system

[118]

Figure 3-7 shows a number of sensors installed around the pipe or vessel to be imaged. The cross-section area of the sensing zone offers useful information on the nature and distribution of components. However, the sensor output signals are significantly affected by the location of the component boundaries within their sensing zones [33]. Experimentally an ERT image reconstruction technique based on the Agilent data acquisition system has shown ERT can effectively detect the particle distribution in a micro-channel [34]. ERT is a technique able to identify solid/liquid distribution in packed beds by identification of the bed conductivity and its subsequent modeling as a function of electrical properties of each phase [35].

Advantages:

- Cheap installation of electrodes;
- Highly redundant measurement conditions for monitoring applications;
- Good evaluation possibilities of inherent error e.g. by reverse current and normal reciprocal error measurements;
- Highly developed computing routines for different applications.

Disadvantages:

- Repeated effort of data quality and error models especially in difficult measurement conditions;
- Expensive measurement devices;
- High level of expertise for the interpretation of measurements.

3.1.6 Acoustic Emission Technique (AE)

Acoustic Emission (AE) technique is briefly described in this section, for full details see Chapter 5. Typical operating frequencies for AE range from 100 kHz - 1 MHz [36]. A key aspect of AE, in comparison to other NDE techniques, is that it can be used to monitor defects during manufacturing. Other conventional NDT methods require that the production line be interrupted to test the materials [37].

The typical instrument for AE applications consists of a transducer/sensor, pre-amplifier and filtering, post-amplifier with threshold and data (signal) acquisition unit. The first step in the AE measurement process is the conversion of the mechanical energy of the elastic wave (signal detected) into electrical energy. The pre-amplifier is used to amplify weak signals, drive the signals over long distances, and minimize electronic noise and/or filter out unwanted frequencies. Data might need further amplification before being processed. Finally, AE signals are processed by using a standard data acquisition board (AEWIN).

3.2 Invasive Techniques

Invasive techniques are those that are used inside the pipes, such as optical or needle probes. Invasive techniques are used in applications when the uses of non-invasive technique are too costly or too difficult, such as measuring high gas holdup. Some invasive techniques are outlined below.

3.2.1 Needle Probes

Needle probes techniques are based on conductivity, capacitance, optical and/or temperature measurements [38, 39, 40]. Needle probes were designed to measure the local void fraction [41] and sand concentration in slurry systems [42]. These probes can be classified into electrical impedance and optical probes. Both types are described below.

3.2.1.1 Electric Impedance Probes

Electrical impedance probes can be further divided based on conductive, resistive or capacitive effects. A conductivity probe makes use of the difference in conductivity of the gas and liquid phases and is quite suitable for aqueous gas-liquid systems. Resistivity probes sense the variation in resistance between two electrodes with the passage of bubbles through the gap between them. Because, their output signals discriminate between the liquid and the gas phase, they can be used to measure not only the time-averaged local void fraction, but also bubble size and speed [43]. They can also be used in non-

polar media and have been often used for solids concentration measurements in fluidized beds and three phase systems.

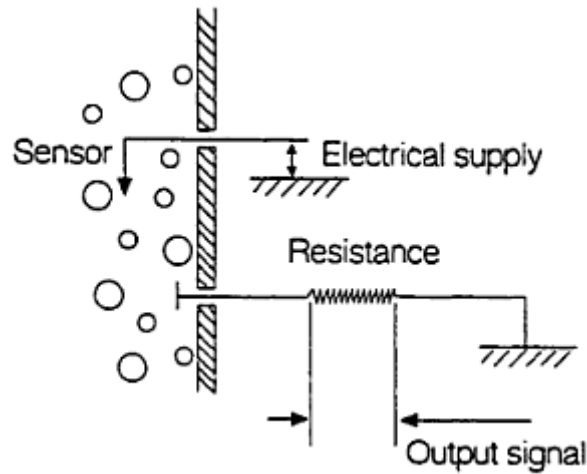


Figure 3-8: Operating schematic of the conductivity probe [43]

The electrical conductivity probe essentially consists of a stainless steel insulated needle exposed only at the tip and a larger electrode mounted on the wall. With the liquid in contact with the probe tip, the electrical circuit between the needle and the wall electrode is closed by the conducting fluid; if the tip is immersed in a bubble the circuit gets broken. The electrical operating schematic is shown in Figure 3-8.

3.2.1.2 Optical Probes

Optical probes exploit the differences in the refractive index of the two phases and rely on the application of Snell's law at the probe-fluid interface. Depending on which phase exists at the probe's tip, the light emitted from the tip is reflected or refracted. The most common optical probe consists of two optical fibres fused and ground to a 45° angle with respect to the probe axis. One of the fibres serves as an emitter and the other as a receiver. Light detection can be achieved with a phototransistor. De Lasa [43] had the optic fibre bent into a U-shape such that the radius of curvature of the U was large enough for the angle of incidence at the turning point to be larger than the angle of total reflection when the fibre was exposed to air (gas). At the same time, the radius

was small enough to secure an angle of incidence at the turning point less than the angle of total internal reflection when the tip is in water (liquid). With this, the light will be conserved in gas and emitted into liquid resulting in a significant difference in the detected signals corresponding to gas and liquid. This principle is illustrated in Figure 3-9.

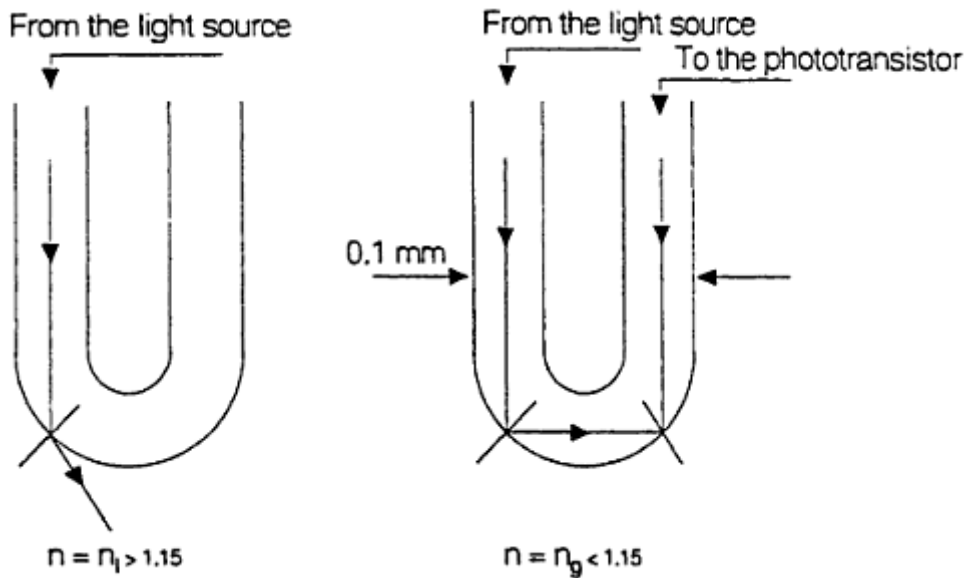


Figure 3-9: Principle of operation of De Lasa optical probe [43]

Optical probe can be used only in transparent media, at low void fractions and at moderate temperatures.

3.3 Acoustic Sand Detectors

A sand detector is an instrument that can be used to detect the sand concentration within a flow stream across a given area. There are two types of acoustic sand detectors, the intrusive and the non-intrusive. The intrusive type detector detects sand by means of monitoring the degrees of erosion on the probe inserted into the flow stream, whereas the non-intrusive method involves “listening” to the flow line for sand related impact noise.

3.3.1 Intrusive Sand Detectors

Electrical intrusive sand detectors are the earliest form of flow line sand detector developed before the acoustic non-intrusive probes, and has been available since the late 1960s. These intrusive probes were designed to be mounted into the surface flow lines. They consist of a thin metal film or a hollow stainless steel cylinder which can be inserted and removed from the pipe under pressure using isolation valves and a lubricator system.

The electrical resistance of the thin metal film exposed to the flow of sand-laden fluids is measured. As the metal film erodes, its resistance increases and this is taken as a measure of loss of metal caused by sand erosion which, coupled with an independent measure of velocity and average size of the sand particles, can be used to calculate the rate of sand production and the mass concentrations of solids in the flow stream [44]. This assumes any increase in resistance is due only to sand erosion. However, if sand is flowing too slowly or the probe is located where there are no sand collisions, the resistance is not necessarily going to increase.

Figure 3-10 shows the installed probe exposed to the impact of sand particles in the flow-line. Without sand particles present, the operating environment has no effect on the performance of the probe. The probe will function effectively as long as it is located in the path of particles.

The resolution of the erosion is determined by the smallest detectable metal loss. The size of element has a proportional relation with the resolution of the probe. Greater resolution may be achieved with thinner elements, but this may negatively affect the probe's service life.

The sensitivity of the probe is an important parameter that determines the accuracy of the metal loss from the surface of the element. This sensitivity depends on the minimum amount of sand that should pass over the erosion probe. The combination of the sensitivity and resolution determines the actual

amount of sand detectable by a measurable metal loss when it passed across the erosion probe at different fluid velocities.

Erosion probes have limitations, such as the need for sealing arrangement to overcome leakage problems caused by loss of adhesion due to the relative thermal expansion of probe and the encapsulating potting. This shortens the service life of the probe.

As a result of their limitations, intrusive erosion probes (ISE) are primarily useful for qualitative sand monitoring. However, probe limitations can be reduced and probes be made more useful by developing more robust models capable which can still determine sand mass flow rate accurately. Improved models of probes may be integrated with other process measurements such as control systems and process data [45].

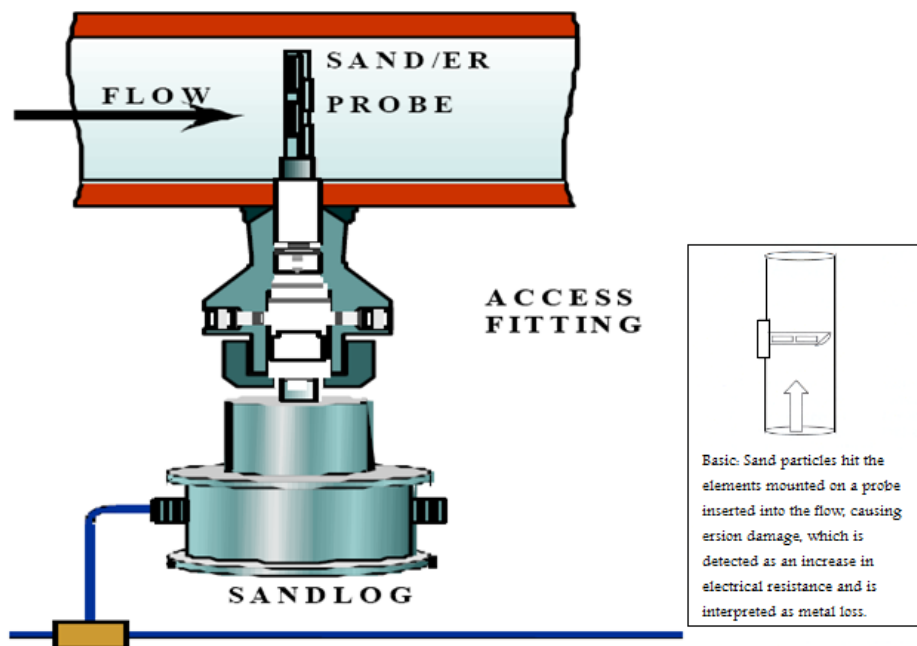


Figure 3-10: Operating principle of ISE probe in flow-line [121]

3.3.1.1 Roxar Intrusive Ultrasonic (RIU) Probe

The Roxar intrusive ultrasonic probe is an intrusive probe that is mainly used to measure oil in water, and is particularly suitable for produced water streams. The measuring techniques are based on ultrasonic backscattering used in

conjunction with acoustic reflectors. The Roxar probe has provided good results when used in produced water systems as well as for water quality with quantitative measurements for use in reinjection [45].

The RIU probe operates as shown in Figure 3-11. It directly transmits highly focused acoustic signals into the produced water stream. Individual solids in the focal region reflect the acoustic energy. By taking a large number of measurements it is possible to calculate the particle size distribution which can then be used to obtain on the corresponding values of concentration.

The Roxar probe operates on the assumption of a well-mixed solid-liquid flow and can provide accurate values as the fluid pass through the widow of measurement. It have been found that the Roxar probe was viable for fluid velocities up to 4 m/s, and a maximum value of Reynolds number of 5,000 [45].

Safety precautions should be followed when installing the Roxar probe, by using an access fitting with an appropriate sealing arrangement.

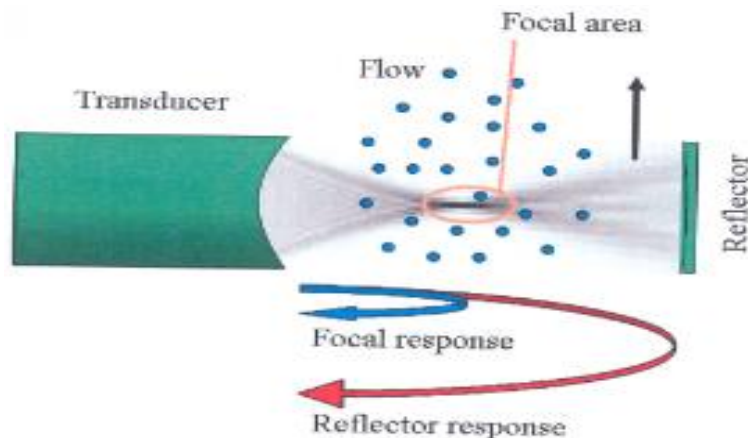


Figure 3-11: Principle of operation of RIU probe [45]

3.3.1.2 Jorin Visual Particle Analyser (ViPA)

The Jorin ViPA uses video microscope imaging to provide online fluid characteristics including particle size distributions, and concentration measurements for both droplets and solids. This device is designed to work at

process pressures and temperatures and can perform batch measurements, as well as record data continuously.

The principle of operation, see Figure 3-12 is video microscope capture with powerful software for imaging analysis. For example, to calculate particle concentration, video images are captured in sequence and particles on each of the images are counted, analysed with their volume determined. The volume related to each of the images is determined by multiplying the image area (width by length) by the focal depth [46]. The Jorin ViPA is suitable for use with transparent fluids.

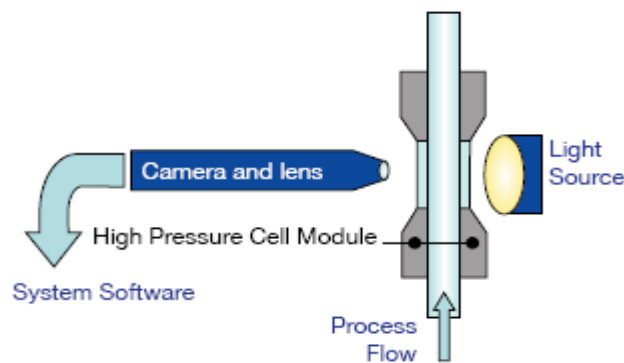


Figure 3-12: Principle operation of Jorin ViPA [46]

3.3.2 Non-Intrusive Detectors

These devices are acoustic and have largely (but not entirely) replaced the intrusive probes due to their greater sensitivity, cheaper installation costs and the ability to be retrofitted (including subsea). An example of an acoustic sand detector is shown in Figure 3-13.

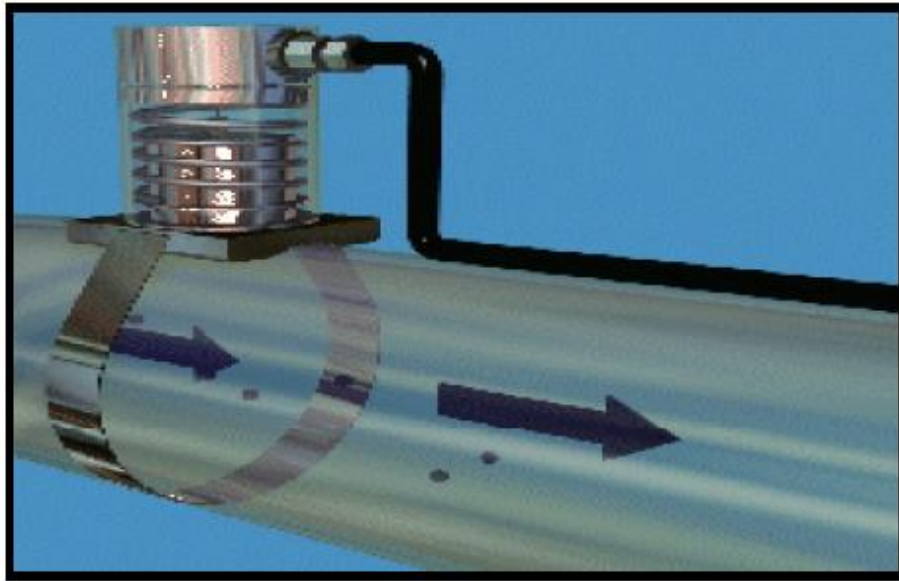


Figure 3-13: Acoustic sand detector located on flow line [121]

Solid particles hitting a flow-line wall will generate high-frequency acoustic pulses (100-500 kHz) in the metal. A sensor (essentially a sensitive, high frequency microphone) detects these pulses and converts them to an electrical signal that can be processed and measured. The sensor determines the kinetic energy of the impact (E_K) which is dependent on the impact velocity (v) and mass of the grain (m) [47]:

$$E_K = \frac{1}{2}mv^2 \quad (3-6)$$

As the sensor physically connects to the flow-line and picks up the impact of a sand particle, it makes sense to place the sensor on the outside of a bend (ideally downstream within two pipeline diameters). Digital processing filters out responses outside the 100-500 kHz band. In this frequency band the sensor picks up sand impacts as well as some flow noise, and signals must be above a threshold level before sand production is reported. Detection (signal to noise ratio) improves with high-gas rates, high GORs, small flow-lines, high velocities and large grain sizes [48]. Detection can be hindered by wax or other deposits and slugging.

The actual sand production rate can be obtained via calibration performed by injecting a known volume with known sand grain size (no lumps or fines) over a fixed period. The sand is mixed with gel and glycol to aid suspension. Brown (1977) [48] reported early use and calibration of these detectors. Excellent calibration can be obtained for sand-producing wells when used in conjunction with a wellhead de-sander to quantify the sand production rate and grain size distribution.

Intelligent processing is built into the CIUs. The CIUs store all the gathered data onto a flash memory which can hold up to 90 days data. Depending on the frequency of the required reading a PC could be used to download data and to display current trends in real time. The PC used to control the service software can be used to configure each CIU on-site.

3.3.2.1 Clamp-On DSP-06 Particle Monitor

This instrument is intended to monitor systems producing gas, oil, or multiphase, in order to minimize sand erosion damage. Early detection of sand can be provided by the device and this makes it possible to protect the system equipment such as valves from in-line process. Sand-free rates or at least sand production at acceptable rates is the target to be achieved by the operators in order to optimize production at higher levels.

Generally, sand monitors are installed in order to keep sand production under control, optimize production, minimize sand removal cost, avoid erosion issues, and avoid reservoir damage or even well collapse. The clamp-on DSP-06 particle monitor is designed to provide a qualitative measurement of solid or particle production in gas, oil and multiphase flows to reduce the risk of erosion damage.

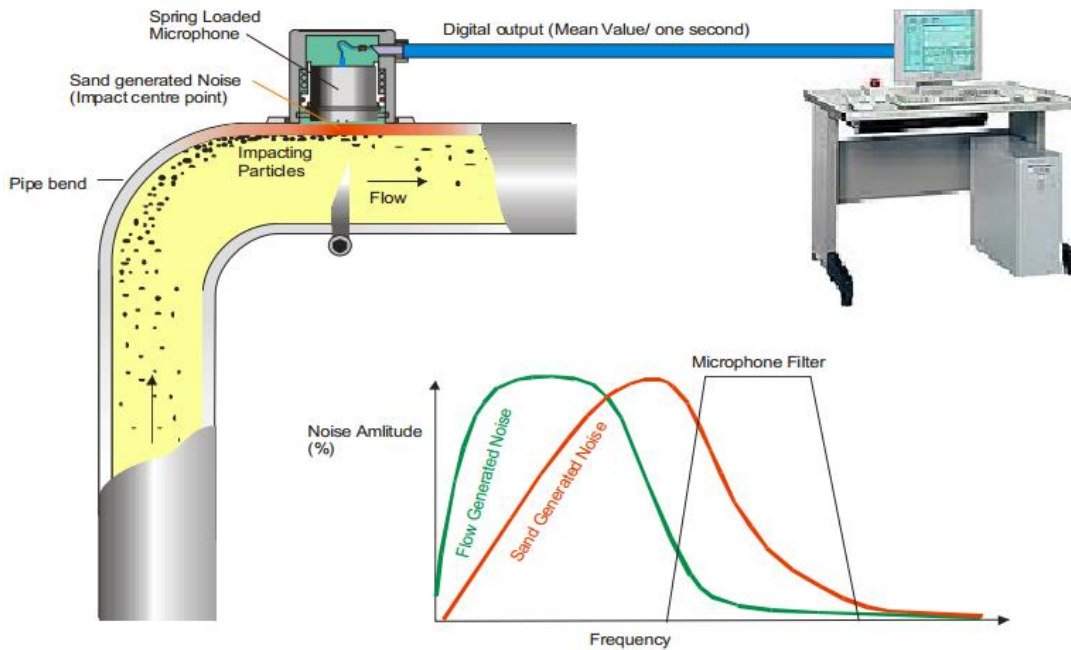


Figure 3-14: Acoustic sand detection principle of operation [49]

The device is based on an acoustic sensor clamped onto the pipe after a 90-degree bend. A microphone picks up the energy of particles hitting the pipe wall at the bend. The signal is filtered to remove information not related to the sand (i.e. flow, mechanical noise etc.), the signal is processed internally by using the built-in electronics which calculate the amount of energy on the spot, and then send results in digital format out of the field [49]. Figure 3-14 shows the principle of operation of the device.

The measured raw signal, representing the energy released by particles hitting the pipe wall can easily be converted to a mass, if the velocity is known then by re-arranging Equation 3-7:

$$m = 2 \frac{E}{v^2} \quad (3-7)$$

3.3.3 Combining Acoustic and Erosion-Based Sand Probes

It is expected that more accurate and reliable measurements can be obtained by combining acoustic and erosion based sand probe technologies into one integrated system, see Figure 3-15. The aim would be to simultaneously optimize the performance of each [50]. The immediate response to sand production is provided by the acoustic monitor, and the erosion-based sand probes can provide measured erosion data that can be used in sand production control. The average size of sand particles can be obtained through a calculation of erosion and sand production when intrusive sand/erosion probes are combined with flow data.

Another benefit from the combination is, if in some unsuitable conditions one system fails the other system is still running and no information is lost. Combining both technologies may provide additional results such as the correlation of internal data and verification of warning messages, as well as setting can be done for more rebuts alarm system.



Figure 3-15: Combination of acoustic and erosion-based sand probes [50]

Combining both technologies could provide a greater range of measurements for velocity, size of sand particles and erosion than for either separately. The

combination of both technologies may also have a significant benefit for such installation that handling the sand with limited capacity topside and operating at low velocity to produce fine sand [50].

Flexibility of calibration is one of the benefits that a combination may afford as the data from one system can be calibrated using the other. This could be done in respect of data comparisons using a single user interface. Consequently, data from the field will be more effective and lead to a better understanding and control of the management processes of gas and/or oil reservoirs.

3.4 Viability and Drawbacks of Techniques

Monitoring of multiphase flows in pipes, especially the presence of sand particles and droplets in oil and gas pipelines can avoid catastrophic failures as well as effectively maintaining the revenue side of industrial projects and reduce maintenance and operation costs. Table 2-1 summarises the viability of the techniques discussed above in monitoring multiphase flow in horizontal pipes with their drawbacks.

Table 3-1: Viability and drawbacks of a number of multiphase measurement techniques

Technique	Viability	Drawbacks
DP Meters	To determine flow velocity, gas void fraction and liquid and/or solid holdup	An old technique, other flow measurement technologies may perform better than differential pressure flow meters in many applications. Solids can plug the impulse piping and cause incorrect measurements.
Electrical Impedance	To measure void fraction and solid concentration of slurry mixtures	Characterised by non-uniformity of electrical field inside the measuring volume. Sensitive to void fraction distribution. Not accurate as signals are affected by the noise of electromagnetic field around the sensors.
Ultrasound	To discriminate the different concentrations of slurries (solid-liquid mixtures)	High initial cost. Not accurate at high velocities
Particle Image Velocimetry, PIV	To measuring velocities in multiphase systems (liquid/solid)	Due to the variations of the particles image intensities may seriously limit the obtainable accuracy of PIV measurements.
Electrical Resistance Tomography, ERT	To detect the particle distribution in micro channels	Repeated effort of data quality and error models especially in difficult measurement conditions. Expensive measurement devices. High level of expertise for the interpretation of measurements.

Technique	Viability	Drawbacks
Needle Probes	To measure the local void fraction and sand concentration in slurry system	Needle probes have limitations regarding the range of substances they are able to measure, the environmental conditions they can be applied to as well as their time resolution
Roxar Intrusive Ultrasound Probe	To measure oil in water, and to detect solids in multiphase flow system	The probe does not work properly if the fluid velocity greater than 4 m/s and value of Reynolds number less than 5,000
Intrusive Erosion Probe	To directly measure sand erosion	The need for sealing arrangement to overcome the leakage of the hydrocarbon caused by loss of adhesion and thermal expansion between the two compounds (probe and potting). This negatively affects the serviceable life of the probe. Need to be replaced when element thickness is reduced by half.
Jorin Visual Particle Analyser	To calculate the concentration and size of the particles in the flow	Not suitable to use with non-transparent fluid.
Clamp-On DSP-06 Particle Monitor	Monitoring sand in oil pipelines to keep sand production under control	No accurate results if probe not installed behind a 90-degree bend, Cannot determine size of sand particle produced.

3.5 Conclusions

The basic fundamentals of multiphase flow such as flow regimes have been outlined. The focus of this chapter was on the multiphase flow in horizontal pipes, and the solid-phase is one of the main components. Multiphase flow can exist in different forms of flow regimes depending on different parameters such as flow rates.

In this chapter, a number of currently available techniques used in monitoring sand concentration in multiphase flow have been outlined, in terms of their design, capabilities and limitations. Monitoring multiphase flow requires robust, reliable and accurate techniques with less limitation as much as possible, which is not available in most of these techniques. For example, ultrasonic techniques and conductivity probe give inaccurate results at high gas flow rates. Therefore, there is still a need to develop the performance of a technique, to be used in monitoring of sand concentration levels in multi-phase flow conditions. The advantages of AE technology appear promising in monitoring of sand concentration in multiphase flow.

4 Sand Deposition and Erosion/Corrosion in Horizontal Pipes

The first section of this chapter discusses the issues that arise from the presence of sand in multiphase flow, and how to overcome sand deposition problems following on from the last section which outlined the findings of previous work that had studied the sand transport characteristics in multiphase flow using a number of techniques.

4.1 Sand Deposition

Sand deposition, which occurs when sand particles are present in a pipeline, is a common problem associated with both oil and natural gas production. If not resolved, it can cause massive damage to the production and transportation systems and carries substantial economic risks.

In order to overcome sand deposition problems, it is necessary to understand the flow characteristics of sand particles in different flows such as liquid-solid and gas-solid in horizontal pipes. It is vital to be able to predict the sand transport velocity and entrainment processes in oil and gas transportation pipelines [51].

Sand particles tend to be deposited (form a bed) when the fluid velocity falls below a certain limit. This velocity is called the sand minimum transport condition (MTC), and is defined as the condition at which the sand particles will continue to keep moving (suspended in the fluid flow) and not be deposited at the pipe bottom [51]. Generally, the smaller the sand particle the easier it is to keep it in suspension. There are some other parameters that affect sand particle deposition, such as sand concentration and pipe size. Figure 4.1 shows the effect of flow velocity on sand particle deposition in pipelines. For a fixed particle size, particle density and kinetic viscosity, observation showed that 100% solid deposition occurs at all flow velocities but the length over which the deposition occurs increases with the increase in average flow velocity (U_{ave}) [52].

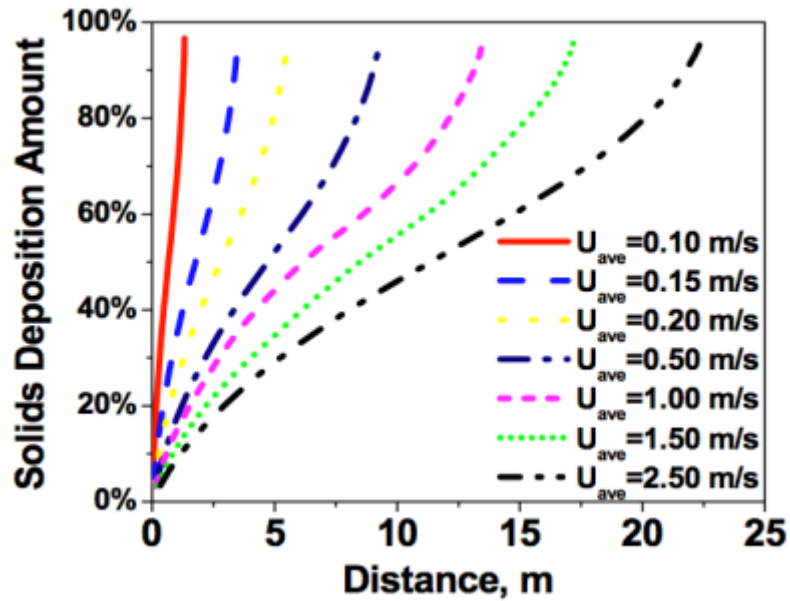


Figure 4-1: Solids deposition as a function of average flow velocity [52]

4.2 Erosion and Corrosion

Depending on the flow rate, production and accumulation of sand particle, sand production can cause erosion and leads to loss of production and high maintenance and operation costs. Erosion is the effect of mechanical wear due to the sand/solids impinging the pipe wall at high flow rates. The erosion effects of sand is difficult to define as all system parameters must be considered – particle size, velocity, flow regime, angle of impact of the particles and materials of construction. As these parameters are always changing, prediction of sand particle flow versus erosion effects cannot be determined accurately in advance or relied upon to operate a healthy system [44].

The erosion rate (ER), is a function of the kinetic energy of impinging particles, which is proportional to the square of particle velocity (u^2) and the frequency of the particle impact which is proportional to the particle velocity [53], thus:

$$ER \propto u^3 \quad (4-1)$$

Impact velocity and impact angle together with the particle density and size are the parameters needed to determine the impact kinetic energy of the particle. In addition,

impact velocity and impact angle are significantly affected by the distributed flow and any increase in impact angle is followed by an increase in erosion [54].

Furthermore, in high speed gas flows repeated discrete impact by particles and/or droplets on the pipe wall generate impulsive and destructive contact pressure, which in turn generate the erosion.

Corrosion occurs as a result of the presence of water in oil/gas pipelines. For instance entrained liquid in a natural gas pipeline can be present in the form of small droplets. These droplets will strike the internal wall of the pipe and accumulate at the bottom and accelerate corrosion of the internal wall of the pipe [55]. Usually, the risk of corrosion increases with low flow rates, whereas erosion increases with high flow rates.

4.3 Forces Acting on a Particle

The single solid particle in fluid flow is affected by several forces including:

4.3.1 Gravitational Force

The gravitational force on a particle (F_{GP}) is expressed in terms of volume and density as:

$$F_{GP} = \rho_P g \frac{\pi d^3}{6} \quad (4-2)$$

where, ρ_P is the density of the particle, d is the equivalent spherical diameter of the particle and g the acceleration due to gravity (9.81m/s^2).

4.3.2 Buoyancy Force

Buoyancy is a force that acts in the opposite direction to gravity. It is found using Archimedes' Principle, which states that the magnitude of the buoyancy force is equal to the weight of the displaced fluid, and so is proportional to the volume and density of the liquid displaced and is determined by the expression [56]:

$$F_{wp} = (\rho_f)g \frac{\pi d^3}{6} \quad (4-3)$$

where: F_{wp} – buoyancy force on particle [N], ρ_f – density of liquid [kg/m^3], g – gravitational acceleration [$9.81 \text{ m}/\text{s}^2$] and d – equivalent diameter of particle [m].

4.3.3 Drag Force

When the surrounding liquid moves relative to a solid particle, a force is exerted by the liquid on the submerged particle. The drag force, F_D , acts in the direction of the relative velocity $V_r = V_L - V_p$ between the liquid and the solid particle. The magnitude of the drag force is calculated from an expression which defines the particle drag coefficient (C_D) [57].

$$F_D = 0.5 C_D A_p \rho_L (V_L - V_p) |V_L - V_p| \quad (4-4)$$

where A_p is the cross-sectional area of the particle ($\pi d^2/4$), $V_L - V_p$ is the velocity of the fluid relative to the particle. The drag force acts in the direction of the relative velocity.

A balance of the gravitational, buoyancy and drag forces on the submerged solid particle determines the settling velocity of the particle.

4.3.4 Lift Force

The lift force is the combination of forces that oppose the settling force on the particle (F_S) which tend to make particles to settle on the pipe bottom. The settling force is the particle weight minus the lift force and has been given as [58]:

$$F_P = [(\rho_p - \rho_f)g/18 \mu] d_p^2 \quad (4-5)$$

Where: ρ_p - particle density, ρ_f - fluid density, μ - fluid viscosity and d_p - particle diameter.

Lift force acting on a single particle (F_L) can be calculated using the expression developed by Saffman [58]:

$$F_L = \frac{20.8 \mu V_r d_p^2 \gamma^{\frac{1}{2}}}{v^{\frac{1}{2}}} \quad (4-6)$$

where: μ and v are absolute and kinematic viscosity respectively, γ is shear rate and V_r is magnitude of the particle velocity relative to the fluid.

At low flow rates the movement of the solid particle is dominated by gravitational and buoyancy forces, which results in deposits of solid particle at the bottom of the pipe. At high flow rates dynamic forces keep the particles suspended in the flow and prevent deposits. The type of movement that occurs when the sum of the forces acting on the particles (buoyancy, lift and drag), is greater than the gravitational force.

At sufficiently high flow velocity, gravitational force has no significant effect on particles compared to viscous forces which leads to homogenous flow where the particles are fully suspended in the flow [59].

4.4 Motion of Particles in Fluids

Motion of particles is controlled by three types of forces: (1) forces acting through the interface between fluid and particles, (2) forces due to the interaction between particles and (3) forces imposed by external fields.

In gas-solid flow, particles can have four types of simple motion: (1) a particle moving with a constant velocity in a uniform flow field, (2) a particle accelerating in a uniform flow field, (3) a particle moving with a constant velocity in a non-uniform flow field and (4) a particle rotating with a constant angular velocity in a uniform flow field [9].

In liquid-solid flow, when the velocity of the flowing fluid is very low, or when the viscosity of fluids is very high and/or size of the particles small, the particles move with a creeping motion in which inertial effects can be ignored relative to viscous resistance.

To avoid sand deposition the fluid flow should be sufficiently fast to suspend particles, this depends on the counterbalance of two actions, gravity and upward

diffusion. Gravity causes the particles to fall and deposit themselves on the bottom of the pipe, whereas upward diffusion of the particles is caused by a concentration gradient of particles.

In multiphase transport systems, flow can exist in different regimes depending on the flow conditions. Stratified and slug flow are the primary regimes that occur in horizontal pipes. Stratified flow takes place at low flow rates which in turn affects the particle motion and causes them to be deposited at the bottom of the pipe. The motion of a sand particle is superior in slug flow as it is characterised by higher liquid loading as well as higher liquid velocity [51].

4.5 Previous Work

This section includes results of investigations of sand particle transport in multiphase flows in horizontal pipes using different techniques.

4.5.1 Conductivity Ring

Al-Lababidi et al. [51] conducted an experimental investigation of sand transport and deposition characteristics to identify the sand MTC in water-sand and in air-water-sand multiphase flows in horizontal and +5° inclined pipelines. A conductivity ring was used to monitor air and water volumetric flow rates, with water temperature, differential pressure and line pressure also recorded.

The two-phase flow loop facility was constructed using ABS plastic (class E) pipes of 50 mm internal diameter, with a total pipe length of 17 m containing a 1.2 m long Perspex pipe window for observation. Flexible pipe was installed at the ends of the pipe to allow for horizontal and inclined arrangements. Water was circulated in the flow loop using a centrifugal pump with a maximum capacity of 40 m³/hr and a maximum discharge pressure of 5 barg. The water flow was metered using an electromagnetic flow meter, ABB K280/0 AS model with 0-20 m³/hr range. The water reservoir tank had a capacity of approximately 1500 litres. A mixture feeder unit was installed upstream of the test section which fed a sand-water mix into the flow loop through a sand injection point installed after the water and air mixing point using a LAFERT centrifugal slurry pump with capacity of 5 m³/hr. Experiments were conducted with different sand volume fractions ranging from 1.61x10⁻⁵ to 5.3x10⁻⁴.

Observations showed that sand behaviour in air-water multiphase flows was different in the horizontal pipe from the upwardly inclined pipe. This was due to backflow of water in the latter. The MTC was influenced by the air supply which can cause a change of flow regime and water flow condition. The concentration of sand had a significant impact on the sand transport condition because sand transport characteristics change with sand concentration. In horizontal air-water flows, MTC occurred mainly in hydrodynamic slug and stratified wavy flow regimes.

4.5.2 Ultrasound Technique

Chemloul [60] conducted an experimental study using pulsed ultrasonic Doppler velocimetry to measure simultaneously the local velocity and the local concentration in a flow of solid-liquid suspension in a horizontal pipe. The closed flow loop facility was constructed using glass pipe of 20 mm internal diameter. The test section was 75 pipe diameters downstream of the pump where the flow was fully developed. Water was circulated in the flow loop using a variable speed centrifugal pump. The flow was maintained at constant temperature using a heat exchanger. Two differential pressure transducers were used. Experiments were conducted with spherical glass beads of density of 2640 kg/m^3 as the solid particles. Four different particle size distributions were tested with volume-averaged mean particle diameters of 0.27, 0.3, 0.4, and 0.7 mm. The particle diameter ranged between 1.30η and 3.38η (η is a Kolmogorov length scale). Kolmogorov length scale is the length scale at which the turbulent fluctuations are dissipated into heat by viscosity [122]. Glass bead volumetric concentrations used in suspension were 0.5%, 1%, 1.5% and 2% and the particle volume fractions ranging between 1.25×10^{-3} and 5×10^{-3} .

A new approach was used to measure the local concentration of particles. It consisted of counting a number NP (number of particles) of the Doppler signals of the solid particles crossing the measurement volume and a number NPt (total number of particles) of the Doppler signals of the solid particles crossing the control volume. The concentration profile is then represented by the ratio NP / NPt. The results obtained show that the suspension of fine particles, which represents a tracer, behaves as a homogenous fluid. For large particles, the author confirmed the existence of slip velocity and that both concentration and size of particle affects the turbulence. The use of two distinct measurement volumes allows the direct

determination of the turbulent length scales. The results show that the turbulence characteristics of the carrier fluid are modified by the presence of the solid particles.

4.5.3 Particle Image Velocimetry (PIV)

Goharzadeh and Rodgers [61] investigated gas-liquid slug flows on solid particle transport inside a horizontal pipe. High speed photography was used to characterise the influence of slug length on the transport of solid particles. PIV and RIM (Refractive Index Matching) with fluorescent tracers (oil-air two-phase loop) were combined and used to measure velocity distribution in the presence of a slug.

This study showed that the mobility of the solid particles was greatly influenced by the presence of a slug body, but that the physical mechanism involved was discontinuous. The region located upstream of the slug nose was found to be “inactive”, in terms transport of the solid particles and the size of the region was a function of the composition of gas-liquid flow and the size of the solid particles. The great reduction in the magnitude of velocity immediately upstream of slug nose meant that the particle MTC occurred further upstream.

4.5.4 Digital Image Analysis

Bello [62] measured sand holdup in oil-gas-sand three-phase slug flow in a horizontal pipeline using a digital imaging technique to obtain accurate local sand particle holdup measurements. The study was performed in a gas-liquid-solid three-phase flow test rig facility. The rig contained an inclinable bench which allowed variation in the angle of inclination of the test pipe. A 6.5 m long transparent plexiglass pipe of 40 mm internal diameter was used as test section. To ensure stabilized flow and to avoid entrance effects, measurement were performed 125 pipe diameters away from the inlet. Water was circulated from a 4 m³ stainless steel slurry tank in the steel pipe of 25 mm internal diameter using a 6 kW stainless steel centrifugal slurry pump. An air compressor was used to feed air into the system through a cooler, filter, regulator valve and porous pipe. Sand particles were used in the tests, with diameters of 0.6 mm. Bello et al., claim that the digital image analysis technique was a powerful tool for visualizing particle movement and to identify local sand holdup profiles under specified conditions of oil-gas-sand three-phase slug flow

in horizontal pipelines. In addition, Bello [62] developed a theoretical model to estimate local sand holdup.

4.5.5 Acoustic Emission (AE) Technique

Duclos [63] carried out an experimental study to monitor erosion rates in pipes using an AE technique. The signals generated by particles impacting on the pipe wall, bubbles bursting and fluid flow, were successfully separated from each other. The test rig facility was constructed using a 3.1 mm thick stainless steel pipe of 26.7 mm inner diameter. Two AE sensors were installed behind a 90-degree bend. The injection point was positioned 2 m upstream of the bend. A controlled quantity of sand particles and droplets were fed into the flow loop using a 60 ml syringe. Observations of the AE waveforms associated with the particle impacts clearly distinguished AE waveforms associated with air bubble bursts. Observations showed a clear distinction between AE signals generated from bubble burst and particle impact in terms of AE event duration; AE event duration of particle impacts was much shorter and the intensities of the emission were much higher comparing to bubble bursts. Finally a clear correlation was established between AE signals and the quantity of sand particles and air bubbles. The increase in the quantity of sand injected led to an increase in the number of sand particles impacting on the pipe wall regardless of particles size, which in turn increased the AE signals generated. The same result was observed with the air bubbles.

Albion [64] carried out an experimental study using AE to investigate the flow regime of powder in horizontal pipes. The test rig facility was constructed using a stainless steel pneumatic transport pipe of 26.7 mm inner diameter. Air was supplied using a compressor with regulator controlled valve. Two AE sensors were located at the bottom and top of the steel pipe test section. In order to record the flow regime under various operation conditions, a high speed video camera was used. Observations showed that dilute phase flow and deposited solid flow could be identified using statistical measures of the AE signal obtained from analysis of its frequency spectrum.

Buttle and Scruby [54] carried out an experimental study to characterise particle impact using AE techniques. The study considered different sized particles. The

parameters obtained from the impact of particles with each other or with the test surfaces were measured and analysed using a method developed by the authors. The output was then compared with the predictions in the literature.

A vacuum free-fall system was designed and used for the particle impact work. The number of particles falling and their velocities could be accurately controlled. Two types of particles were used in this work, spherical bronze particles 53 μm – 75 μm in diameter, and glass particles 57 μm – 90 μm in diameter. The particles were dropped from different heights so that impact velocities were between 2.5 – 7.1 m/s. The target consisted of either a pure aluminium plate with a thickness of 5.8 mm or a mild steel plate with a thickness of 6.3 mm. AE signals from individual particle impacts upon the surfaces generated elastic waves which were detected using a broad bandwidth piezo-electric capacitance transducer placed on the opposite side of the target plate at the epicentre of the impact.

The impacts were assumed elastic and the impact forces were obtained by deconvoluting the AE signals. Two useful parameters, the peak impact force and the impact time were both extracted. It was observed that the peak impact force increased consistently with the increase in velocity of the impact particle, but the impact time was not dependent upon the velocity of the impact. Both observations were in good agreement with the theoretical models. The particle size distribution that optically measured was in good agreement with the size distribution obtained experimentally.

4.5.6 Acoustic Non-Intrusive Sand Monitor and Intrusive Erosion Sand Measurement Detectors Techniques

Shirazi [3] evaluated sand monitors for multiphase flow using acoustic non-intrusive sand monitor and intrusive erosion sand measurement detectors. On-site calibration is required for an acoustic sand monitor to be able to determine the quantity of sand production. Whereas, an erosion prediction model is required for intrusive detectors in order to be combined with the monitor and enable the rate of sand production to be assessed.

By comparing data obtained experimentally with data obtained from a particle impact velocity and erosion prediction mechanistic model, this study led to the conclusion that the particles were significantly retarded by the fluid before they came in impact with the wall. The data from the acoustic sand monitor showed a direct correlation existed between data obtained from the monitor and the erosion model. A direct correlation also existed between data obtained from the intrusive sand detector and the erosion rates predicted for an elbow.

These results indicated that the particle impact velocity and erosion model could be used to interpret output from sand monitors as well as to assess sand production and erosion rates of pipe components.

4.5.7 Mechanistic Model

Mazumder [65] developed a mechanistic model to predict erosion in multiphase annular flow by considering the effects of sand particle distribution and particle velocities in an annular film and in the gas core region of three-phase flow. The mechanistic model predictions were compared with annular flow erosion results and showed good agreement.

A procedure to calculate liquid droplet velocity in the gas core region was also presented and the calculated droplet velocities showed good agreement with experimental results.

Different erosion rates were observed at test sections with flow development lengths of 70 and 160 inner diameters, for both horizontal and vertical flows. Higher erosion rates were observed when the flow development length was 160 pipe diameters because it required a greater pipe length for the annular three-phase flow to become fully developed.

Also greater erosion was found in specimens placed in the vertical test section than in the horizontal test section due to different sand distribution profiles in horizontal and vertical flow. Sand distribution was nearly uniform in the vertical test section for the annular flow condition. In the horizontal section, a larger annular liquid film and higher sand concentrations were found at the lower section of the pipe due to gravity effects and this had a significant influence on erosion because the sand in the liquid

film moves at a much slower velocity than the sand in the core region of annular flow.

The uniform sand distribution assumption used in the mechanistic model agrees with measured sand distributions in vertical annular flow. Generally, the mechanistic model erosion predictions were higher than the experimental results.

4.6 Conclusions

Typically, each technique has its own advantages and disadvantages. For example, the accuracy of data measured by the ultrasonic technique has been criticized because it is affected by gas void fraction and it has been observed that the accuracy of the ultrasound technique significantly decreases at high gas flow rates. Thus, it is important to find an online technology characterised by its reliability, sensitive to the presence of sand particles and which requires little or no maintenance.

To date is still conducted researches on monitoring sand particles in multiphase flow using the AE technique. Thus, this research will investigate the use of acoustic emission technology as a tool having the required capabilities to successfully detect and quantify the presence and properties of sand particles in multiphase flow in horizontal pipes.

5 Acoustic Emission (AE)

Acoustic emission is a naturally occurring phenomenon where transient high frequency elastic waves are emitted by the sudden release of energy from localised sources within a material. Such sources could be the cracking of timber, fracture of materials under pressure, turbulence in fluids and fluid leakage [66, 67]. In solids, the source is usually micro cracking within the material, which results in rapid releases of energy in the form of transient elastic waves [68].

The earliest use of acoustic emission analysis probably occurred in seismology. Elastic waves produced by an earthquake were analyzed to characterize fault movement in terms of energy released, location, and depth. Also, the possibility of detecting rock burst in coal mines was anticipated early in the studies.

Early observation of audible emissions in metals was made by tin smiths who noted “tin cry”, or twinning, during deformation of tin. As deformation occurs, atomic planes slip past each other through the movement of dislocations. Because the amount of atom movement during twinning is small, the resulting plastic deformation is also small [123]. Audible sounds or clicks noted during heat treatment of steel were related to martensitic transformation. In fact, later studies showed that martensitic transformations in general are prolific sources of AE. Joseph Kaiser and his co-workers in Germany in the early 1950s are generally credited with initiating the present effort in AE. Several years after Kaiser’s work, Schofield and Tatro initiated research in the middle 1950s and did much to improve the instrumentation and to clarify the sources of AE. They found that emissions from metals were primarily due to dislocation motion accompanying plastic deformation rather than being entirely due to grain boundary sliding, as proposed by Kaiser.

In the decade of 1960s, many engineers and scientists became interested in AE and utilized this technique in studies relating to materials research, material characterization and evolution, non-destructive testing, and structural evaluation. In addition, emission techniques have been found for such uses as detecting boiling

and cavitation in fuel systems. Extensive improvements in instrumentation in the early 1960s made possible many advances in AE technology.

During the last few decades AE has received a great deal of attention and recent publications have shown that its use can offer reliable quantitative information about the process being monitored, though, there remain difficulties in its effective application [69,70]. AE has been classified as a non-destructive testing (NDT) technique with no harmful effect on the future usefulness of the objects tested [71].

5.1 Definition of Acoustic Emission (AE)

The elastic waves associated with AE are typically in the frequency range from 100 kHz to 1 MHz. They propagate on the surface of the material as Rayleigh waves and within a material as Lamb, longitudinal and shear waves. The waves are usually detected by an AE sensor placed on a suitable surface of the material [36].

The detection sensors are, of course, analog devices attached to fully digitized data recording and analysis systems [72].

5.2 Mechanism of Acoustic Emission

The first step in the AE measurement process is the detection of AE waves by a sensor, which converts dynamic motions or mechanical energy of the elastic wave at the surface of a material into electrical signals. Due to the low amplitude of the AE signals, amplifiers is used to drive the signals produced by the piezoelectric sensor over long distances (i.e. from sensor to data acquisition device). The signal-to-noise ratio of equipment should be low. Digital filters are used to minimize the electronic noise, or to filter out unwanted frequencies [73]. Finally, the AE signals are processed using a data acquisition board. Figure 5.1 shows the principles of the AE process.

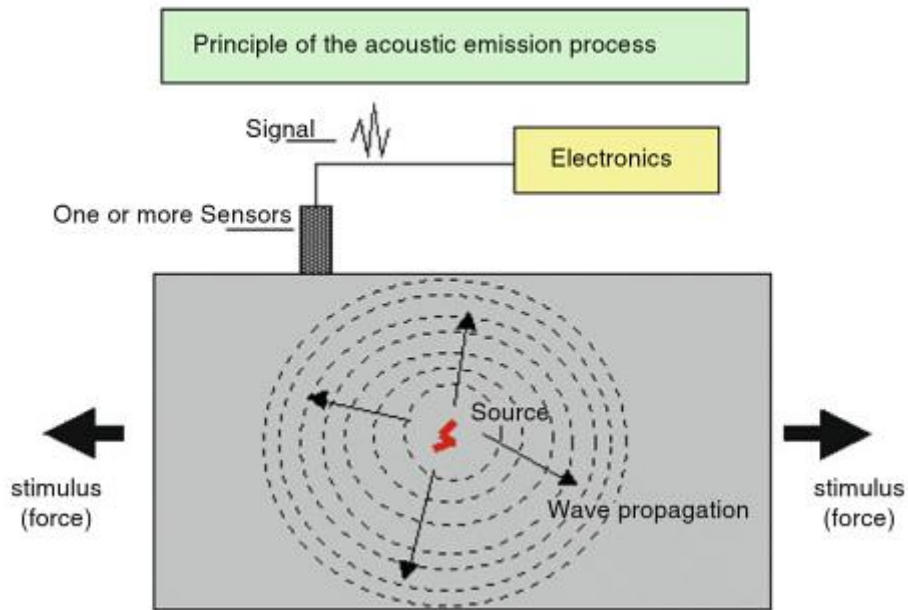


Figure 5-1: Principle of Acoustic Emission process [119]

5.2.1 Kaiser Effect

Joseph Kaiser in Germany in the early 1950s was the first to use electronic instrumentation to detect audible sounds produced by metals during deformation. Kaiser reported that all metals examined, including zinc, steel, aluminium, copper, and lead exhibited the emission phenomena. Kaiser also observed that AE activity was irreversible, AE was not generated during the reloading of a material until the stress level exceeded its previous maximum. This irreversible phenomenon has become known as “Kaiser Effect” [74].

Figure 5.2 illustrates this phenomenon. When the load increases the emission counts increase from point “A” to point “B”. If the load decreases to point “C”, the emission count remains constant. The emission count will stay constant when the load increases again, until it reaches the previous level at point “D” = “B”. If the load increases beyond that, the emission count starts increasing again [36, 67].

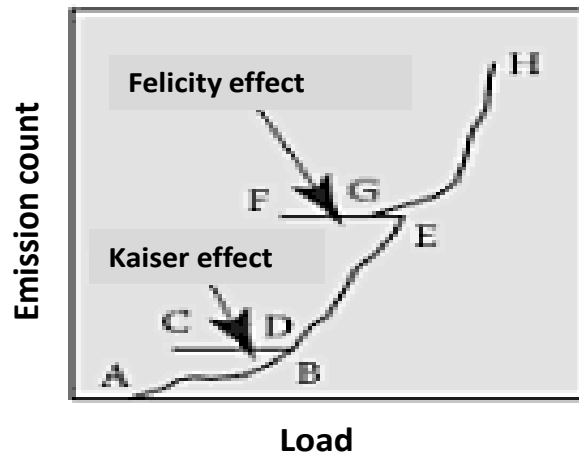


Figure 5-2: Kaiser and Felicity effects [36, 37]

5.2.2 Felicity Effect

At higher stress levels the Kaiser effect does not hold true. In such a situation, emission can occur at load levels that are lower than the previous maximum load level. As can be seen from Figure 5.2, if a higher load level “E” the load decreases to level “F” the emission count remains same. When the load starts increasing again from “F” to “G” the emission count remains same. However, at level “G”, a level that is less than the previous maximum load, “E”, the emission count starts increasing. This effect is known as the Felicity Effect [67].

5.3 Acoustic Emission System

The basic AE measurement system consists of an AE sensor, amplifier(s) and AE signal analyzing equipment, schematically shown in Figure 5.3. Each of these units is briefly described;

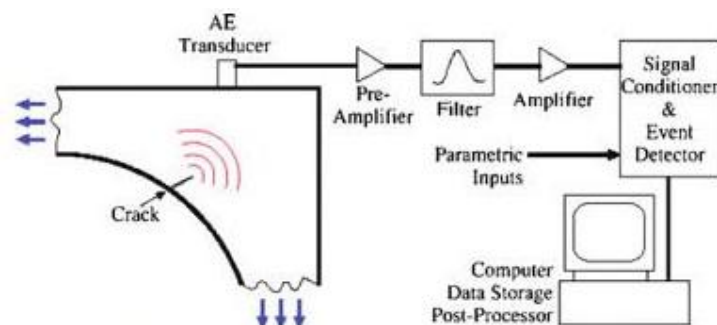


Figure 5-3: Typical Acoustic Emission system [119]

5.3.1 Acoustic Emission Sensors/Transducers

The AE sensor, see Figure 5.4 is the most important part of the AE equipment and fundamental to any effective monitoring process [75].



Figure 5-4: Acoustic Emission sensors [78]

The most widely employed AE sensors for detection and recording of AE are piezoelectric sensors characterized by a wide-range frequency response, high sensitivity, low cost, and ease of use. Piezo-ceramic is widely used in AE sensors because of its high sensitivity and robustness. Piezoelectric sensors are classified into two categories according to their frequency response: resonant and high fidelity. Resonant sensors are termed narrowband but may have multiple resonances with high sensitivity peaks over a wide frequency range. High fidelity sensors provide an output that is flat with frequency and thus more closely approximates the ideal sensor. Typically, high fidelity sensors have lower peak sensitivity than resonant sensors, but more accurately reproduce the actual wave displacement.

Figure 5.5 shows the basic construction of an AE sensor. When piezoelectric material is mechanically strained, an electric charge is generated. The resonance frequency of the sensor will be determined by the thickness of the piezoelectric element. The area over which the sensor averages surface motion can be defined by the diameter. Piezoelectric materials include [76]:

Some natural crystals such as Quartz,

- Specially formulated and processed ceramics such as Lead Zirconate Titanate (PZT),
- Specially formulated and processed polymers such as Polyvinylidene Fluoride (PVDF).

The electric signals obtained are different for the different of the materials used as the sensor. For example, a typical AE sensor with a Lead Zirconate Titanate (PZT) element will produce an electric signal of almost 1 mV for a displacement of 1 picometer.

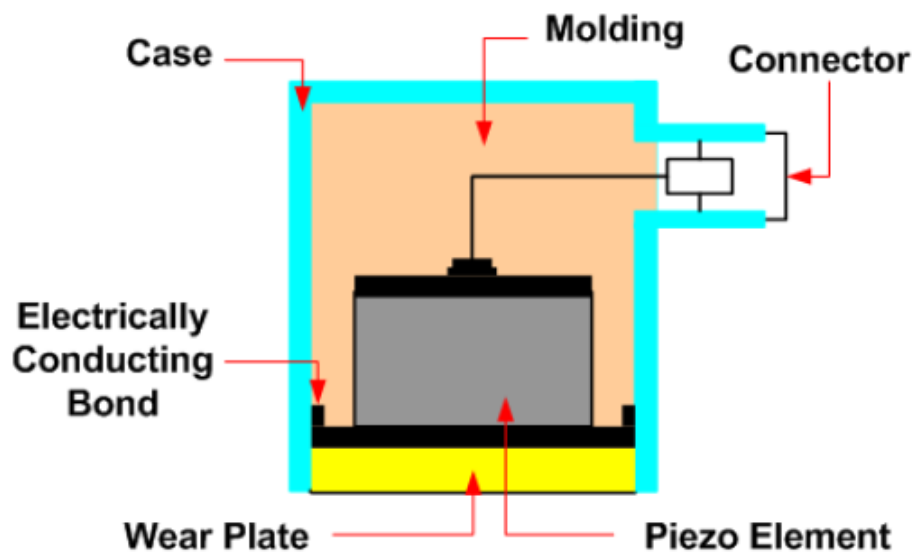


Figure 5-5: Basic construction of an AE sensor [37]

5.3.2 Acoustic Emission Preamplifier

The sensor is accompanied with a preamplifier so that it increases the signal transmitted. The preamplifier should have low noise, moderately high power gain (The gain of the amplifier = $20 \log_{10} (V_o/V_i)$ dB; where, V_i is the reference voltage = 1μ volt, and V_o is output voltage). To maximise accuracy, the cables connecting the sensor to the pre-amplifier should be as short as possible – traditionally it was said less one meter long, as well as being shielded (co-axial or BNC) – but today the pre-amplifier will usually be contained within the sensor.

Filters are designed for different band widths and can be plugged in to meet specific requirements, such as to minimize the electronic noise and to filter out unwanted frequencies.

The pre-amplifier output signal has to be amplified further (post-amplification) before it travels a “long distance” (this might be 1 metre) before being processed. Further amplification with selectable gain is incorporated in this unit. To better eliminate unwanted background noise, only signals exceeding a certain threshold voltage are detected and analysed, [77, 78].

5.3.3 Data Acquisition (DAQ) Board

AE signals are processed and analysed using a DAQ board to sample the analogue signal and converting it to a digital signal. The DAQ board can have more than one channel. Each channel serves a signal detection unit (sensor and preamplifier) and is connected to a computer. PCI bus signals, analysed by the DAQ board, are processed to show AE duration, rise time, RMS value, etc.

5.4 Mounting Conditions for AE Sensors

The three most important factors in ensuring an undistorted signal and maximum sensitivity are [75];

- The couplant material between the sensor and the medium through which the AE wave is propagating,
- Mounting pressure (mechanical force required to hold the sensor against the structure or the specimen), and
- Surface condition of the specimen.

These factors affect not only the overall sensitivity (e.g. peak voltage) and arrival time but also the resonant frequency of the mounted sensor and the phase relations of the different components of the AE sensor signal [75]. Thus, when AE waves are analyzed in the time domain, it is important to know the characteristics and reproducibility of the mounting condition.

5.5 Acoustic Emission Signals

There are two types of AE signals encountered in practice: these are burst and continuous signals as illustrated in Figure 5.6.

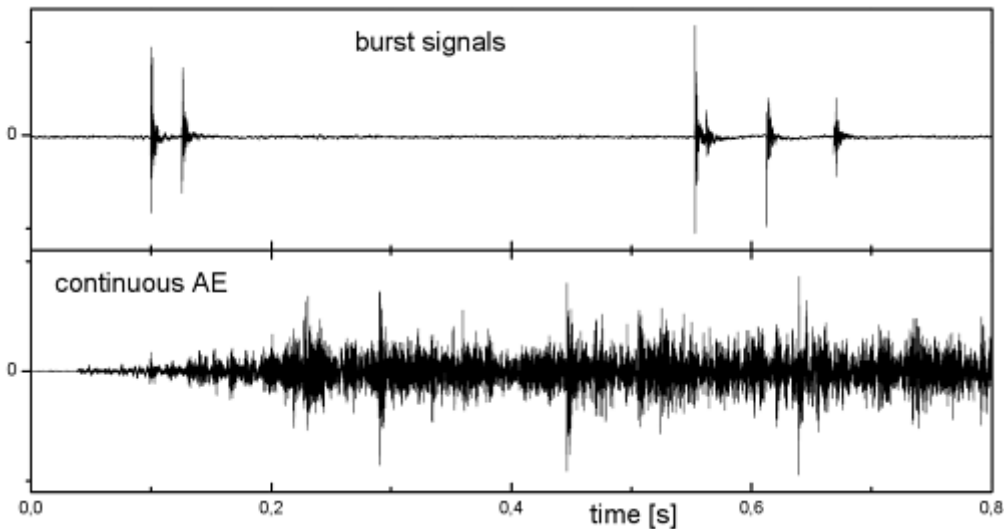


Figure 5-6: Burst signals compared to continuous Acoustic emissions [80]

- **Burst signal** - is a type of emission related to individual events occurring in a material that results in discrete acoustic emission signals. Such bursts tend to be random in timing and size. Burst signals are separated in time, i.e. beginning and end of these signals can be identified and it is this characteristic that usually separates them from continuous signals.
- **Continuous signal** - is a type of AE signals that cannot be separated in time. They are produced by overlapping phenomena, e.g. when there are sufficiently numerous AE individual bursts in plastic deformation or friction. These signals often include background noise from both mechanical and electrical disturbances [79]. Such continuous signal is often analysed using root-mean-square (RMS) techniques.

5.6 AE Wave Propagation Modes

AE waves are elastic waves due to dislocation motions (discontinuity of displacements as cracking) in a solid. They consist of P-waves (longitudinal waves), S-waves (transverse or shear waves), and other interfacial waves as surface waves

(Rayleigh waves), reflected waves, diffracted waves and guided waves (Lamb waves and other plate waves) [80], see Figure 5.7.

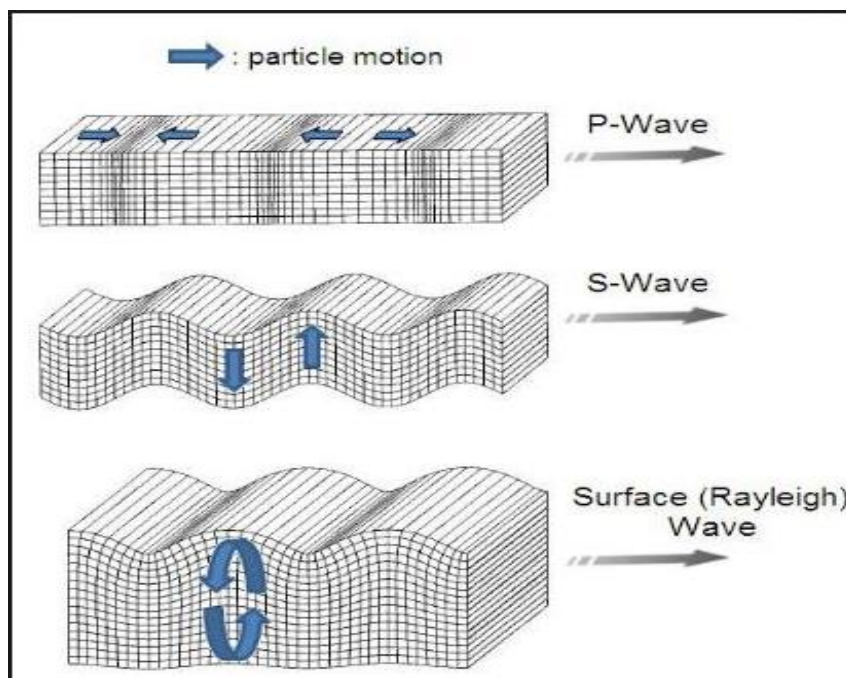


Figure 5-7: Typical P-, S - and surface waves [81]

AE waves are elastic waves but because they are high frequency they attenuate rapidly with distance.

- **P-wave (longitudinal wave)** - is a wave in which the oscillations (particle displacements) occur in the direction of the wave propagation, longitudinally.
- **S-wave (shear/transverse waves)** - is a wave in which the oscillations occur perpendicular to the direction of the wave propagation.
- **Rayleigh or surface wave** - is a wave in which the particle motion (combination of longitudinal and shear waves) is elliptic motion in planes normal to the surface and parallel to the direction of the wave propagation.
- **Lamb wave (or plate wave)** - is a wave with particle motion parallel to the test surface and perpendicular to the plate.

Aspects of the wave propagation process that are important in AE technology include attenuation and wave velocity;

- **Attenuation** - the loss of amplitude as the wave travels outward from the source. Attenuation is due to several factors such as geometric spreading,

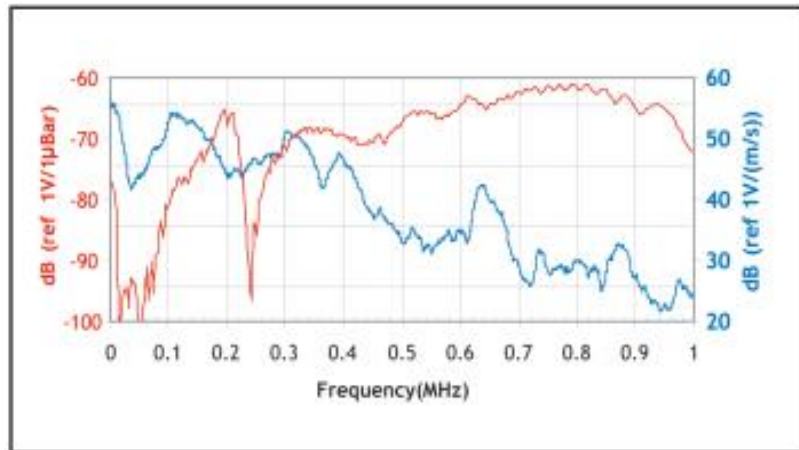
scattering at structural boundaries and absorption. When the source is a short distance from the sensor, geometric spreading is the most influential factor, whereas at longer distances energy absorption and structural scattering can be the most influential [67].

- **Wave velocity** - the velocity with which the disturbance travels through the structure is important for some source location techniques [67, 78, 81]. To improve the accuracy of source location, arrival times of different wave modes should be detected separately and their velocities evaluated.

The effects of propagation velocity as a function of frequency (dispersion) together with the material and surface attenuation - which are also functions of frequency - will change the pulse as it propagates. These effects should be measured prior to each monitoring test as the geometric and structural conditions will vary.

5.7 AE Sensor Calibration and Attenuation Test

A calibration test is defined as a test during which known values of the parameter to be measured are applied to the sensor and corresponding output readings are recorded under specific conditions [82]. Usually, manufacturers provide AE sensors with calibration certificates. These certificates are a calibration record, issued by an accredited calibration facility and certifying its traceability to national and international standards such as ASTM-E1106 (Standard for primary calibration of AE sensors) and ASTM-E976 (standard for determine the reproducibility of AE sensors response). Figure 5.8 shows an example of wideband AE sensor calibration certificate which display the sensitivities of the sensors as frequency response diagrams (output voltage vs. frequency).



Frequency response of the WSα. Calibration based on ASTM E1106;
 Calibration based on ASTM E976.

Figure 5-8: Example of wideband AE sensor calibration certificate [81]

To guarantee the quality of measurements, AE sensor calibration should be performed regularly using the attenuation test. To determine the signal strength as a function of distance from the source is important as it depend on the attenuation. The value of the attenuation is affected by factors such as, the type and thickness of the medium [68]. Each type of medium has its own attenuation coefficient (β) that can be used to identify the decay in amplitude of AE signals as a function of frequency. Attenuation can be determined using the following expression;

$$A_t = \beta * r * f \quad (5-1)$$

where, A_t is the attenuation, β is medium coefficient, r is transmission distance and f is the signal frequency.

The amplitude of a given signal is defined as the maximum of the AE signal (positive or negative) generated from an AE hit, and determined as;

$$SA = 20 \text{Log}_{10} \left(\frac{V_{max}}{10^{-6}} \right) \quad (5-2)$$

where, SA is the amplitude of a given signal, V_{max} is the maximum amplitude of a given signal and 10^{-6} is a standard reference value.

The attenuation for two different locations can be calculated if their signal voltage (V_s) or signal power (P_s) is known.

If P_s is a source signal power at location 1 and P_d is signal power at location 2, then At_p the attenuation between location 1 and 2 is given by:

$$At_p = 10 \text{Log}_{10} \left(\frac{P_s}{P_d} \right) \quad (5-3)$$

Similarly if V_s is source signal voltage at location 1 and V_d is a signal voltage at location 2, then At_v the attenuation between location 1 and 2 is given by:

$$At_v = 20 \text{Log}_{10} \left(\frac{V_s}{V_d} \right) \quad (5-4)$$

$$SE = \int_0^{T(\text{sec})} v^2(t) dt \quad (5-5)$$

where, $v(t)$ is the time dependent voltage from the AE sensor, and T is the duration of the entire event over which the integration is performed.

$$SP = \frac{SE}{T(\text{sec})} = \frac{1}{T(\text{sec})} \int_0^{T(\text{sec})} v^2(t) dt \quad (5-6)$$

An AE sensor attenuation test usually precedes any AE test.

Calibration of AE sensors can be carried out in a number of ways, the most widespread is excitation of a sensor with a standard broadband source and noting the resulting frequency response. This can be complicated, time consuming and expensive.

Thus a great deal of effort has gone into using mechanical sources such as fracture of lead pencils and glass rods, calculating the transfer function from the source to the sensor locations and comparing these to the sensor output. This has also been done in conjunction with laser measurement.

An easy and simple method of calibration of AE sensors is the Hsu-Nielsen, see Figure 5.9. This technique is based on pencil lead breakage [83]. A standard graphite pencil lead (2H) of 0.5 mm thickness and length 3 mm is placed as shown in Figure 5.9. A guide ring rests on a steel surface and the pencil is guided obliquely towards the surface. The lead is broken as the pencil is rotated around the point of contact, towards the vertical. The calibration signal is generated as the lead breaks [84].

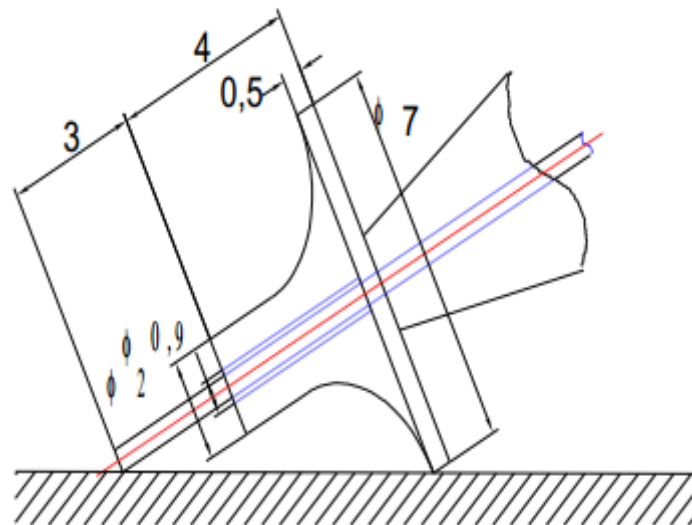


Figure 5-9: Hsu-Nielsen source [81]

5.8 Acoustic Emission Measurements

Data collected using AE systems can be analyzed to extract useful information using various signal processing techniques. Typically, Hit and time driven data measurements are the two methods used to record data from AE system. These two methods are briefly described below.

5.8.1 Hit Driven Data Measurements

AE measurement systems have the capability to measure parameters of individual discrete AE signals. These parameters are used to analyse AE events. Figure 5.10 summarises typical AE parameters. AE signal detection parameter measurements are based on signals equal to or greater than a pre-set voltage threshold. The most common measured parameters of AE signals include:

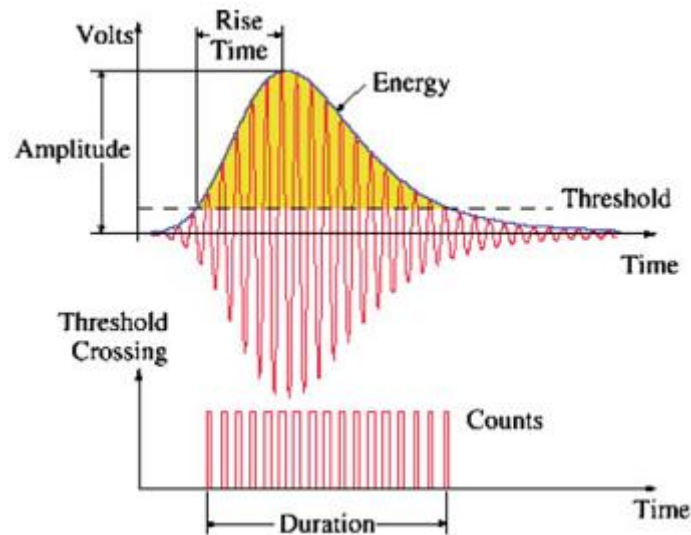


Figure 5-10: AE signals measurement parameters [119]

- **Threshold** - is equivalent to a voltage level on an electronic comparator;
- **Peak amplitude** - is the maximum amplitude of the signal;
- **Arrival time** - is determined by the first signal excursion above the threshold voltage, and is used to calculate source location;
- **Duration time** - is the difference in time between the first threshold crossing and the last. This parameter can be used to identify different types of sources and to filter out noise;
- **Rise time** - time interval between the first threshold crossing and the peak amplitude;
- **Ring down count** - number of threshold level crossing;
- **Energy** - the measured energy value is an integrated measurement of the square of the voltage signal with respect to time.

5.8.2 Time Driven Data Measurement

This method is characterised by a continuous record of the AE waveform during an AE test. The analogue AE waveform detected by AE sensor is transformed into a digital signal and stored. Today, AE systems generally have the capability of acquiring AE waveforms continuously at a range of sample rates. The data collected is then subject to more comprehensive analysis and further characterisation to determine the nature of the source. Figure 5.11 shows samples of typical AE waveforms.

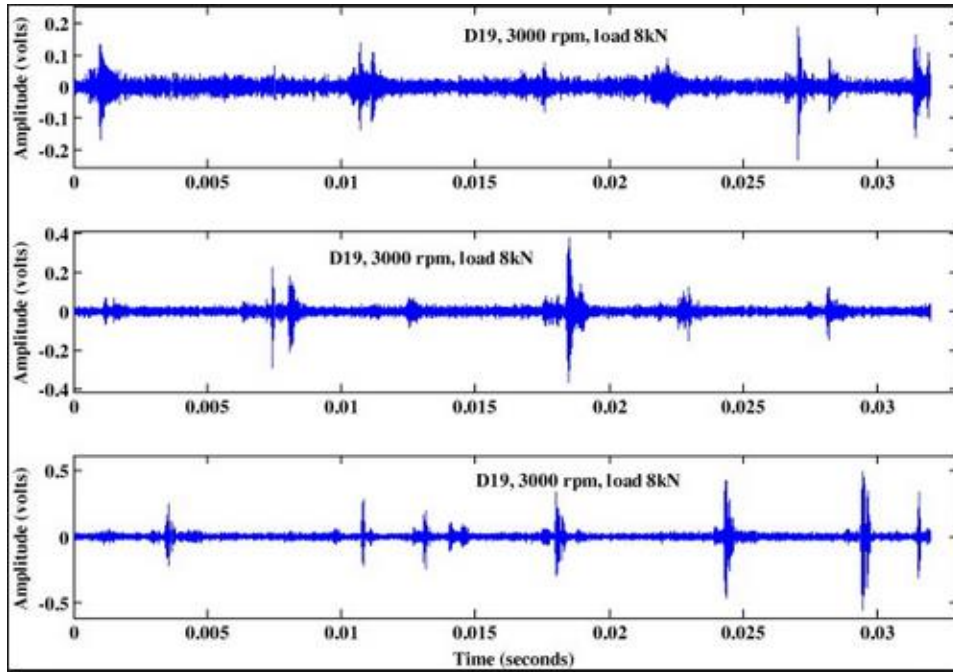


Figure 5-11: Typical AE waveforms [online source]

5.9 Location of AE Sources

There is a variety of different location methods for different structural geometries and applications. Most are based on evaluation of time difference between wave arrivals at different sensors. When arrival time is difficult or impractical to detect using one method, another is applied. These include cross correlation methods or zone location method based on the effect of attenuation with distance. Figure 5.12 schematically shows calculation of AE source location based on detecting time difference between wave arrivals at the sensors with a known wave velocity.

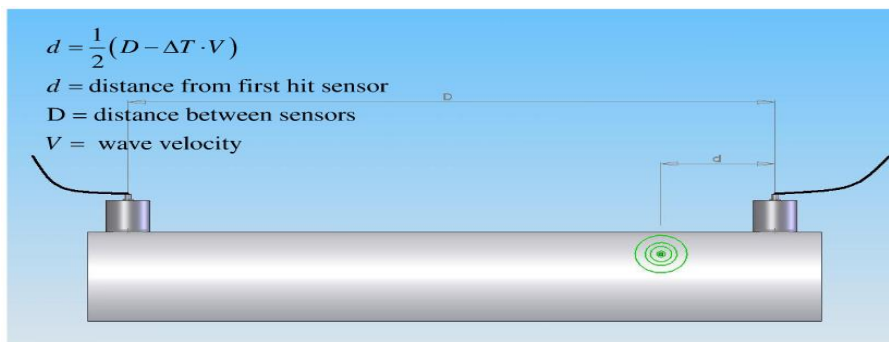


Figure 5-12: Acoustic Emission source location [81]

Zone location method is another simple method to locate an AE source. The exact source coordinates are not determined, but the defect is located within the radius of the sensor's sensitivity range. This method is used to monitor large structures such as pipes and vessels. Figure 5.13 shows the basic principle of the zone location method applied to monitor for leaks in pipes. Sensors are distributed on the surface of the structure within detection range from the most critical locations (leak or failure). If an AE signal is recorded by a particular sensor, a technician should inspect the vicinity around this sensor for leaks or cracks [80].

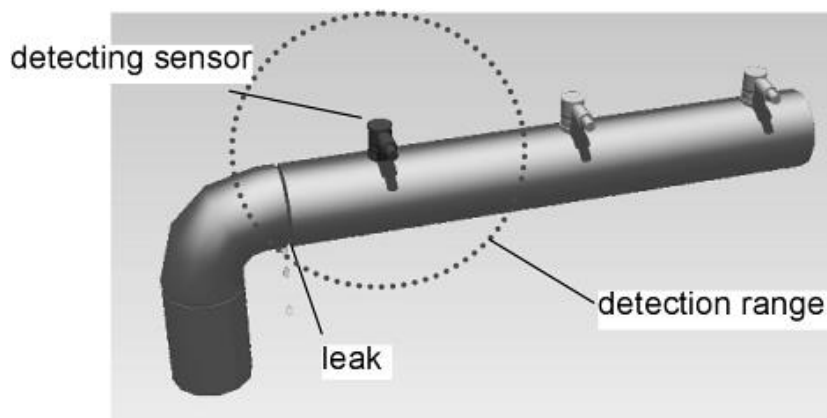


Figure 5-13: Zone location method to monitor leakage in the pipe [80]

5.10 Energy Measurement

AE is effectively a process of energy release in the form of acoustic pulses. There are two parameters commonly used for measuring the acoustic energy emitted;

The first parameter is the root mean square (RMS) value of the output voltage, a relatively simple process without electronic complications. Traditionally this would be done using an RMS voltmeter and the power is proportional to the square of the RMS voltage. Such measurements are very suitable for continuous signals where no threshold voltage is imposed. Background noise, which is generally of constant amplitude, will have an RMS value which remains constant and any variation of the RMS above this value will be indicative of emissions occurring from the material tested.

The second parameter measures the absolute energy. Absolute energy is a measure of the true energy of the AE hit and is derived from the integral of the squared

voltage signal divided by the reference resistance (10 k-ohms) over the duration of the AE signal [85]. The following equation can be used to calculate the AE energy:-

$$\text{AE-Energy} = 1/R \int_0^T v^2(t) dt \quad (5-7)$$

where $v(t)$ is the time dependent voltage from the AE sensor, and T the duration of the entire event over which the integration is performed. This energy is directly proportional to the electrical energy of the AE signal in the measured bandwidth by a constant of system electric impedance [86], which in this instance was 10 k Ω .

The advantage of energy measurement over ring-down counting is that, energy measurement can be directly related to important physical parameters such as deformation mechanisms or impacts without having to model the AE signal. Energy measurement can also improve the AE measurement when emission signal amplitudes are low, as in the case of continuous emission.

5.11 Sources of Acoustic Emission in Process Industries

AE sources vary depending on type of material and in the process industries are classified in two main groups: AE generated from mechanical sources and AE generated from hydraulic sources. Examples of mechanical sources are cracks, friction, impacts and cyclic fatigue such as occurs at heavily stressed spots (e.g. moving parts of gears, bearing, pumps in rotating machinery). Hydraulic sources might include erosion/corrosion in pipes and pipe leakage occurring due to chemical reactions, solid impacts, water-droplets, etc.

As this research is dealing with multiphase fluid flow the AE sources are hydraulic. The main AE sources in multiphase flow are; gas bubble formation and collapse, impacting of solid/droplets on the internal pipe wall and turbulence produced by flow vortices.

5.11.1 AE Generated from Bubbles

The presence of gas bubbles in pipes is a result of gas-liquid mixtures and impacting of droplets on the liquid surface [87]. The initial formation of bubbles (prior to

reaching a state of equilibrium) is accompanied by pressure waves. These waves originate mainly from volumetric bubble oscillations [88]. The oscillatory motion of bubble wall generates acoustic emission [89]. Gas bubbles emit AE because the compressibility of the trapped gas and the mass of the surrounding liquid produce a natural oscillator [90].

In gas-liquid flow in a horizontal pipe, bubbles can be seen in some flow regimes such as dispersed and slug flow. Bubbles in slug flow are large and varied, see Figure 5.14. Slug flow occurs as a result of gradual increase in liquid velocity. Typically, in slug flow a cluster of bubbles coalesce into a single bubble, this might be due to turbulent flow and/or pressure drop [91]. The source of the AE is the dynamic behaviour of the bubbles during formation, oscillation and break-up [90].

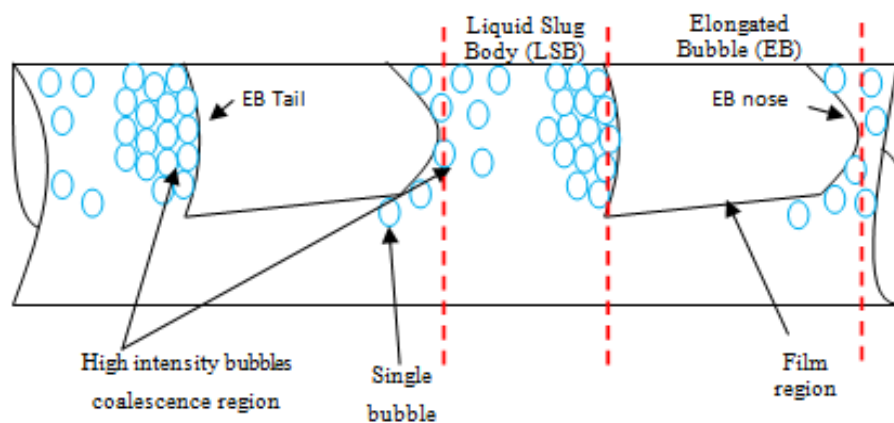


Figure 5-14: Schematic of the bubbles generated in slug flow in a horizontal pipe [69]

Underwater noise is a result of bubble oscillations, where bubble size can determine amplitude and frequency of the signal. Usually a low pressure pulse is generated by bubble oscillations and a higher pressure pulse is generated by bubble coalescence and break-up. High pressure pulses are propagated in the form of shockwaves and can be picked up by AE sensors [92].

Normally, the rate of coalescence and break up is high for elongated bubbles due to the high concentration of bubbles at the nose and tail (see Figure 5.14), which are as result of drag forces [1].

5.11.2 AE Generated from Solid Particle Impacts

In gas-solid flow in horizontal pipes, AE can be generated as a result of particle-particle collision and particle-wall collision. Figure 5-15 shows motion of solid particles in a horizontal pipe.

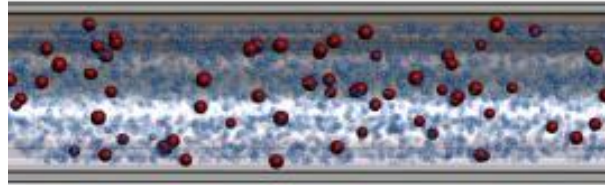


Figure 5-15: Solid particles in horizontal pipe [online source]

The collision/impact of solid particles with the pipe wall will generate AE in the form of elastic waves that propagate through the pipe and can be detected by AE sensors. The other source of AE is particle-particle collision/impact. In this case very low amplitude AE signals may be detected by sensors located on the pipe's surface. The impacts themselves do not often generate a large AE signal and the medium (gas/liquid) between the solid particles and the pipe wall will attenuate those signals. The AE emitted is proportional to the quantity of solid particles injected into a pipe. The increase in the number of solid particles impacting on the pipe's walls results in an increase in number of elastic waves generated. Also, increase in flow rates increases the velocity of solid particles in the stream which increases their kinetic energy and the probability of their hitting the pipe wall, both resulting in an increase of AE signal levels [1, 2, 51, 54].

5.11.3 AE Generated from Turbulent Flow

Typically, fluid generates noise as it flows through a pipe due to such factors as turbulence generated at sharp bends and pressure differentials at valves. Turbulence is described as a flow in which the velocity of the fluid is a random function of position and time and (where) inertia forces are significant [1, 93, 94, 95]. In the case of solid-liquid flow, AE signals generated by turbulence can be differentiated from other AE signals by, for example, first running the liquid without

the solids present. Thus, the AE signals generated by the turbulence can be determined and separated from AE signals generated from solid collisions.

Sound waves generated in a pipe are continuously reflected by the walls so that the sound is guided along its path; hence, a pipe forms an acoustic 'waveguide' [96].

5.12 Advantages and Disadvantages of AE Technology

AE technology like any non-destructive techniques has its own advantages and disadvantages, as listed below.

The most common advantages are:

- The ability to detect and locate defects from only a few static sensor locations. Due to of the relatively low attenuation in the typical AE frequency range (hundreds of kHz), it is possible to detect emissions that originate several meters away from the sensor. This in turn means that an AE test can be quickly set up on site,
- The established link between AE activity and stress intensity such as for high strength materials in which linear elastic fracture mechanics are well defined. AE can locate short critical cracks (i.e. highly stressed regions) around cut-outs or profile changes which are difficult to inspect using, for example, ultrasonic techniques,
- AE is a dynamic inspection method that provides a response to discontinuity growth under an imposed structural stress; static discontinuities will not generate acoustic emission signals,
- AE can detect and evaluate the significance of discontinuities throughout an entire structure during a single test,
- Since only limited access is required, discontinuities may be detected that are inaccessible to the more traditional non-destructive methods,
- Vessels and other pressure systems can often be re-qualified during an in-service inspection that requires little or no downtime,
- The AE method may be used to prevent catastrophic failure of systems with unknown discontinuities and to limit the maximum pressure during containment system tests.

The most common disadvantages are:

- AE waves will be attenuated through the structure under test,
- AE requires professional technicians,
- The assessment provided by AE is qualitative but not quantitative,
- The difficulty in detecting faults not produced in the material, such as imbalance. Static discontinuities will not generate AE signals,
- Due to its low amplitude signals, sensors should be located very close to the source of emission,
- Sources of high frequency signals emitted from nearby electromagnetic and turbulence may disturb the AE.

5.13 Applications of AE Technology

AE technique have been successfully applied to a wide variety of research in civil and industrial fields, these include [1, 37, 68, 88, 97]:

- **Material testing** - such as crack testing of materials, fatigue testing of metals and alloys, and corrosion detection.
- **Chemical and petroleum industries** - such as integrity testing of pressure vessels, spherical tank testing and cryogenic tank testing.
- **Electric and power plant industries** - such as high pressure vessel testing, power plant monitoring and diagnostics.
- **Aircraft and aerospace industries** - such as aircraft proof testing, aircraft ageing tests, fatigue testing of complete structures/aircraft.
- **Civil engineering** – such as structural testing of concrete buildings, bridges, tunnels and dams: continuous surveillance for flaw or crack propagation of structures and cranes.
- **Transportation application** - such as detecting and locating flaws in tube trailers, railroad cars and tank trucks: crack detection in railway tracks and structures.
- **Other application** - such as, pinpointing defects in welds, drought stress monitoring of crops and woods, wear and friction testing, geological and seismological applications, on-line process monitoring of engines and rotating machinery, crack detection in steel rollers, automobile shaft strengthening

process monitoring, casting process monitoring, charge and discharge monitoring of Li/MnO₂ battery cells.

5.14 Methods for Acoustic Emission Signal Analysis

AE signal processing includes time-domain, frequency domain and combined time frequency domain analysis. Recording and analysing of AE signals can be divided into: parameter-based (classical) and signal-base (quantitative) techniques [98].

Parameter-based techniques are where the AE event is recorded and relevant parameters such as duration, amplitude, counts, rise time and absolute energy are extracted from the signal and stored on a PC hard drive. This approach has the advantage of high recording and data storing speeds that facilitates fast visualization of the data. If many signals are recorded and stored, along with their waveforms then this approach has the advantage that comprehensive analysis of the data is possible [98, 99, 100, 101].

Analysis of AE waveform data can be divided into: threshold based and envelope based. In the threshold based approach, a threshold level is pre-set and only signals with an amplitude exceeding the threshold are considered and signals lower than the threshold are considered to be background, see Figure 5.11. The parameters usually extracted are:

AE counts – This hit feature simply counts the waveform signals which exceed the AE threshold.

AE events – AE events and AE counts are operates on the same principle, whereas AE waveform signals are counted.

Threshold envelope analysis is a statistical technique, whereas oscillatory waveform data is analysis. In this technique a modulating function is extracted from an amplitude modulated signal.

An advantage of using signal-based AE analysis is that different post processing analysis methods are available. This software will include advanced mathematical transformations such as the Fast Fourier Transform (FFT) and wavelet transform

(WT) which can be used to extract useful information from the recorded AE waveform [101].

The FFT requires signal information not only in the time domain but also in the frequency domain [102]. The FFT is used to produce a spectrum of the energy which sometimes leads to misinterpretations of the characteristics of the data [103]. In order to overcome the disadvantage of the global nature of the FFT, the Gabor wavelet [101, 104] was developed, this consists of localizing the analysis by selecting a portion of the signal around a specific time position (a time window), conducting the Fourier analysis and then sliding the time window along the signal to its next (adjacent) position and repeating the transform process.

The wavelet transform (WT) is a tool that cuts up data, functions or operators into different frequency components, and then studies each with a resolution matched to its scale [105]. Wavelet transform is a time-frequency analysis using a Gabor wavelet [106]. Unlike the FFT which is localized in the frequency domain but not in the time domain, WT is well localized in both the time (or position) domain and the frequency (or scale) domain. Furthermore, compared with the FFT, a large number of basis functions are available with WT. Thus, it may decompose a signal into its components directly according to the frequency [107]. An example is given in Figure 5.16. With the help of wavelet transform the relationship between time and frequency can be clearly demonstrated in one single diagram.

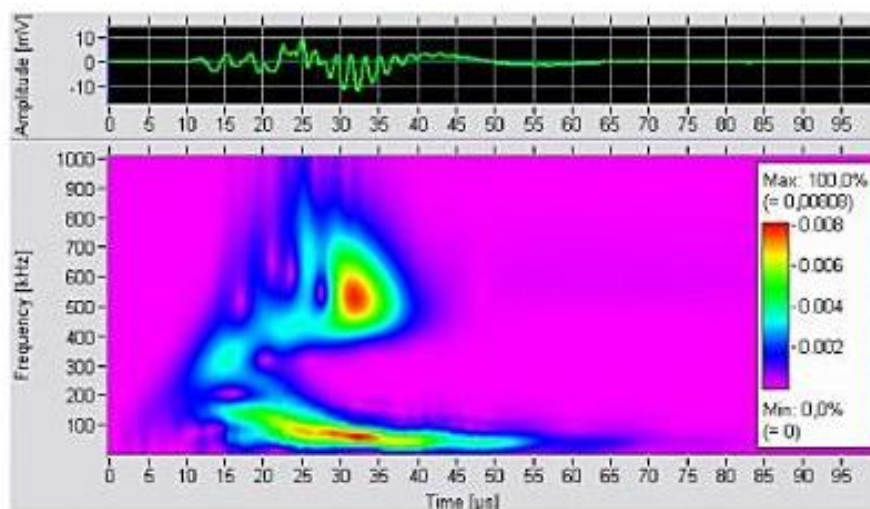


Figure 5-16: Original signal and wavelet analysis of an AE event [120]

Wavelet transforms are a class of a functions used to localize a given function in both space and scaling. The applications of wavelet transform (WT) are expanding. It has been successfully utilized for detection of a signal in low signal to noise applications, such as to analyse the pressure fluctuations in fluidized bed and for studying of transition velocity from bubbling to turbulent fluidization [108, 109, 110, 111].

5.15 Conclusion

The chapter has outlined different aspects regarding Acoustic Emission technology, such as the AE system and its mechanisms. AE advantages and disadvantages are also outlined, and was noted that the AE technology is a robust investigative technique. Thus, AE technique has been employed in different applications, such as crack detection and sand detection at elbows in pipes etc. AE technology has been selected for use in this research to test its capability as an online monitoring tool to detect and quantify the presence of sand particles in multiphase flow in horizontal pipes.

6 Experimental Investigation and Methodology

In this research work five experiments were carried out using acoustic emission technology:

- Assessing the capability of AE technology to detect the sand particles in terms of size and distance,
- Monitoring sand particle characteristics in air-sand two-phase flow,
- Monitoring sand transport characteristics in multiphase flow (air-water-sand flow),
- Identifying the minimum transport condition (MTC) for sand in air-water two-phase flow,
- Monitoring the characteristics of water droplets and water-sand-droplets.

Two different test rigs were used. The initial test investigated the feasibility of AE to detect sand particle impacts on two different types of metal plates, see Figure 6.1. The second to examine multiphase flow in the horizontal section of a closed loop system, see Figures 6.3 and 6.10.

6.1 Initial Test-Rig Design and Layout

This initial experiment was performed to provide a basis for the application of AE technology to detect sand particle impact prior to performing tests in multiphase flow conditions. The schematic diagram of the initial test is shown in Figure 6.1.

The test rig consists of a ruler on which three locations were marked (20 cm, 40 cm and 60 cm) from which the sand particles were dropped. The diameters of sand particles ranged from 150 μm – 710 μm in diameter. Steel and aluminium plates of thickness 1.5 mm were used as targets.

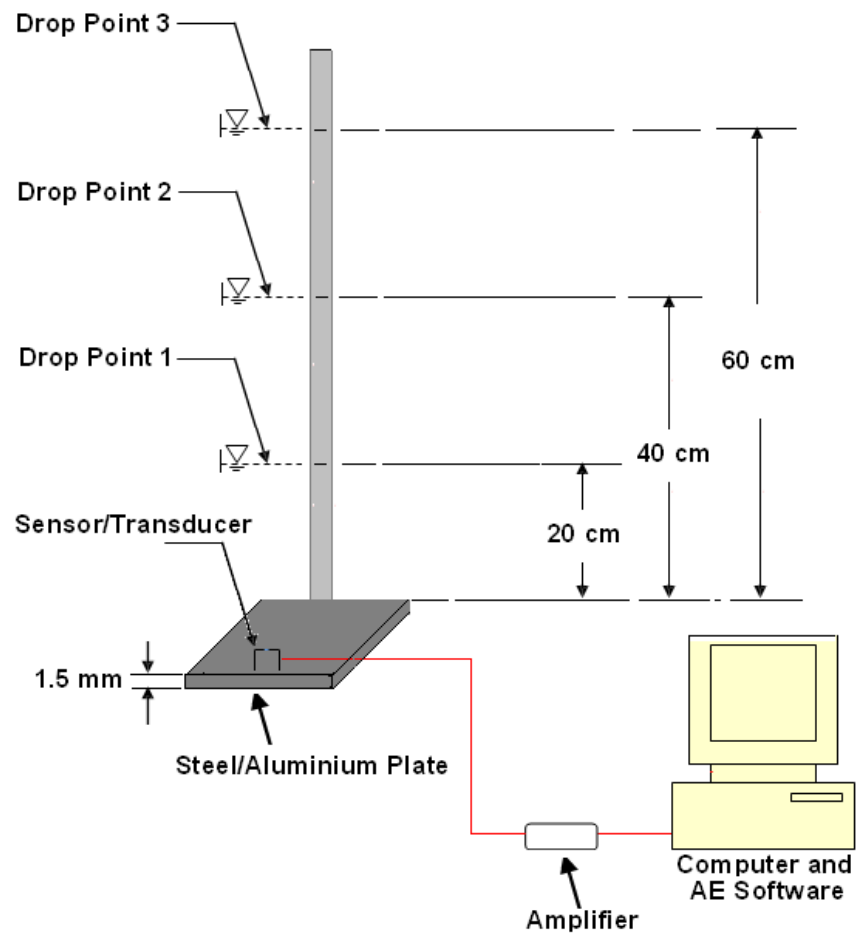


Figure 6-1: Schematic diagram of initial experimental test

6.1.1 Instrumentations and Experimental Setup

AE waves were detected with a calibrated broad bandwidth piezoelectric transducer positioned on the top face of the target plates, see Figure 6.2. The Physical Acoustic Corporation type WD piezoelectric sensor / transducer is 18 mm in diameter and 17 mm high. Wideband sensors had an operating frequency of 100 kHz – 1 MHz. Pre-amplification of 40 dB was used. The sampling rate for acquisition of AE waveform was set at 2 MHz. A threshold level of 30 dB was set for the electronic background noise of the acquisition system.

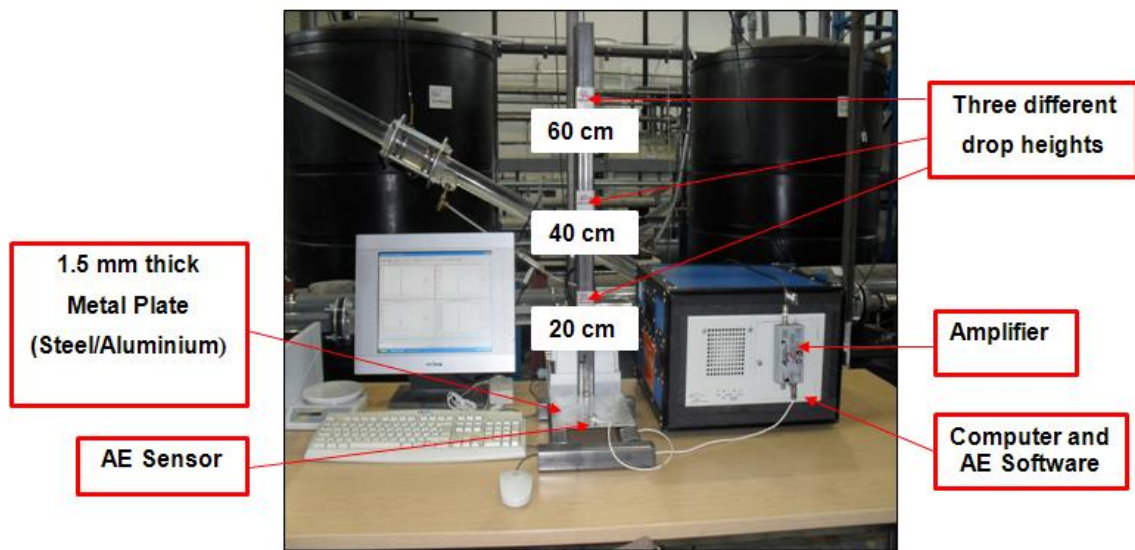


Figure 6-2: Initial experimental test

AE waveforms were obtained from hit driven data which was determined by three timing parameters; the hit definition time (HDT), hit lockout time (HLT) and peak definition time (PDT).

The function of HLT is to eliminate the measurement of reflections and those parts of AE signal arriving late, this enables data from wave arrivals to be acquired at a faster rate. An accurate setting of HLT avoids spurious measurements during signal decay, essentially it defines the period between successive hits.

The function of HDT is to enable the system to determine the end of the hit, close the measurement processes and store the measured attributes of the signal. Accurately setting the value of HDT will ensure that each wave generated from the structure is reported as one hit, as it defines the time-period over which a hit can be acquired.

The function of PDT is to enable determination of the time of the true peak of the AE waveform [77]. Correctly setting the PDT will ensure accurate measurement of peak amplitude.

HLT, HDT, and PDT were set at 500 μ s, 3000 μ s and 500 μ s respectively.

The system was set to continuously acquire AE absolute energy (atto-Joules) over a time constant of 10 ms - a sampling rate of 100 Hz. The absolute energy

is a measure of the true energy and is derived from the integral of the squared voltage signal divided by the reference resistance (10 kΩ) over the duration of the AE signal [85].

$$\text{AE-Energy} = 1/R \int_0^T v^2(t) dt \quad (6-1)$$

where $v(t)$ is the time dependent voltage from the AE sensor and T is the duration of the event over which the integration is performed.

This energy is directly proportional to the electrical energy of the AE signal in the measured bandwidth by a constant ($1/R$) where R is the system electric impedance [86], which in this instance was 10 kΩ.

6.1.2 Experimental Procedure

In this initial investigation, a series of experimental tests were conducted to assess the capability of an AE sensor to detect AE from sand particles impacting on a metal plate. The experimental investigation required recording measured AE energy levels for four different sizes of sand particles in the range 150 μm – 710 μm dropped from three heights (20 cm, 40 cm and 60 cm) onto the target plates (steel/aluminium). The AE Energy levels (atto-Joules) obtained from the AE system resulting from a single sand particle impact, were correlated with size of particles and drop-height, see Figure 6.3. In this experiment, the impact point of the sand particle on the plate was fixed throughout the test-period (in the centre).

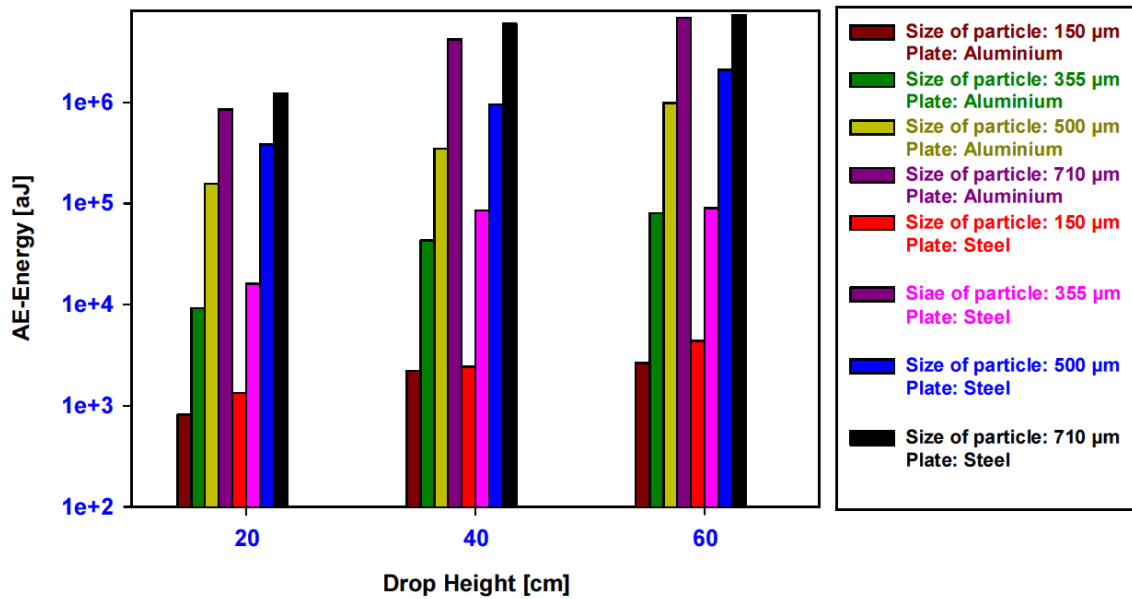


Figure 6-3: AE Energy vs drop height for different size of sand particles

6.1.3 Results of Monitoring

Tables A-1 and A-2 in Appendix A, summarise the experimental measurements. General trend of AE transit signals generated by sand particle of diameter 500 µm dropped from heights of 20 cm and 60 cm onto a 1.5 mm thick steel plate are shown in Figures 6.4 and 6.5, respectively. The waveform results show that a sand particle rebounds after the initial impact with the metal plate which caused many transient/pulse at the waveform (amplitude-time plot).

It can be seen that the maximum amplitude clearly increases with drop-height. At drop-height 20 cm, the peak is at 2 mV, while the maximum amplitude at drop-height 60 cm is 3.5 mV.

The waveform show very distinctive result at different height of the test performed as a result of the height of the rebound particle at drop-height 20 cm is lower compared with the higher drop-height 60 cm.

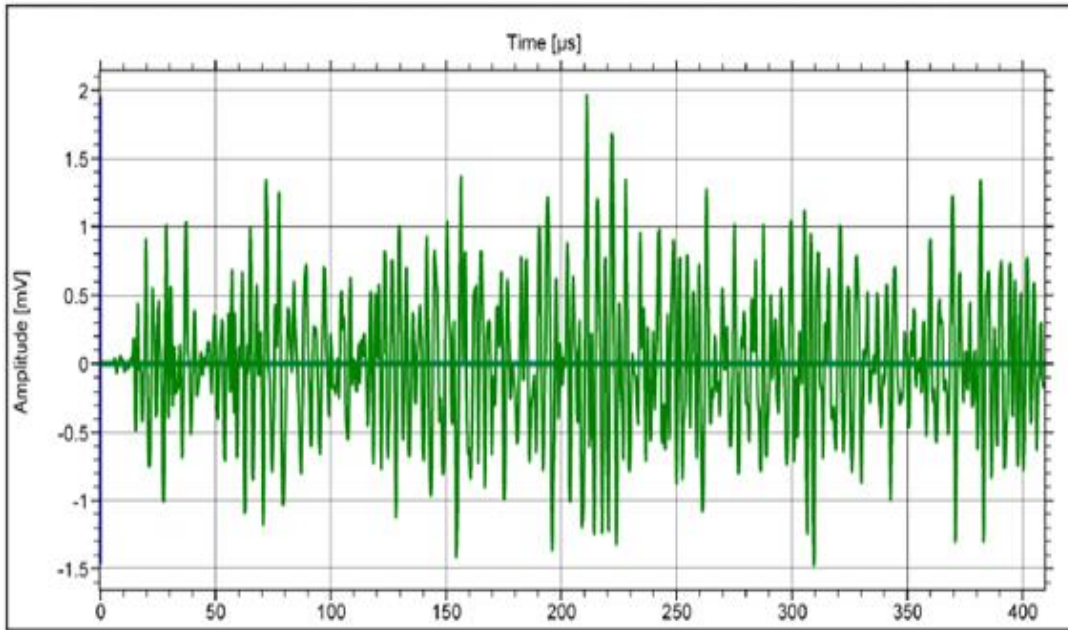


Figure 6-4: Example of AE transient signal from sand particle impact dropped from 20 cm

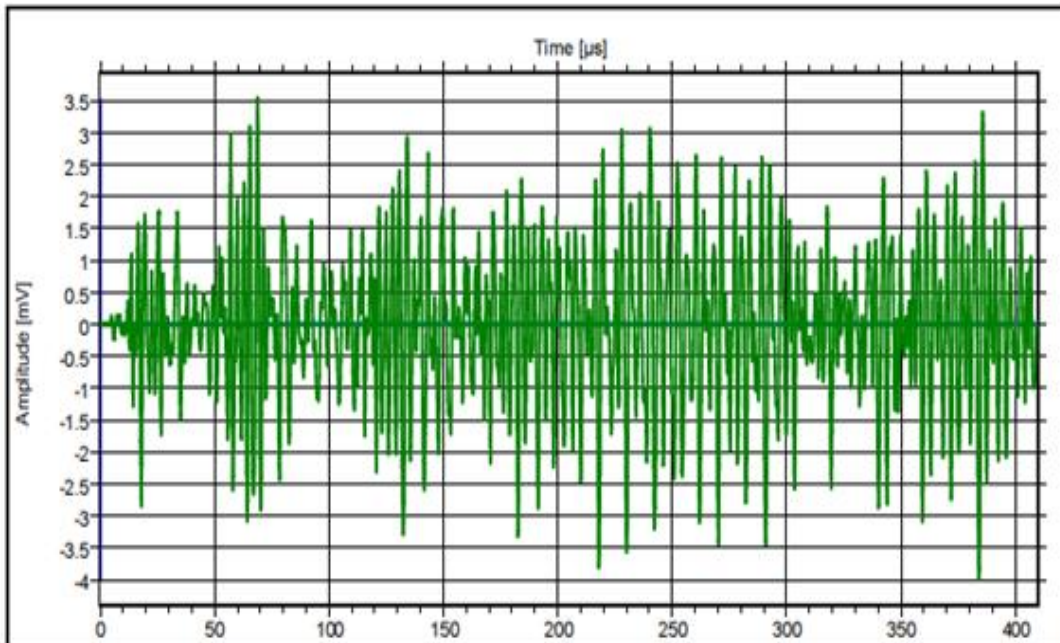


Figure 6-5: Example of AE transient signal from sand particle impact dropped from 60 cm

6.2 Multiphase Flow Test-Rig Design and Layout

Several tests were undertaken using the multiphase facility. Figure 6.6 shows the schematic diagram of the test rig facility built for the experiments. The experimental test rig was constructed using ABS plastic (class E) pipes. The total flow length of the loop is 32 m, with the inner diameter equal to of 50 mm. A steel pipe was inserted in between two Perspex pipes of 50 mm. The Perspex pipe was used for visual observation, whereas steel pipe was used for AE sensor installation. The test rig is equipped with an air supply unit, water supply unit, water-sand mixture supply unit, data acquisition system (DAS) and acoustic emission (AE) system, see Figure 6.7. The use of this equipment's will be discussed in more detail in the following section.

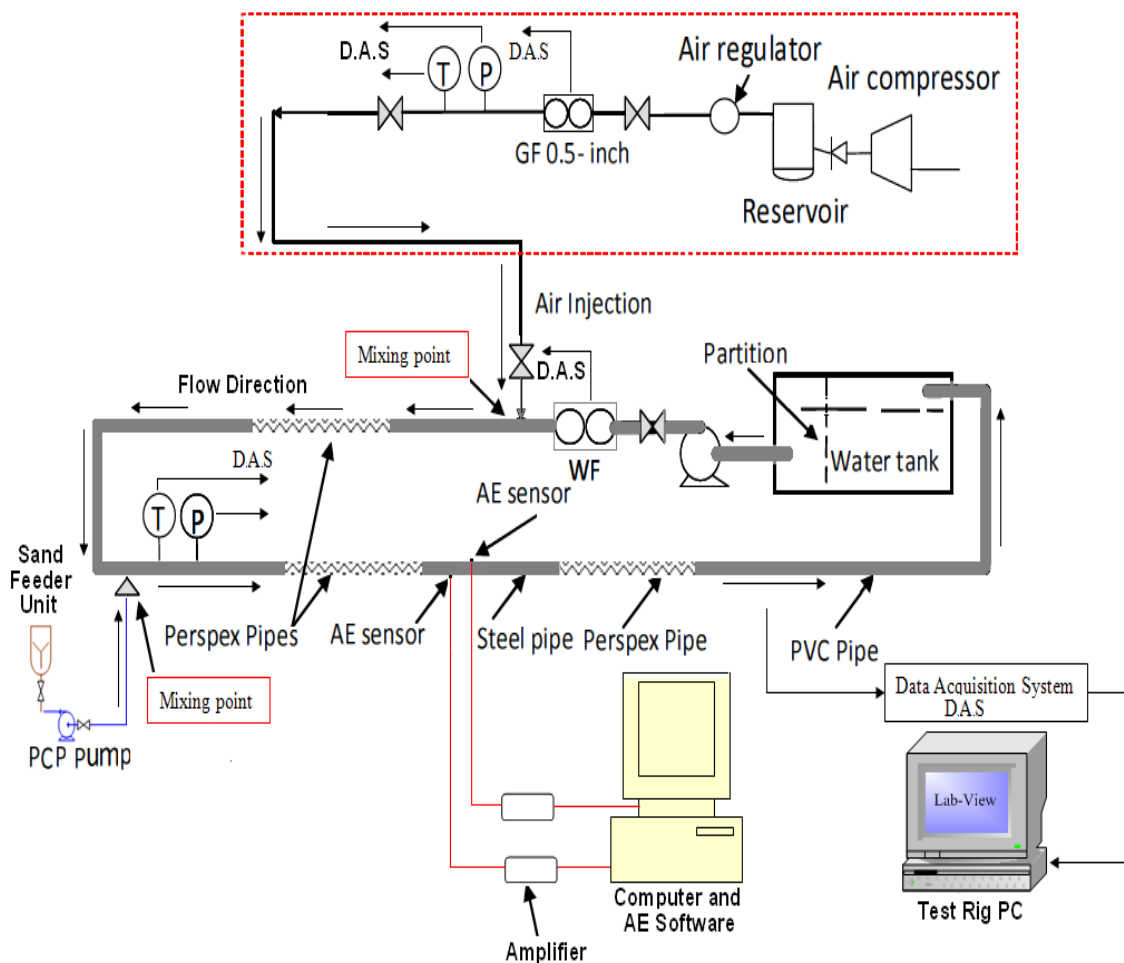


Figure 6-6: Schematic diagram of three-phase flow test facility

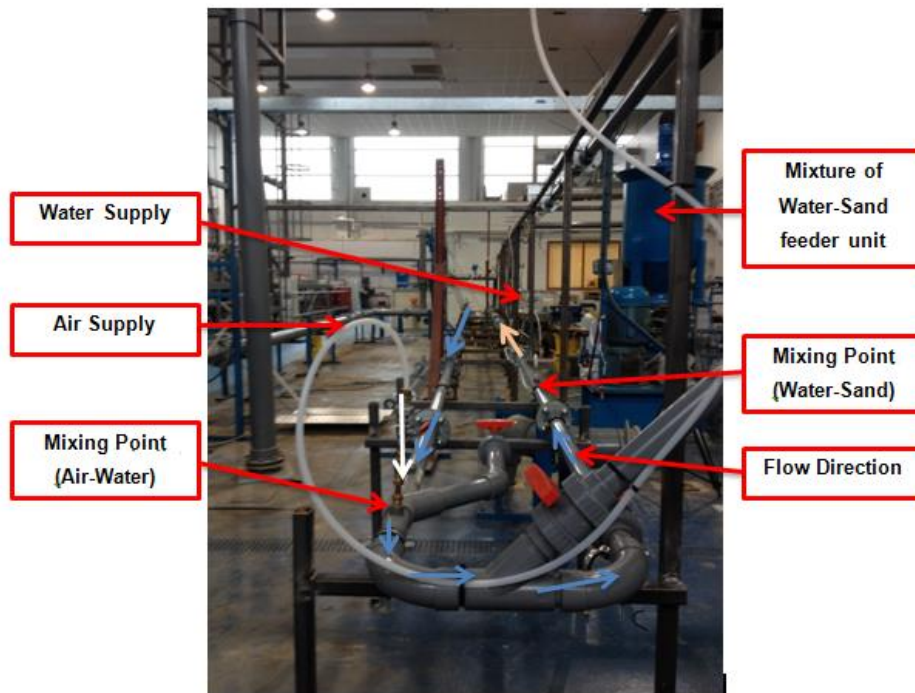


Figure 6-7: Multiphase flow test facility

➤ **Air Supply**

Air was supplied from a screw compressor with a maximum capacity of 400 m³/hr, and a maximum discharge pressure of 10 barg. Air flow was metered using an electromagnetic flow meter (GF) ABB K280/0 AS model with 0 – 20 m³/h range. At the gas metering point, temperature and pressure values were also measured using a thermocouple (T) and a pressure transducer (P), in order to obtain the volumetric flow rate of the gas entering to the test section.

➤ **Water Supply**

The water used in this test experiment is tap water. The water is supplied by a reservoir tank with a capacity of approximately 1500 litres, at atmospheric pressure. Water is circulated in the flow loop using a centrifugal pump with a maximum capacity of 40m³/hr and a maximum discharge pressure of 5 barg (500 kPa) installed at the bottom of the water reservoir tank. The water flow was metered using an electromagnetic flow meter, ABB K280/0 AS model with 0-20 m³/hr range.

➤ Water-Sand Mixture Feeder Unit

The water-sand mixture feeder unit, as seen in Figure 6.8, was installed at the upstream end of the test section. The unit consists of a cylindrical stirred vessel (800 mm diameter and 500 mm high), with a 365 mm diameter axial flow impeller. The mixture is pumped to flow line using variable speed progressive cavity pump (PCP) with capacity of 5 l/m and 5 barg maximum discharge pressure. The mixture of water-sand was injected into the test rig through an injection point installed after the water and air mixing point.

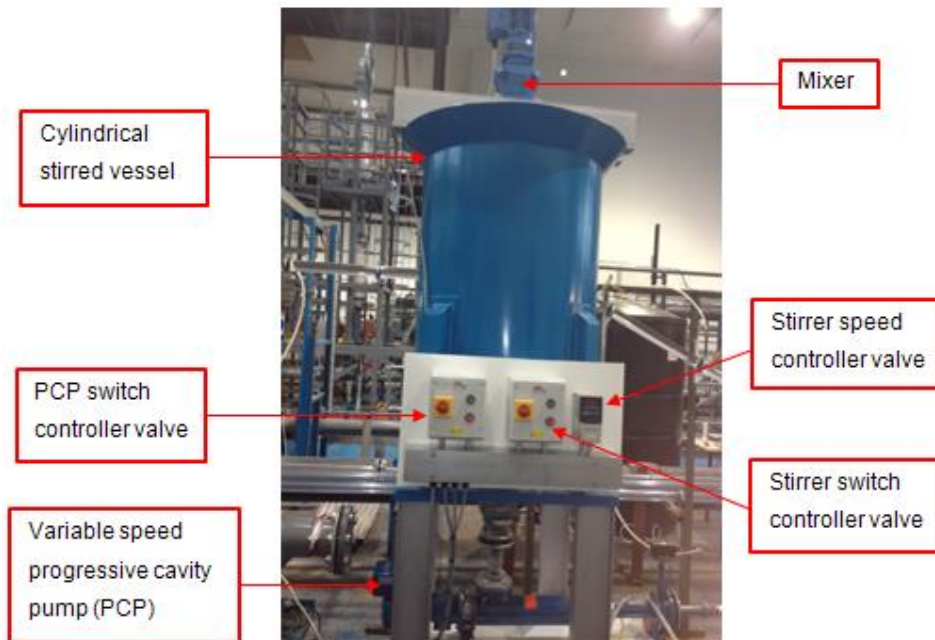


Figure 6-8: Water-Sand mixture feeder unit

The mixture feeder unit is used to supply an homogeneous sand-water mixture flow at atmospheric conditions. The mixture is injected into the flow loop at a speed of 0.128 m/s using a pump. The type of sand used in the test was Congleton HST50 with an average sand particle diameter of 200 μ m and a density of 2650 kg/m³.

➤ Data Acquisition System (DAS)

Data obtained from associated instruments including air volumetric flow rates, water volumetric flow rates, line pressure, differential pressure and temperature were acquired using a DAS consisting of a 16 channel parallel port multiplexer (SCB-68), see Figure 6.9, connected to the PC via an analogue-to-digital converter (ADC) card. The data collected are converted to an appropriate digital signal and displayed on a computer monitor using National Instrument software (Lab-View version 2010).



Figure 6-9: Data acquisition system (channels box)

➤ Acoustic Emission (AE) System

The Physical Acoustic Corporation type WD wideband piezoelectric sensors (see Section 6.1.1) were positioned with one at the top and the other at the bottom of the steel pipe. The acoustic sensors were connected to pre-amplifier set at 40 dB. The AE waveforms were acquired at a sampling rate of 5 MHz for 30 seconds for each superficial gas and water velocity. For the acquisition of traditional AE generated from the flow, the detection threshold was set at 32 dB, approximately 32 dB above background noise. AE streamed waveforms were captured for every crossing of a 32 dB threshold for a duration of 3 seconds throughout the entire test run for all air, water and sand three-phase flows.

AE waveforms were obtained from hit driven data which was determined by hit definition time (HDT) of 60000 μs , hit lockout time (HLT) of 6000 μs and peak definition time (PDT) of 1000 μs .

6.2.1 Monitoring sand transport characteristics in multiphase flow (air-water-sand flow)

The experimental investigation involved the assessment of concentration of sand in three phase flow (air-water-sand) in a horizontal pipe, using a multiphase flow test rig. The sand used in the test was Congleton HST50 with sand particle diameters distributed between 50 μm and 500 μm (average sand particle diameter 200 μm) and mixture density 2650 kg/m^3 . The mass of sand to input in the mixture feeder unit is calculated as follows:

For sand production rate of 300lb/1000bbl, the sand mass fraction is:

$$(300 \text{ lb} * 0.4536) / (1000 \text{ bbl} * 0.159 * 2650 \text{ kg/m}^3) = 3.23\text{E-}04 \text{ kg of sand/ kg of fluid}$$

The liquid mass flow rate for $V_{\text{SL}} = 0.5 \text{ m/sec}$ is:

$$(\pi D^2/4) * V_{\text{SL}} * \rho \text{ (density of water)} \tag{6-2}$$

$$(3.14 * (0.05)^2 / 4) * 0.5 * 1033 = 1.0134 \text{ kg/sec}$$

The sand mass flow rate = sand mass fraction * liquid mass flow rate

$$= 3.23\text{E-}04 * 1.0134 \text{ kg/sec} = 0.0000327 \text{ kg/s}$$

The mixture feeder pump delivers a constant flow rate of 0.128 kg/s

The mass fraction in sand mixture tank = 0.000327 / 0.128

$$= 0.0026 \text{ kg of sand / kg of fluid}$$

For tank of 200 litres in volume or 200 kg of water

The mass of sand to weight = 0.0026 * 200 * 1000 = 520g of sand

The sand concentrations studied are listed in Table 6.1.

Table 6-1: Sand weight of different sand concentrations used in test

Sand concentration (SC) (lb/1000bbl)	Sand volume fraction (C_V) %	Sand weight (g)
300	3.23E-04	520
400	4.31E-04	683
500	5.38E-04	852
600	6.46E-04	1023
700	7.54E-04	1194

The distribution of sand particle sizes for Congleton HST50, used in the tests, is shown in Figure 6.10.

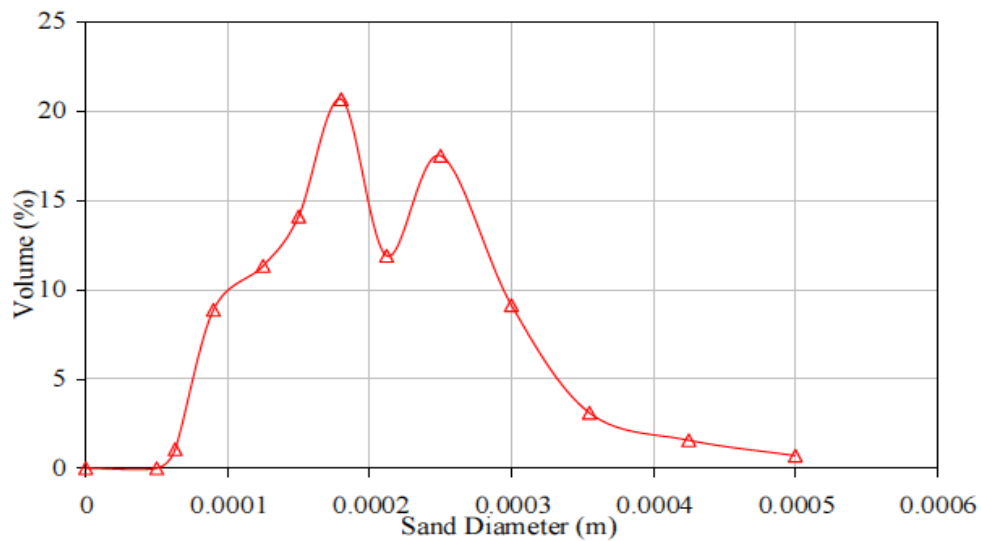


Figure 6-10: Distribution of sand particle diameters in Congleton HST50 sand [51]

6.2.1.1 Experimental Procedure

The experimental investigation assessed the effects of concentrations of sand of 300lb/1000bbl to 700lb/1000bbl at increments of 100lb/1000bbl (equivalent to

0.856 kg/m³ to 1.997 kg/m³ at increments of 0.285 kg/m³) in three phase flow (air-water-sand) in a horizontal pipe. The method was based on recording AE energy levels for each sand concentration at different values of V_{SG} and V_{SL} ranging from 0.2 ms⁻¹ to 2.0 ms⁻¹ and 0.2 ms⁻¹ to 1.0 ms⁻¹, respectively, at increments of 0.1 ms⁻¹. The homogeneous water-sand mixture was fed/injected from the sand-water mixture unit into the flow pipe at a speed of 0.128 ms⁻¹. The flow regimes are defined in Table 6.2

The influence of segregated and intermittent flow regimes on sand transport were studied by monitoring the corresponding AE energy levels generated. Figure 6.11 shows the test section with the location of AE sensors. Only the bottom sensor was used in this test.

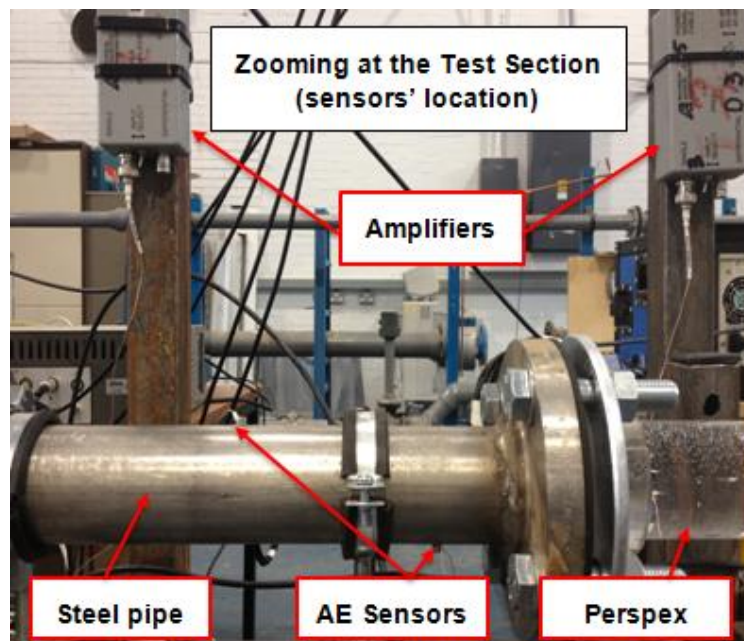


Figure 6-11: Test section for three-phase flow

6.2.1.2 Results of Monitoring

One hundred and fifty tests were conducted. For each test the V_{SG} was fixed and the V_{SL} varied. For instance with V_{SG} = 0.2 ms⁻¹, and V_{SL} was varied from 0.2 ms⁻¹ to 1.0 ms⁻¹ at increments of 0.1 ms⁻¹. The first twenty five tests were conducted without sand, after which five different sand concentrations as described above were used sequentially. Table B-1 in Appendix B summarises

the experimental measurements. The AE Energy levels (atto-Joules) obtained from the AE system for different sand concentrations were plotted as functions of VSL and VSG, see Figure 6.12. The remainder of Figures are in Appendix B.

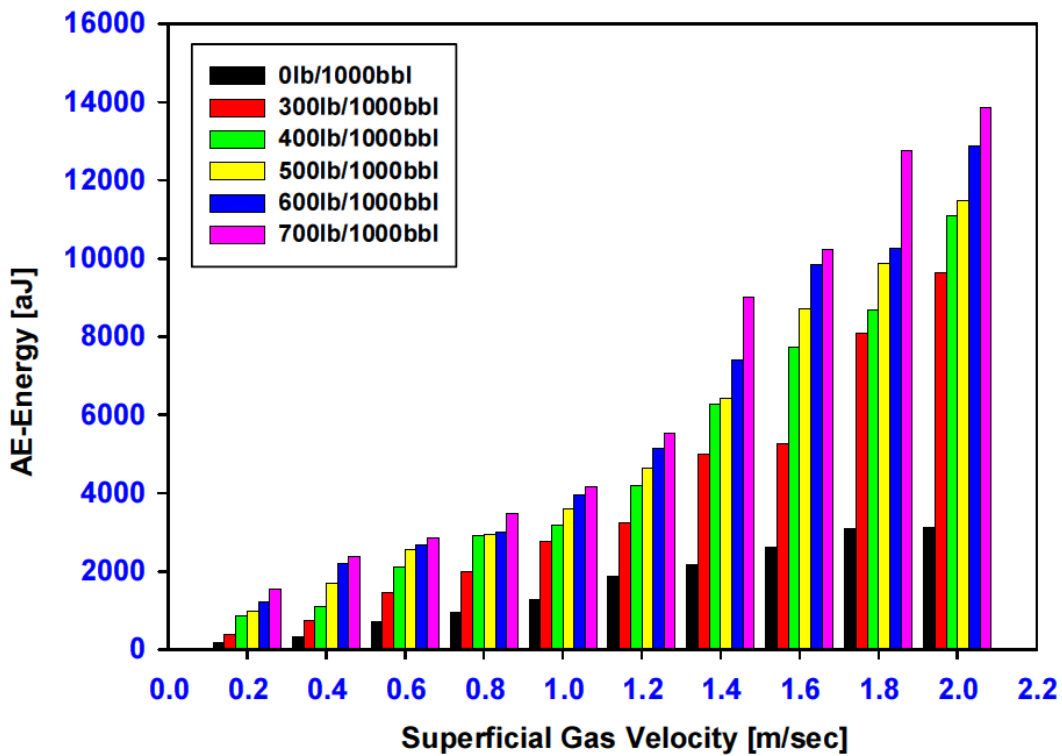


Figure 6-12: AE Energy VS Superficial Gas Velocity (Vsg) for Different Sand Concentration and fixed Superficial Liquid Velocity (Vsl) of 0.2 ms⁻¹

The influence of a segregated flow regime (stratified and stratified-wavy flow) and an intermittent flow regime (plug and slug flow) on sand transport was studied using the same range sand concentrations as in Section 6.2.1.1. Table 6.2 summarises the experimental measurements. AE Energy levels (atto-Joules) obtained from the AE system of different sand concentrations were correlated to the VSL and VSG, see Figures 7.19, 7.20 and 7.21, chapter 7.

Table 6-2: AE-Energy levels as a function of sand concentration for different flow regimes

Sand Concentration (SC) (lb/1000bbl)	Flow Regime	AE-Energy (atto-Joules)
0lb/1000bbl	Stratified Flow	181.00
	Stratified-Wavy Flow	1283.00
	Plug Flow	1380.00
	Slug Flow	2096.00
300lb/1000bbl	Stratified Flow	372.00
	Stratified-Wavy Flow	2766.00
	Plug Flow	3982.00
	Slug Flow	6818.00
400lb/1000bbl	Stratified Flow	876.00
	Stratified-Wavy Flow	3180.00
	Plug Flow	4311.00
	Slug Flow	9327.00
500lb/1000bbl	Stratified Flow	989.00
	Stratified-Wavy Flow	3609.00
	Plug Flow	4459.00
	Slug Flow	11632.00
600lb/1000bbl	Stratified Flow	1202.00
	Stratified-Wavy Flow	3946.00
	Plug Flow	8344.00
	Slug Flow	17939.00
700lb/1000bbl	Stratified Flow	1540.00
	Stratified-Wavy Flow	4162.00
	Plug Flow	8532.00
	Slug Flow	19896.00

6.2.2 Identification of Minimum Transport Condition (MTC) for Sand in Sand-Water Two-Phase Flow

This experiment used the multiphase flow facility shown in Figures 6.6 and 6.7. Only one broadband Physical Acoustic Corporation AE sensor type WD was used. This was located at the bottom of the steel pipe test section, see Figure 6.13. The sensor had a pre-amplification of 40 dB. The sampling rate for acquisition of AE waveforms was 5 MHz for 30 seconds for each superficial water velocity. AE streamed waveforms were captured for every crossing of a

32 dB threshold level above the electronic background noise for a duration of 3 seconds throughout the entire test run for all water and sand two-phase flow.

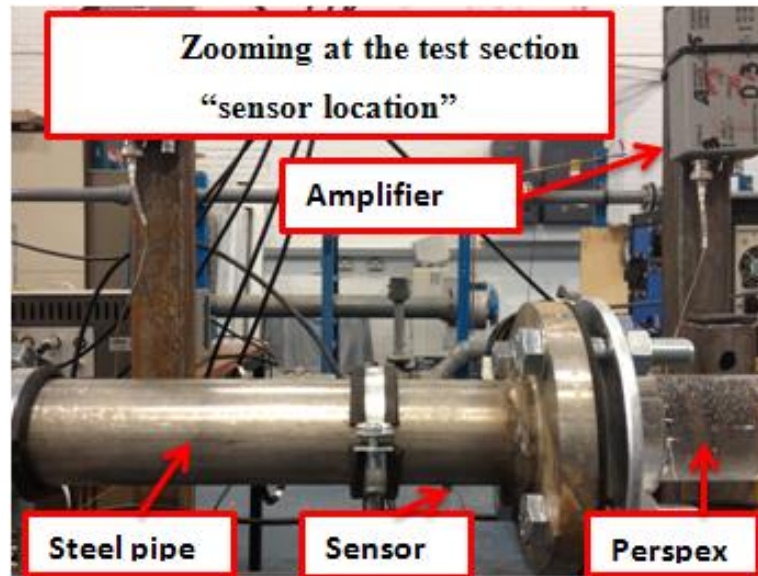


Figure 6-13 Test section for two-phase flow

As previously the homogeneous water-sand mixture was fed/injected from the sand-water mixture unit into the flow pipe at a speed of 0.128 ms^{-1} .

6.2.2.1 Results of Monitoring

The experimental investigation used the same sand concentrations as previously, see Section 6.2.1.1, under two-phase flow conditions (sand-water) to monitor sand transport characteristics and identify sand MTC. The V_{SL} used was varied from, 0.1 ms^{-1} to 1.2 ms^{-1} in increments of 0.1 ms^{-1} . Visual observations for varied V_{SL} ranging from 0.1 ms^{-1} to 1.0 ms^{-1} at increments of 0.1 ms^{-1} for different sand concentrations are presented in Appendix C. The measured AE Energy levels (atto-Joules) for the different sand concentrations are presented as functions of slug velocity (V_s), V_{SL} and MTC, see Figures 7.22, 7.23 and 7.24, chapter 7. Tables 6.3 and 6.4 summarise the experimental measurements.

Table 6-3: AE-Energy against VSL for a range of sand concentration

VSL (ms ⁻¹)	AE-Energy (atto-Joules) (SC=0lb/1000bbl)	AE-Energy (atto-Joules) (SC=300lb/1000bbl)	AE-Energy (atto-Joules) (SC =400lb/1000bbl)	AE-Energy (atto-Joules) (SC =500lb/1000bbl)	AE-Energy (atto-Joules) (SC =600lb/1000bbl)	AE-Energy (atto-Joules) (SC =700lb/1000bbl)
0.1	3.14	30.65	49.10	76.24	80.21	84.85
0.2	6.30	47.57	63.48	78.85	80.89	85.27
0.3	6.92	84.54	85.62	88.94	90.46	97.62
0.4	7.20	205.22	298.98	316.24	346.08	759.10
0.5	7.47	609.67	731.99	707.79	948.21	858.02
0.6	7.50	1280.86	829.45	910.78	2467.73	1176.73
0.7	7.53	809.98	1795.46	1880.76	2850.07	3106.48
0.8	7.59	756.66	841.44	2691.40	3157.01	3680.50
0.9	7.93	419.34	444.52	501.23	5043.39	4041.45
1.0	8.29	262.24	327.08	378.52	841.48	5553.03
1.1	8.30	205.22	214.06	241.03	596.39	622.43
1.2	8.72	100.73	102.68	129.33	572.01	597.63

Table 6-4: Sand minimum transport velocity (V_{MTC}) for a range of sand concentrations

Sand Concentration (SC) (lb/1000bbl)	V_{MTC} (ms^{-1})
300	0.70
400	0.80
500	0.90
600	1.0
700	1.10

6.2.3 Monitoring Sand Particle Characteristics in Air-Sand Two-Phase Flow

The same basic two-phase facility described in Section 6.2 was modified as shown Figure 6.14, to assess the effects of sand concentrations in the range from 0.1 g to 1.0 g in increments of 0.1 g. The total flow length of the loop is 22 m, with the inner diameter equal to 0.05 m. The sand was injected at the same point as previously.

The AE sensor used in this test was a Pico sensor 5 mm in diameter, 4 mm in high and with a frequency range of 100 kHz – 750 kHz. Two AE sensors are used, one positioned at the top and the other one at the bottom of the steel pipe, see Figure 6.15. The sensors had a pre-amplification of 40 dB. The sampling rate for acquisition of AE waveform was set at 2 MHz for 30 seconds for each superficial gas velocity. AE streamed waveforms were captured for every crossing of a threshold level of 30 dB above electronic background noise for a duration of 1 second throughout the entire test run for all air and sand two-phase flow.

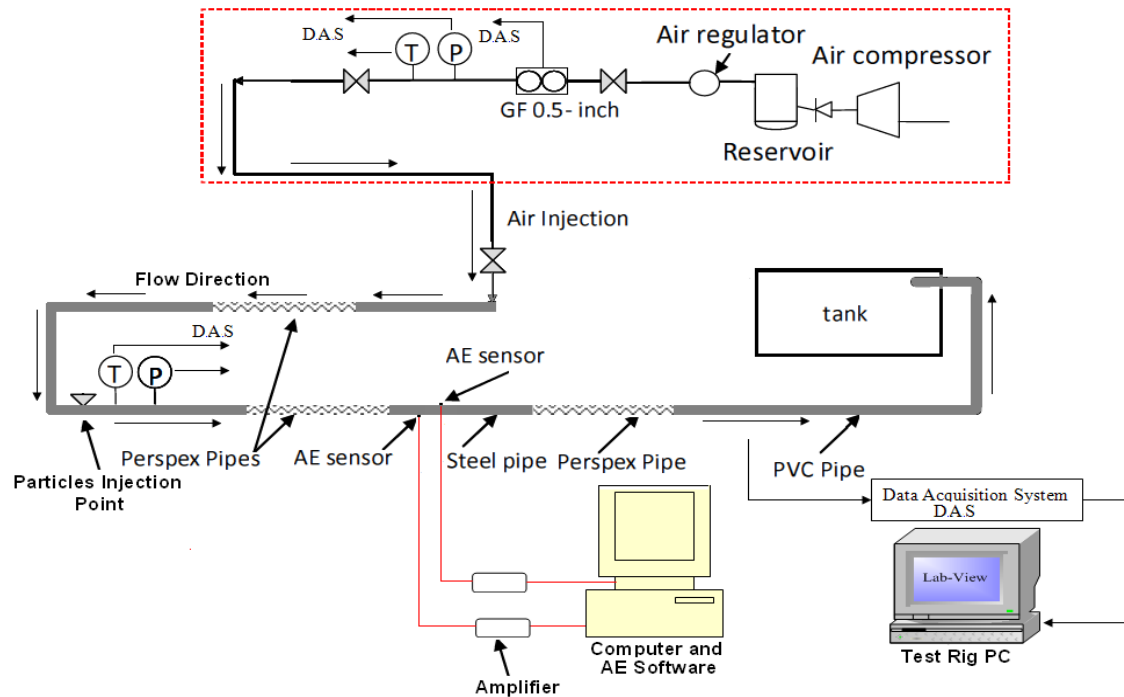


Figure 6-14: Schematic diagram of two-phase flow test facility

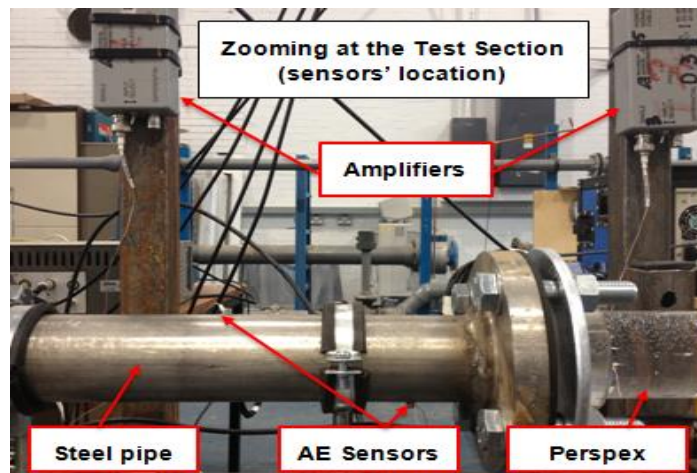


Figure 6-15: Test section of air-sand two-phase flow facility

AE waveforms were obtained from hit driven data for which HLT, HDT, and PDT were set at 500 μ s, 3000 μ s and 500 μ s respectively.

6.2.3.1 Results of Monitoring

The experimental method was based on record of AE energy levels for each quantity of sand at five gas flow rates. Fifty tests were conducted, each test involve on assessing the concentration of sand range from 0.1 g to 1.0 g at increments of 0.1 g

fed/injected into the pipe at selected VSG values (8 ms^{-1} , 9 ms^{-1} , 10 ms^{-1} , 11 ms^{-1} and 12 ms^{-1}). The results of AE Energy levels (atto-Joules) obtained from the AE system on different quantities of injected sand were correlated to the VSG and quantity of sand, see Figure 6.16. Table 6.5 summarises the experimental measurements.

Table 6-5: Experimental measurements AE – Energy for air-sand two-phase flow

Quantity of sand (gram)	AE-Energy atto-Joules ($V_{SG} = 8 \text{ ms}^{-1}$)	AE-Energy atto-Joules ($V_{SG} = 9 \text{ ms}^{-1}$)	AE-Energy atto-Joules ($V_{SG} = 10 \text{ ms}^{-1}$)	AE-Energy atto-Joules ($V_{SG} = 11 \text{ ms}^{-1}$)	AE-Energy atto-Joules ($V_{SG} = 12 \text{ ms}^{-1}$)
0.1	1378.68	1947.85	7091.41	9005.65	16593.66
0.2	2160.74	2904.70	13415.26	15666.74	19459.97
0.3	2214.55	9429.17	14196.23	16134.11	21649.22
0.4	3435.84	9795.30	16123.08	19400.56	26985.87
0.5	5331.89	21730.08	36760.00	43715.72	50152.13
0.6	10239.67	30665.75	39601.91	49459.08	51386.12
0.7	11545.98	33095.72	42308.90	52423.11	58416.77
0.8	18061.86	37583.33	44080.75	60682.31	84832.99
0.9	21556.81	39016.82	52131.31	85214.49	118817.80
1.0	42469.23	56969.97	72632.75	116994.28	141575.97

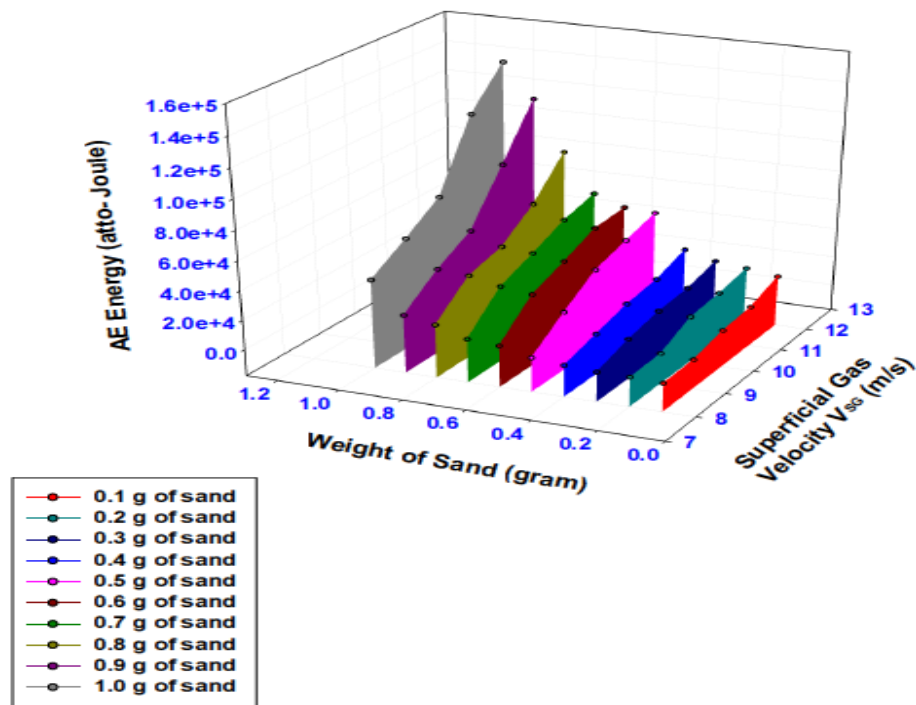


Figure 6-16: AE energy levels as a function of VSG for a range of sand injection rates

6.2.4 Monitoring the Presence of Droplets in a Horizontal Pipe

AE measurements can also be used to assess the effect of the presence of droplets in flow in horizontal pipes. To accomplish this, the two-phase flow facility, shown in Figures 6.14 was re-arranged slightly. The test section was re-positioned about 30 cm downstream of the droplet injection point as shown in Figure 6.17. The flow was considered to be fully developed by the time it reached this section. The injection point is the position where a stream of droplets is continuously fed into the flow loop. Acoustic Emissions were detected using a Physical Acoustic Corporation type WD piezoelectric transducer located at the bottom and top of the steel pipe test section. The acoustic sensor was connected to the DAS via a preamplifier, set at 40 dB gain. The system was set to acquire AE waveforms at a sampling rate of 2 MHz for 30 seconds for each superficial gas velocity. AE streamed waveforms were captured for every crossing of a threshold level of 30 dB t above the electronic background noise for a duration of 3 seconds throughout the entire test run for all air and droplet two-phase flow.

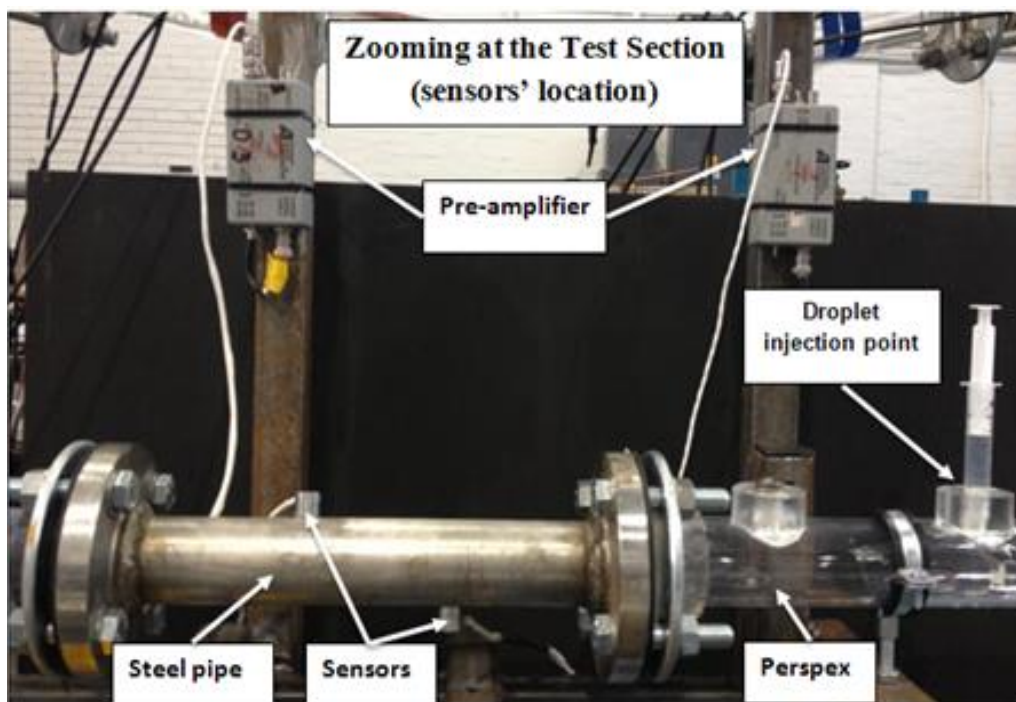


Figure 6-17: Test section of two-phase flow

AE waveforms were obtained from hit driven data where HLT, HDT, and PDT were again set at 500 μ s, 3000 μ s and 500 μ s respectively.

6.2.4.1 Results of Monitoring

The experimental investigation assessed the ability of the AE technology to detect the presence of droplets of volumes ranging from 1 ml to 5 ml in a horizontal pipe within a V_{SG} of between 9 ms^{-1} and 11 ms^{-1} . The number of droplets for 1 ml, 3 ml, and 5 ml was 14 ± 1 , 39 ± 2 and 67 ± 3 respectively. The diameter of the droplet was taken to be the diameter of the injection nozzle. The first type of droplet consisted of water only and the second type was a homogeneous mixture of water and sand produced by mixing 2 grams of sand in 10 ml of water. Eighteen tests were conducted the first nine tests assessed the three different volumes of water droplets at selected V_{SG} , whereas the other nine tests assessed water-sand droplets. The results of AE Energy levels (atto-Joules) obtained from the AE system for the range of injected droplet volumes were correlated to the V_{SG} and total droplet volume, see Figures 7.25, 7.26, 7.27 and 7.28, chapter 7. Tables 6.6 and 6.7 summarise the experimental measurements.

Table 6-6: AE-Energy as a function of V_{SG} for a range of droplet volumes (water & water-sand droplets) captured at bottom sensor

Droplet Type	Droplet volume (ml)	AE-Energy (atto-Joules) ($V_{SG} = 9 \text{ ms}^{-1}$)	AE-Energy (atto-Joules) ($V_{SG} = 10 \text{ ms}^{-1}$)	AE-Energy (atto-Joules) ($V_{SG} = 11 \text{ ms}^{-1}$)
Water-Droplet	1	12.54	30.65	32.52
	3	30.30	49.42	50.67
	5	44.40	54.40	64.27
Water-Sand-Droplet	1	159.24	253.90	958.06
	3	764.75	1926.84	3048.06
	5	1223.20	3510.09	6905.63

Table 6-7: AE-Energy as a function of V_{SG} for a range of droplet volumes (water & water-sand droplets) captured at top sensor

Droplet Type	Droplet volume (ml)	AE-Energy (atto-Joules) ($V_{SG} = 9 \text{ ms}^{-1}$)	AE-Energy (atto-Joules) ($V_{SG} = 10 \text{ ms}^{-1}$)	AE-Energy (atto-Joules) ($V_{SG} = 11 \text{ ms}^{-1}$)
Water-Droplet	1	10.36	110.86	471.60
	3	18.03	486.16	784.74
	5	25.70	767.50	1226.02
Water-Sand-Droplet	1	122.92	199.15	522.74
	3	366.25	583.98	921.00
	5	464.17	863.04	1252.71

6.3 Conclusion

This chapter has discussed the test rig and various components used for conditioning the flow and recording experimental measurements. Experiments have been carried out using acoustic emission technology to assessing the capability of AE technology to detect the sand particles in terms of size and distance, monitoring sand particle characteristics in air-sand two-phase flow, monitoring sand transport characteristics in multiphase flow (air-water-sand flow), identifying the minimum transport condition (MTC) for sand in air-water two-phase flow and monitoring the characteristics of water droplets and water-sand-droplets.

7 Analysis and Discussion

The experimental set up and methodology were discussed in the chapter six, whereas this chapter discusses the results of five experiments that have been carried out in order to monitor the sand particle/sand concentrations in multiphase flow in horizontal pipes. The monitoring of sand concentration is based on the ultrasound signals emitted from the sand particles impacted the inside of the pipe wall. The ultrasound signal is transmitted through the pipe wall and picked by the AE sensor. The signal is amplified and filtered and then processed internally by the AEWIN version 3.2 software package from physical Acoustic Corporation. The software can be used to record the AE parameters such as AE amplitude (dB), AE duration, AE absolute energy (atto-Joules) and AE rise time at a maximum sampling rate of 5 MHz. The sensitivity of these parameters was established in most dated research work. In this particular research project, the trend of AE energy generated by the particles/solids impact the inside of the pipe wall was studied. The reason behind this selection was attributed to relatively higher sensitivity observed in AE energy levels, due to the variation of flow rates and sand concentration used in tests, comparing to the other AE parameters. The following sections discuss results that have been achieved in monitoring sand particles/sand concentrations in air-sand, air-water-sand, air-water and air-droplet flows.

7.1 Sand Particle Impact Test

This initial experiment was performed to provide a basis for the application of AE technology to detect sand particle impact prior to tests in multiphase flow conditions. The experiment set up was outlined in previous chapter, see section 6.1. Tables A-1 and A-2 in Appendix A, summarise the experimental measurements.

Sand particles of sizes ranging from 150 μm – 710 μm in diameter, were dropped from a height of 20 cm – 60 cm onto the target plates. The waveforms obtained due to the impact of 500 μm diameter sand particles dropped from a height of 20 cm onto a 1.5 mm thick steel plate were recorded, and a typical AE time domain waveform is

shown in Figure 7.1 (top). A corresponding Gabor wavelet was generated, and can be seen in Figure 7.1(bottom). The wavelet shows the intensity of the AE waveform at each frequency over the duration of the signal.

Observations of the AE waveforms in Figures 7.1 and 7.2 showed the first 50- μ s to be associated with the initial impact of the sand particle on the steel plate. Thereafter, the sensor measured AE reflections from the edges of the plate and the secondary impacts of the sand particle on the plate. The corresponding time-frequency plot obtained from AE waveform data, as shown at the bottom of Figures 7.1 and 7.2, shows high frequency content at various time locations. The waveforms show distinctive results for each different height test performed, where the maximum amplitude of the waveform for drop height of 60 cm was greatest. Similar results were obtained for the aluminium plate.

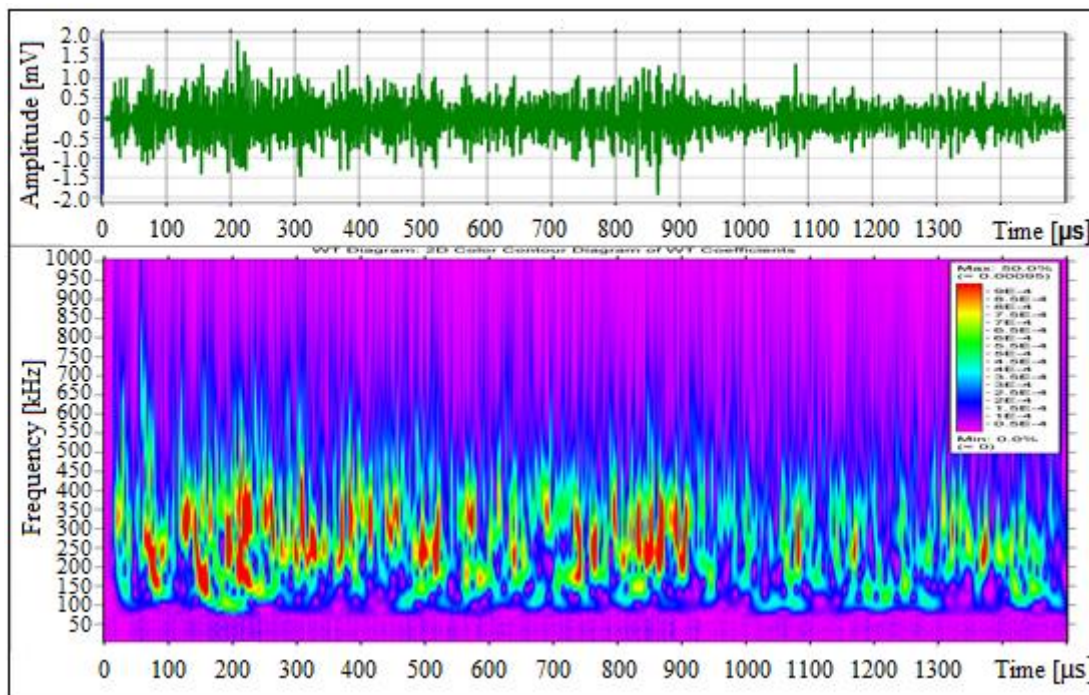


Figure 7-1: Time domain (top) and time frequency (bottom) plots for single sand Particle of 500 μ m in diameter dropped onto a 1.5 mm thickness steel plate from a height of 20 cm.

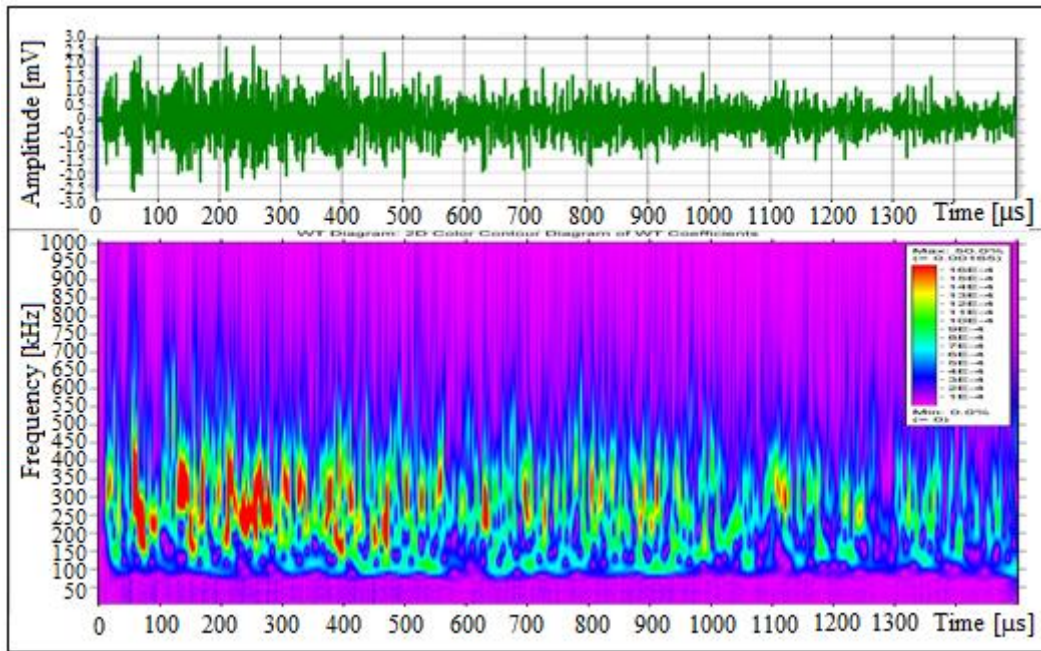


Figure 7-2: Time domain (top) and time frequency (bottom) plots for single sand particle of 500 μm in diameter dropped onto a 1.5 mm thickness steel plate from a height of 60 cm.

It is well known that, when a solid particle impacts onto a metal plate, it produces an elastic waves that propagates away from the target site [54], and can be detected by an appropriate sensor. These waves contain frequencies that range from just over 0.1 Hz to several MHz, however, the measurements of AE are restricted to between 100 kHz – 1 MHz. Observation of Figures 7.1 and 7.2, reveals that the sand particle impact excited a broad frequency range covering 100 kHz to 700 kHz, with the dominant range between 100 kHz to 400 kHz. Also, interestingly, the time-frequency map associate with the initial impact ($< 50 \mu\text{s}$) shows remarkable similarity in the distribution of frequency intensity irrespective of drop height. Figure 7.3 shows that the AE absolute energy was influenced by the size of particle and drop height. AE energy levels increased with an increase of size of particles and drop height, with the steel plate demonstrating more AE energy levels for each impact. This was to be expected given the propagation of the elastic waves is significantly influenced by material properties such as elastic modules and damping.

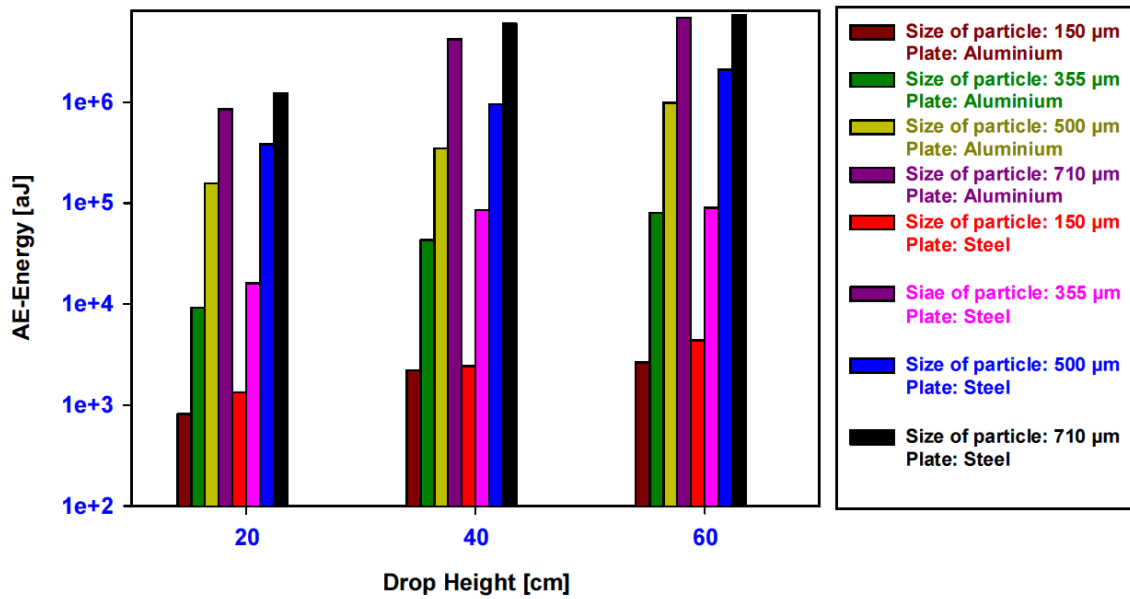


Figure 7-3: AE Energy vs drop height for different size of sand particles

On average the AE energy levels were higher on the steel plate in comparison to the aluminium plate. Also for a fixed drop height, an incremental increase in particle size resulted in between 84% to 96% increase in AE energy for both Steel and Aluminium plates, see Table 7.1. The standard deviation was 0.05% on average.

Table 7-1: AE energy change in % for different sand sizes for a fixed drop height

Drop height (cm)	Size of sand particles (μm)							
	Aluminium Plate				Steel Plate			
	150 μm	355μm	500 μm	710μm	150μm	355μm	500 μm	710μm
20	-	-	-	-	-	-	-	-
40	-	95 %	90 %	93 %	-	94 %	85 %	91 %
60	-	95 %	88 %	94 %	-	96 %	91 %	84 %
Avg.	-	95 %	89 %	93.5 %	-	95 %	88 %	87.5 %

7.2 Two-Phase Flow Test

For experimental set up and method, see section 6.3. These experiments were conducted with different quantities of sand (0.1 g to 1.0 g at increments of 0.1 g). The sand was fed/injected into the pipe at selected V_{SG} values (8 ms^{-1} , 9 ms^{-1} , 10 ms^{-1} , 11 ms^{-1} and 12 ms^{-1}). Table 6-5 in chapter 6, summarise the experimental measurements.

In gas-solid flows, the flow regime depends not only on the initial conditions and physical boundaries of the flow system but also on the mechanisms of momentum transfer or the interacting forces between the phases. The flow regimes of gas-solid phases in horizontal pipes include homogeneous, dune, slug and packed bed flows [8]. Under this two-phase condition forces controlling the motions of particles may be classified into three groups: (1) forces of the interface between the fluid and particles; (2) forces due to the interactions between particles; and (3) forces imposed by external fields [86]. As such this implies that three basic sources of acoustic emissions (AEs) include particle-particle collision, particle-wall collision, and, air turbulence. The only AE source considered in this work is particle-wall collision/impact, as signals generated from the other sources were assumed to be insignificant. For instance, AE generated from particle-particle collision/impact within the pipe will not be detectable by an AE sensor located on the pipe wall due to attenuation of the air medium between the source and the sensor on the pipe.

Typical AE waveforms for a 0.2 g and 1.0 g of sand at V_{SG} of 11 ms^{-1} are shown in Figures 7.4 and 7.5. These time domain waveforms show that the AE transient events observed were so closely coupled as to be of a continuous nature. The authors attribute this to multiple impacts resulting in significantly more AE energy accumulated over a wider frequency range. The time-frequency plots (Figures 7.4 and 7.5), for sand impacts on the pipe was different for the two cases, both in terms of intensity and frequency range.

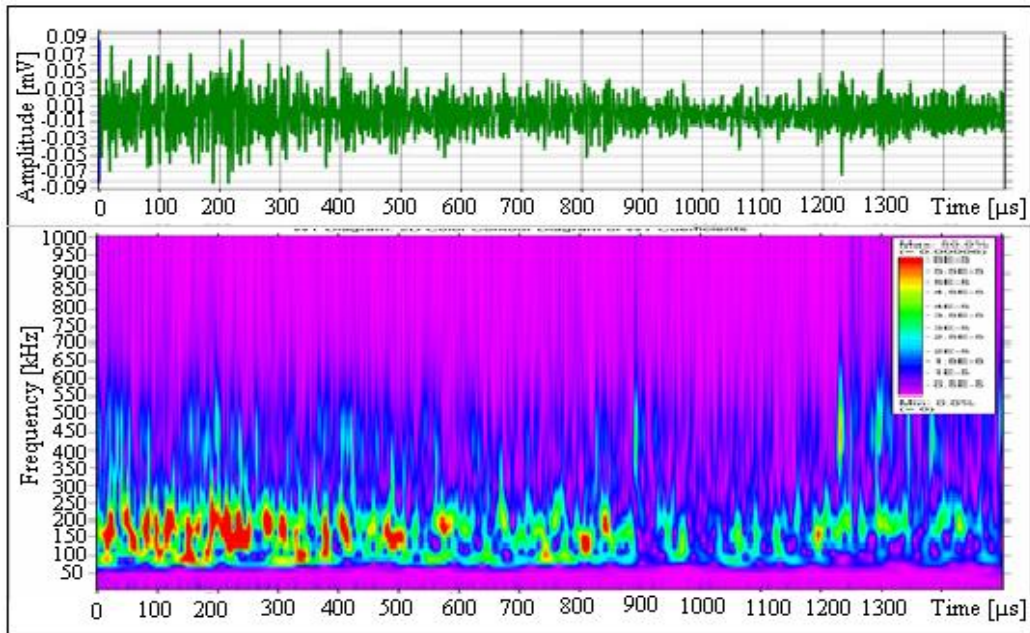


Figure 7-4 Time domain (top) and Time Frequency domain (bottom) plots for sands of 0.2 g impacting on a steel pipe with V_{SG} of 11 ms^{-1}

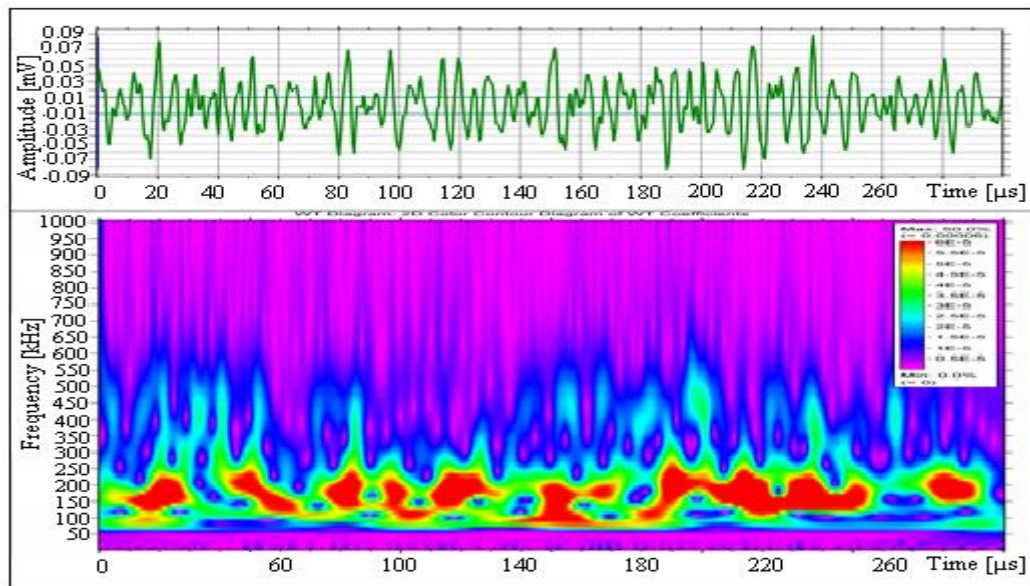


Figure 7-5: Time domain (top) and Time Frequency domain (bottom) plots for sand mass of 0.2 g impacting on a steel pipe with V_{SG} of 11 ms^{-1} (0 to 300 μsec)

A time/frequency trace of an AE waveform response at 11 ms^{-1} (0.2g) is depicted in Figure 7.5. It was evident that the energy intensity levels between 100 kHz to 550 kHz were highest at the point of particle impacts (0 to 300-μs). This level of intensity

decreased significantly as a function of time due to the attenuation; evident by decreasing energy levels at 1000- μ s in comparison to 100- μ s of Figure 7.4. Figure 7.6 shows the maximum intensity of the AE energy for 1.0-g sand injection to be frequencies of up to 800 kHz. These figures, which are typical of all other test results, also demonstrate that there are variations in the frequency content as a function of time. For instance, in Figure 7.4 the frequency content at 50 μ s ranged from 75 kHz to 550 kHz whilst at 1100- μ s the frequency content ranged from 75 kHz to 250 kHz. This would suggest that particle impacts are responsible for the higher frequency content whilst the lower frequency, observed a few microseconds later, are attributed to attenuations and reflections. Comparison of Figures 7.4 and 7.6 show that the higher mass concentration of sand (1.0 g, Figure 7.6) showed significantly more particle impacts on steel pipe, evident by the presence of higher frequency content (above 550kHz) across the recorded time frame in comparison to that recorded for 0.2grammes of sand (Figure 7.4). This wasn't surprising given that there are significantly more sand particles (1.0-g) in the waveform response, presented in Figure 7.6. These results suggest that it may be feasible to investigate the concentration of sand particles by correlating particular high frequency bands over a time period to generated AE energy.

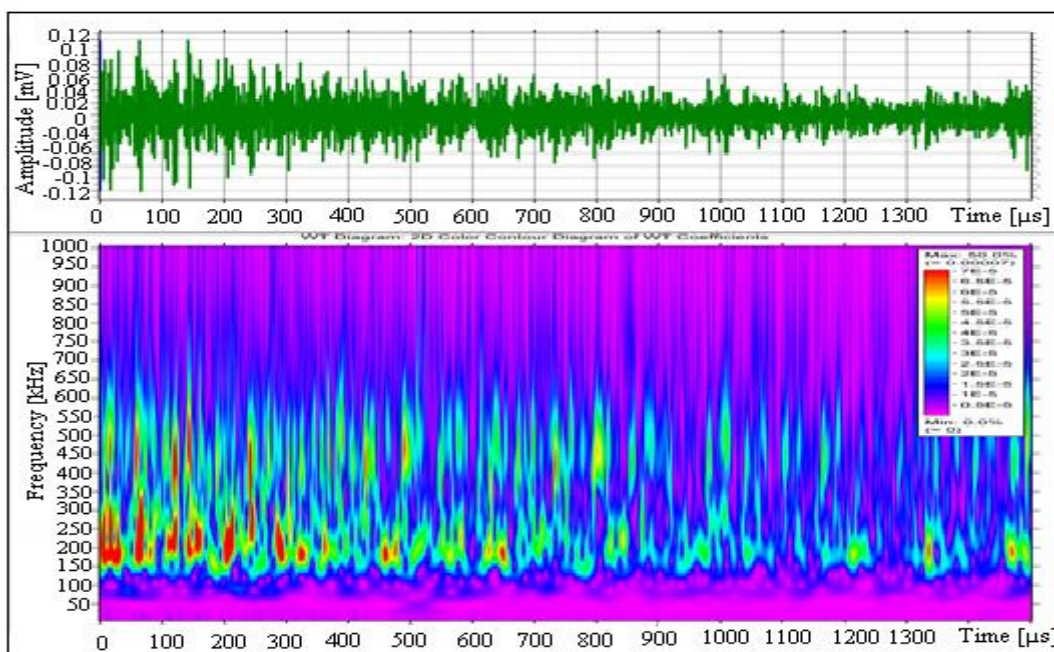


Figure 7-6: Time domain (top) and Time Frequency domain (bottom) plots for sands of 1.0 g impacting on a steel pipe with V_{sg} of 11 ms^{-1}

Figure 7.7 presents a summary of all the results and clearly shows a correlation between AE energy levels, quantity of sand injected and V_{SG} . The observations showed an increase in the AE energy levels as the V_{SG} increased from 8 ms^{-1} to 12 ms^{-1} for the same quantity of sand injected. Also, AE energy levels increased with an increase in the quantity of sand injected for the same V_{SG} . The increase in the quantity of sand injected leads to an increase in the number of sand particles impacting on the pipe's walls. This results in an increase in number of elastic waves generated by the impact. Also, the increase in V_{SG} significantly accelerates the velocity of sand particles in the stream. Therefore, the probability of the sand particles hitting the steel pipe will increase as the V_{SG} increases, resulting in an increase of AE energy levels.

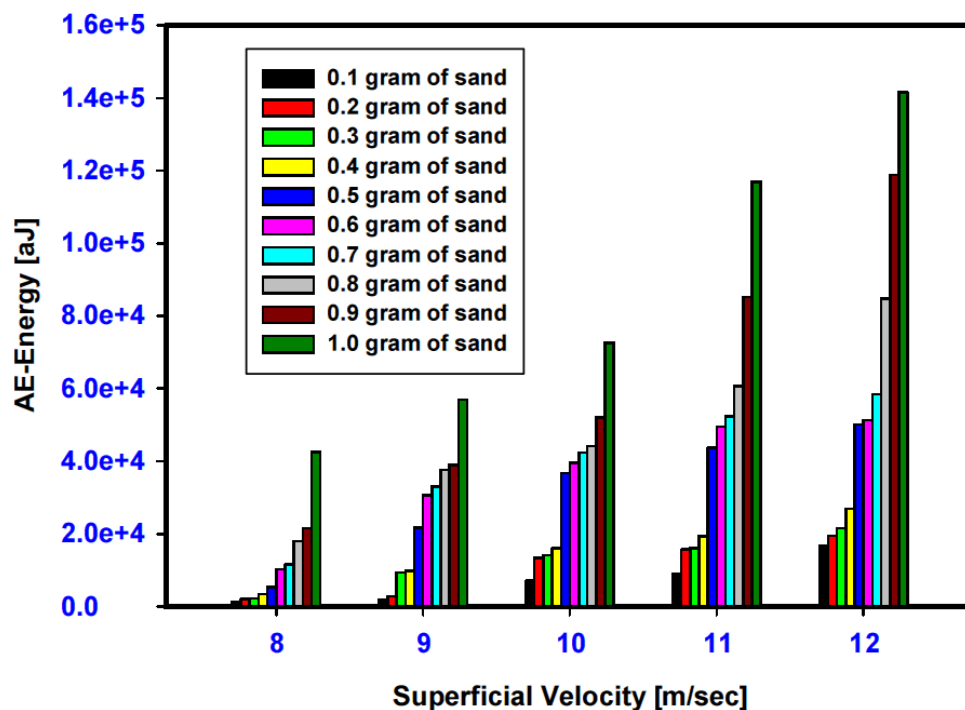


Figure 7-7: AE energy levels VS V_{SG} for a range of sand injections

Figures 7.7 and 7.8, display all results for various quantities of sand and V_{SG} ranges. In addition, Table 7.2 details observations for relative changes in sand quantity and V_{SG} . It was evident (Table 7.2), that for a fixed V_{SG} level an incremental increase in sand quantity resulted in an average increase of between 26 % to 42 %, depending on the specific V_{SG} level. These values were obtained by comparing the relative increases in AE energy for different quantities of sand for varying V_{SG} levels. The

standard deviation was 3.55 % on average. This wasn't unexpected given the probabilistic influences in the generation of AE for this particular investigation. The rate at which the sand particles impact the horizontal pipe, and the degree to which the particles are carried in the main velocity stream, will greatly influence the level of measured AE energy. Irrespective of this probabilistic variation, on average, an increase in sand quantity for a fixed V_{SG} resulted in a linear increase in AE energy levels, see Figure 7.8. This shows an exponential relationship between AE energy levels and the quantity of sand, irrespective of the varying V_{SG} levels.

In order to establish an empirical relationship between the V_{SG} , AE energy and sand quantity the following relationships were established:

- For $V_{SG} = 8$ m/s $AE\text{-Energy} = 619.77e^{4.17(QoS)}$
- For $V_{SG} = 9$ m/s $AE\text{-Energy} = 5683.98e^{2.30(QoS)}$
- For $V_{SG} = 10$ m/s $AE\text{-Energy} = 10057.49e^{1.95(QoS)}$
- For $V_{SG} = 11$ m/s $AE\text{-Energy} = 9254.42e^{2.51(QoS)}$
- For $V_{SG} = 12$ m/s $AE\text{-Energy} = 11178.41e^{2.56(QoS)}$

The quantity of sand may be deduced from these relationships for a given V_{SG} and AE energy level. Though, it should be noted that this relationship only applied to the pipe characteristics presented in this work.

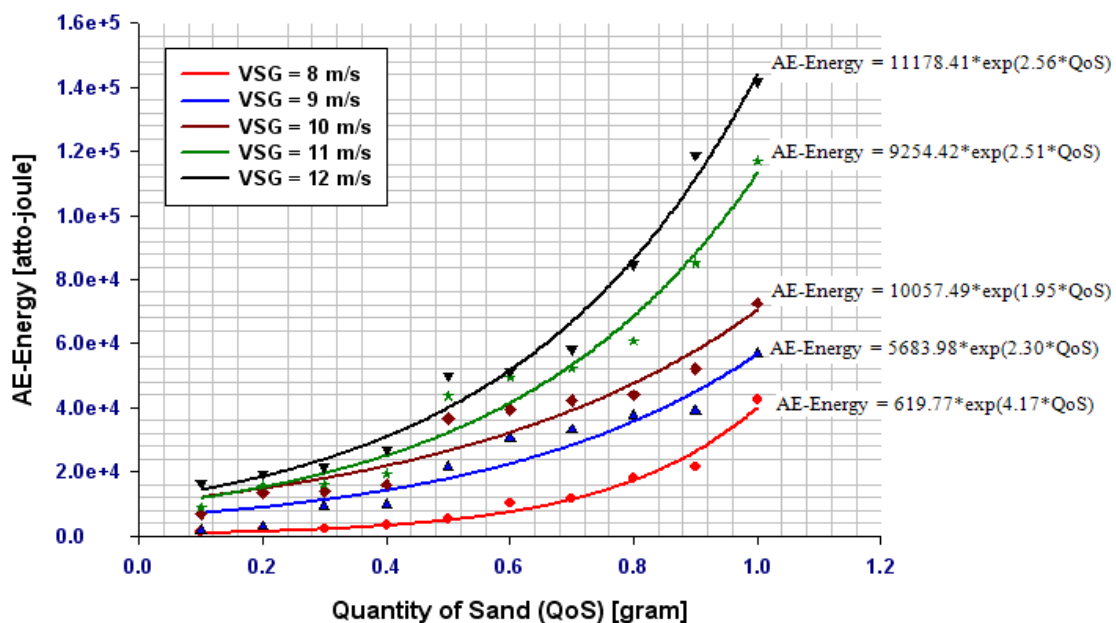


Figure 7-8: AE energy levels plotted against V_{SG} for a range of sand injections

Table 7-2: AE energy change in % for constant sand quantities and varying V_{SG}

V_{SG} (ms^{-1})	Quantities of sand (gram)									
	0.1	0.2	0.3	0.4	0.5	0.6	0.7	0.8	0.9	1.0
8	-	-	-	-	-	-	-	-	-	-
9	29 %	26 %	77 %	65 %	75 %	67 %	65 %	52 %	45 %	25 %
10	73 %	78 %	34 %	39 %	41 %	23 %	22 %	15 %	25 %	22 %
11	21 %	14 %	12 %	17 %	16 %	20 %	19 %	27 %	39 %	38 %
12	46 %	19 %	25 %	28 %	13 %	4 %	10 %	28 %	28 %	17 %
Avg.	42 %	34 %	37 %	37 %	36 %	29 %	29 %	31 %	34 %	26 %

Typically, pipe erosion rate greatly increases with higher particle velocity. In a two-phase gas-solid flow, sand (solid phase) is normally entrained/suspended in the gas phase. Thus, it is reasonable to assume that sand particles have the same velocity as the gas velocity (V_{SG}). Therefore, the increase in V_{SG} will lead to an increase in erosion rate. In addition, the erosion rate is dependent upon the incident angle of the eroding particle, with the erosion process much more efficient for a larger angle of incidence [54]. An increase in quantity of sand within the pipe will cause an increase in the number of the particle impacts, which will also lead to an increase in erosion rate.

7.3 Monitoring Sand Transport Characteristics in Multiphase Flow in Horizontal Pipelines

For experimental set up and method, see section 6.2. The experimental investigation involved the influences of segregated and intermittent flow regimes on sand concentration in a horizontal pipe, Table 6-2 in chapter 6, summarise the experimental measurements. Also the experimental investigation involved assessing the concentration of sand for a three phase air-water-sand flow in a horizontal pipe, where the V_{SG} had a range of between $0.2 ms^{-1}$ to $2.0 ms^{-1}$ and V_{SL} had a range of

between 0.2 ms^{-1} to 1.0 ms^{-1} , Table B-1 in Appendix B, summarise the experimental measurements.

7.3.1 Sand Transport Characteristic in Segregated Flow

The segregated flow is characterized by two-phase flows of liquid and gas in separate regions of the pipe while still interacting at the interface between the regions. The segregated regime is usually subdivided into stratified flow and stratified wavy flow. For the transition boundary between the stratified flow and stratified wavy flow based on the relative velocity of the two phases.

7.3.1.1 Sand Transport Characteristic in Stratified Flow

This regime occurs when the gravitational separation is complete. The liquid flows along the bottom of the pipe and the gas along the top part of the pipe, see Figure 7.9. During this investigation it was observed that, stratified flow regime occurred at low superficial gas velocity (V_{SG}) and superficial liquid velocity at (V_{SL}) was 0.15 ms^{-1} - 0.30 ms^{-1} and V_{SG} was 0.15 ms^{-1} - 0.35 ms^{-1} .

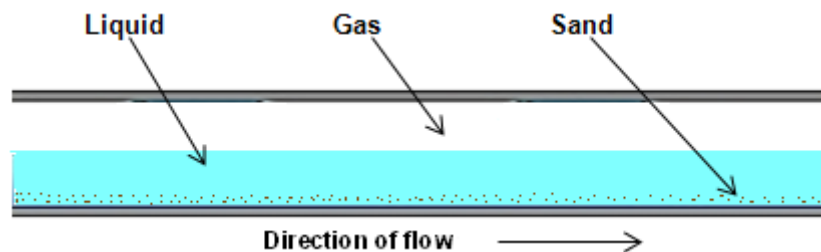


Figure 7-9: Schematic of sand behaviour in stratified flow regime

Figure 7.10 presents the results of monitoring stratified flow regime, where relatively low AE energy levels were noted in comparison to other flow regimes. This can be attributed to the movement of sand particles slid and creep in the film, which makes collision between the sand particles and the pipe significantly low as a result of lower V_{SL} and V_{SG} . Though AE tests were relatively low, it was also observed that AE energy levels increased with increasing sand concentration.

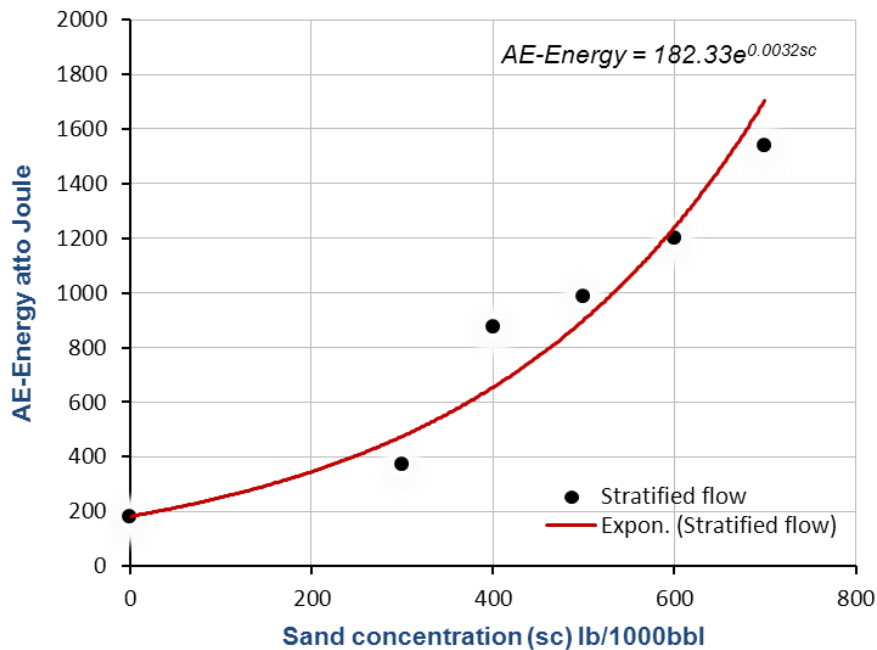


Figure 7-10: AE energy levels plotted against sand concentration (stratified flow)

7.3.1.2 Sand Transport Characteristic in Stratified- Wavy Flow

When higher gas velocity is applied to stratified flow, waves are produced on the gas-liquid interface and this is referred to a wavy or stratified-wavy flow regime. The transition boundary between the stratified flow and stratified wavy flow is based on the relative velocity of the two phases. Experimental observations in this study showed that stratified wavy flow was observed at $V_{SL}=0.15 \text{ ms}^{-1} - 0.3 \text{ ms}^{-1}$, and V_{SG} was $0.4 \text{ ms}^{-1} - 0.9 \text{ ms}^{-1}$. Also was noted that the transportation of sand particles were relatively influenced by the sand concentration. At lower sand concentration, particles were suspended within rough wave. This led to steady exchange and settlement in the film zone. As the sand concentration increased, sand particles that are located in the film zone will be dragged by the coming wave and wrap them by its movement. Figure 7.11 shows schematic behaviour of sand particles in stratified wavy flow.

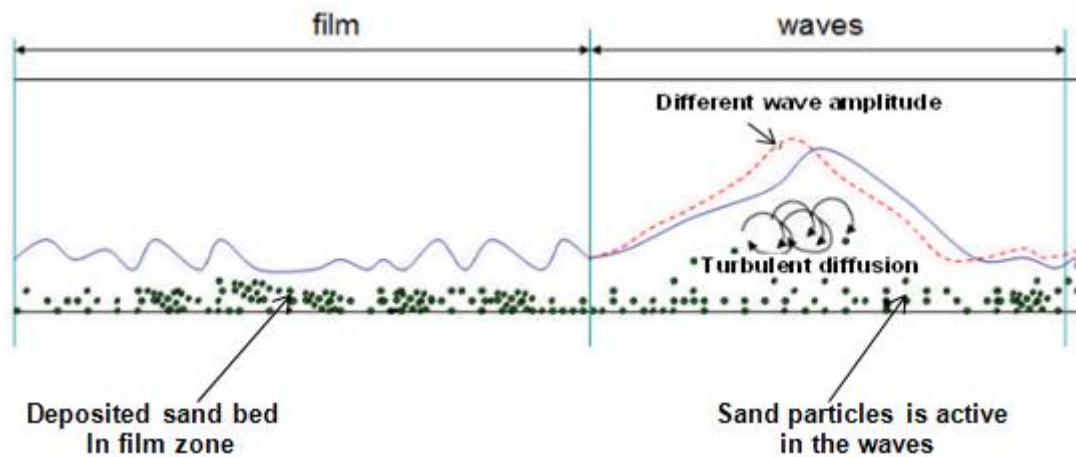


Figure 7-11: Schematic of sand behaviour in stratified wavy flow regime [17]

Interestingly, it was noted that an increase in the AE energy levels were recorded as sand particles entered into waves and become active; thereby resulting enhancement of the impact energy. Further, the increase in V_{SG} significantly accelerated the velocity of sand particles in the stream, and therefore-the probability of the hitting the steel pipe by sand particles increased with increasing V_{SG} . This has in turn led to resulting in an increase in AE energy levels, see Figure 7.12.

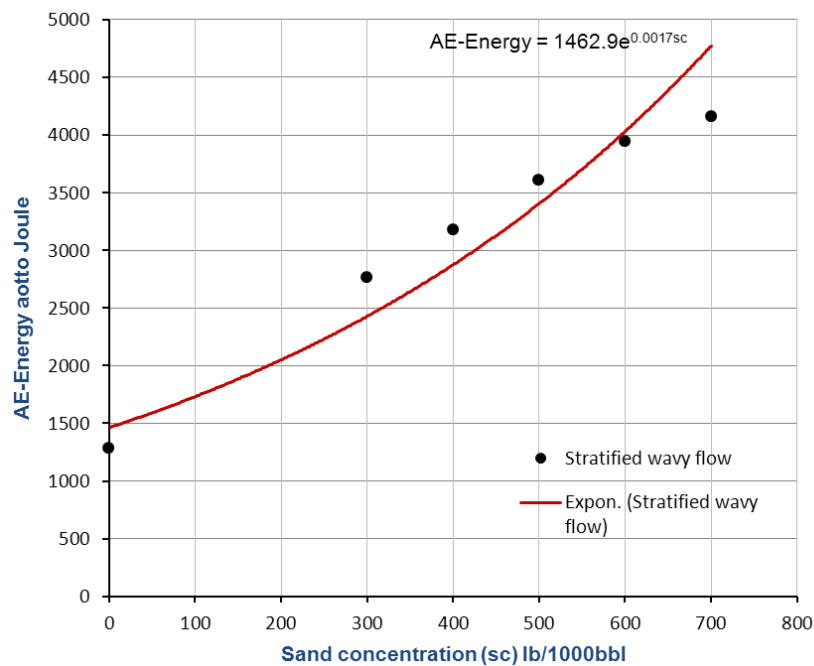


Figure 7-12: AE energy levels plotted against sand concentration (stratified wavy flow)

7.3.2 Sand Transport Characteristic in Intermittent Flow

The intermittent flow is characterized by alternate flow of liquid and gas. The intermittent regime is usually subdivided into plug flow and slug flow. For the transition boundary between the plug flow and slug flow, based on the quantity of the gas bubbles contained in a slug body.

7.3.2.1 Sand Transport Characteristic in Plug Flow

This is a transition regime between stratified wavy flow and hydrodynamic slug flow. In this flow regime most of the liquid flows at the bottom of the pipe and the gas flows at the top. In plug flow, plug bodies of liquid fill the entire pipe cross section area, and are separated by gas pockets. Gas pockets tend to travel in the upper half of the flow pipe, and the liquid plug is free of gas bubbles or includes very few gas bubbles [51].

Plug flow was observed at V_{SL} was $0.95 \text{ ms}^{-1} - 1.0 \text{ ms}^{-1}$ and V_{SG} was $0.1 \text{ ms}^{-1} - 0.15 \text{ ms}^{-1}$. For low sand concentration, sand particles were observed moving as streak lines separated by liquid plug body. As the sand concentration increased, leads to a higher intensity of sand concentration in streaks, and gradually directed toward the centreline. Further increase in sand concentration result in the intensity in streaks and sliding sand layer increases, see Figure 7.13.

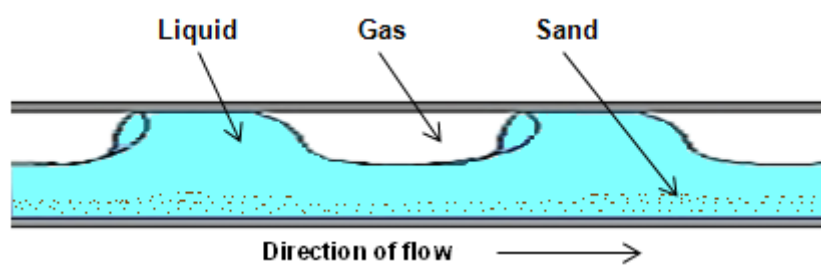


Figure 7-13: Schematic of sand behaviour in plug flow regime

In plug flow, gas pockets move along the top of the pipe having little effect upon the solid behaviour as long as the gas velocity is increased, the gas pocket gets depth and the fluctuating velocities affect the sand transportation. Under this flow regime, it can be seen that either the sand is transported in the plug body and in the film region, or the sand particles settle in the gas plug zone (film region), and are only

transported into the plug body of collided sand particles are formed, moving in the liquid plug body.

Observations from monitoring of this flow regime indicated that the movement of sand particles in the liquid plug body eventually motivated sand particles to generate AE energy higher than that observed in the stratified wavy flow. The influence of the increase in the sand concentration on the AE energy levels is presented in Figure 7.14.

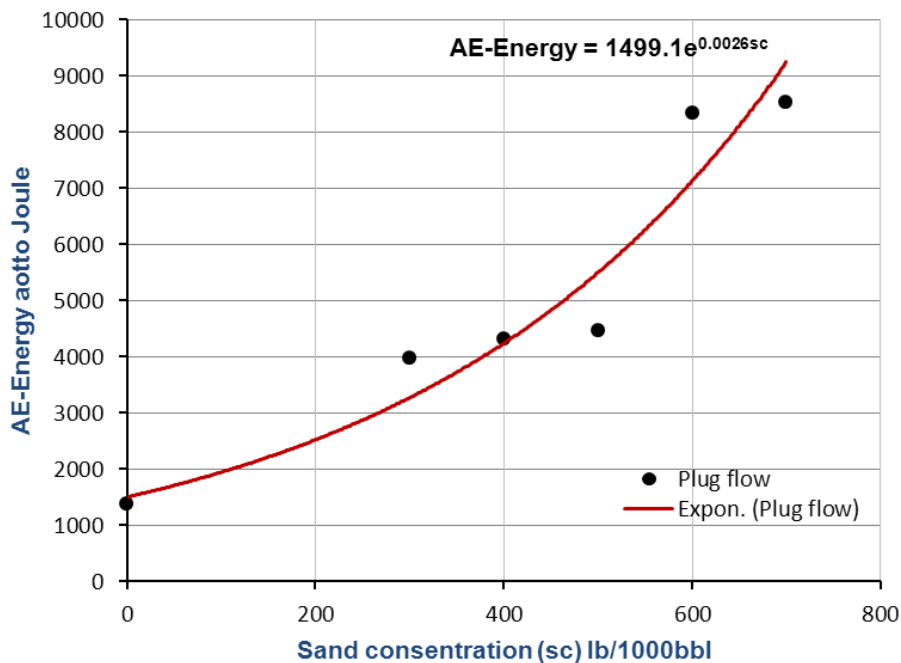


Figure 7-14: AE energy levels plotted against sand concentration (plug flow)

7.3.2.2 Sand Transport Characteristic in Slug Flow

Slug flow consists of the slug body and the gas pocket zone (film zone). The liquid in the slug body may be aerated by small bubbles, which are concentrated towards the front of the slug body and at the top of the pipe. In slug flow regimes, turbulence is generated at the front of the slug, high amplitude of slug impacts the top of pipe wall, long film zone was formed due to the gas was enwrapped between each slug body, the obviously distinguish of plug and slug flow is the length and depth of the gas pocket zone, gas pocket zone area in slug flow is more expanse.

The slug flow was observed at V_{SL} 0.5 ms^{-1} to 2.0 ms^{-1} and V_{SG} was between 1.0 ms^{-1} to 5.0 ms^{-1} . This flow regime is characterised by a formation of turbulence at the front of slug [113]. Under different conditions of sand concentration distribution, some sand particles accommodated on the pipe wall is collected by the energy produced from the turbulent, then the sand particles is lifted into the turbulent core of the slug body. The behaviour of sand particles in slug body and gas pocket zone are schematically depicts in Figure 7.15.

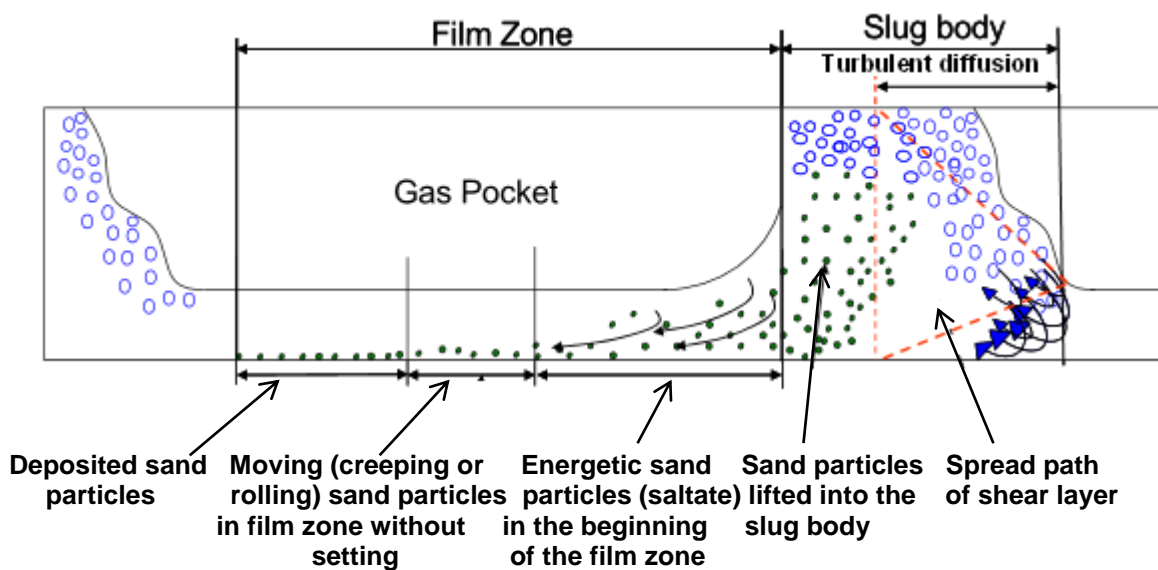


Figure 7-15: Schematic of sand behaviour in slug flow regime [17]

At the slug back region, sand and water started sprayed into the gas pocket zone. The sand particles subjected to slow their speed gradually as it entered to the gas pocket zone, this is as a result of the effect of counter-current flow in the gas pocket zone. In case of short gas pocket zone, active sand particles are moving to the front, then slide, while in case of long gas pocket zone, the particles tend to settle (length of gas pocket zone affected by consumption of kinetic energy generated by friction force). By increasing the gas superficial velocity, the length of the gas pocket zone increases. The process repeated once again with passing other slug.

For low sand concentration, sand particles were transported with the flow as they are left up by the turbulence generated at the front of slug. As increases in sand concentration, part of sand particles having passed rolling through the front of gas pocket zone, and settle at the end length of gas pocket zone.

It is worth noting that the relationship between the AE energy and the sand concentration in different flow regime was non-linear. It is also worth mentioning that the AE sensor recorded the highest values of AE energy in slug regime comparing to the other flow regimes, see Figure 7.16.

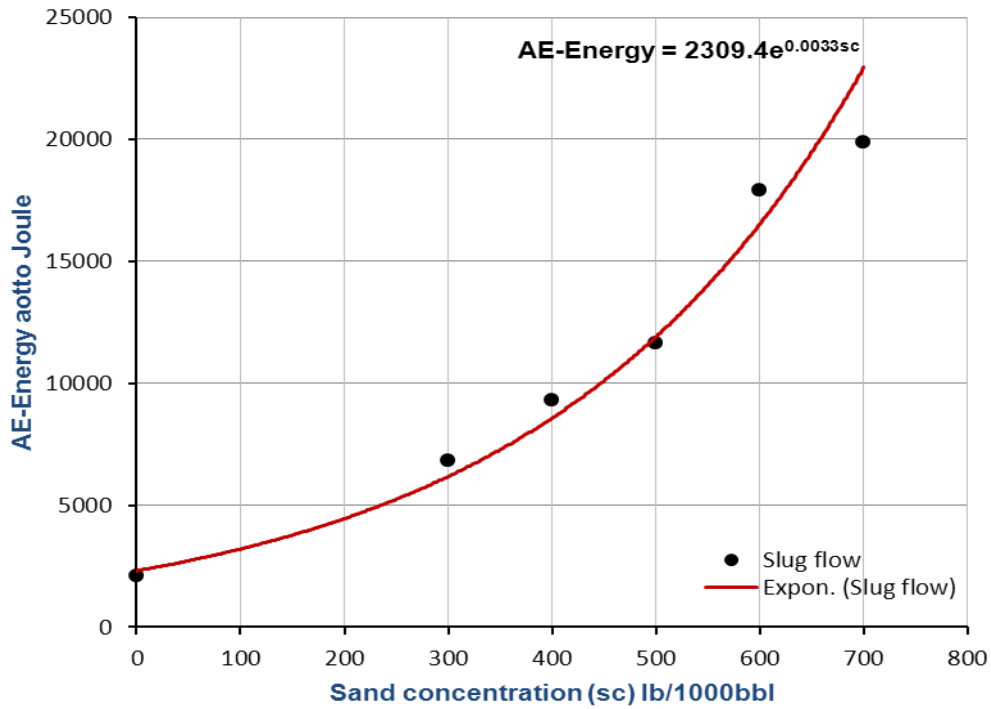


Figure 7-16: AE energy levels plotted against sand concentration (slug flow)

Figure 7.17 presents a summary of all results that clearly shows a correlation between AE energy levels, quantity of sand injected for the investigated flow regimes. The observations showed greatest AE energy levels measured in slug regime due to high flow rates (V_{SL} and V_{SG}), whereas lower AE energy levels was measured in stratified flow regime due to the low flow rates.

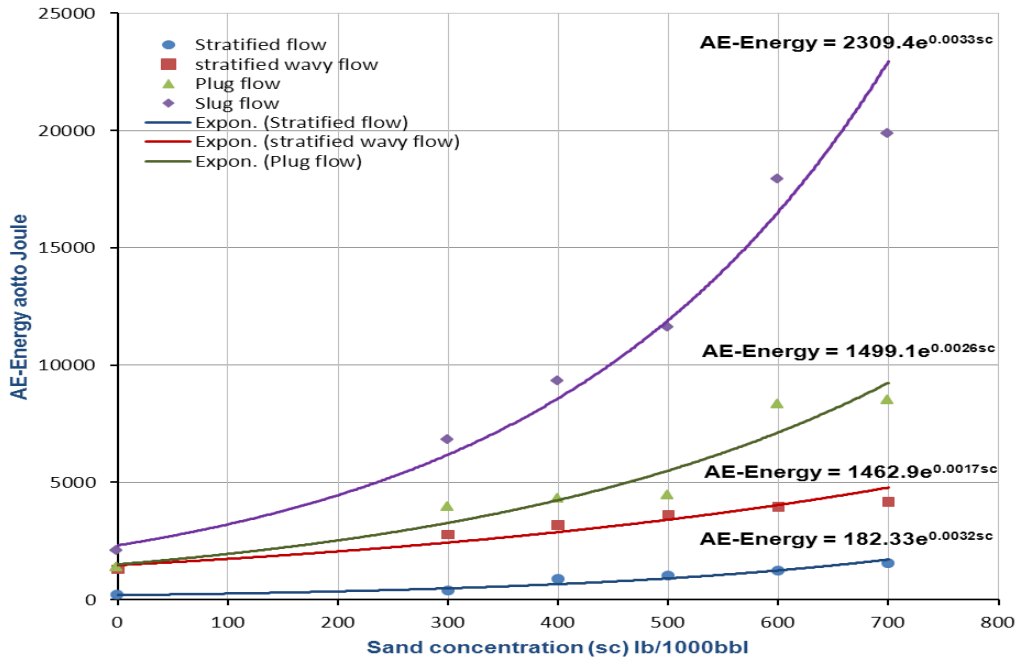


Figure 7-17 AE energy levels plotted against sand concentration for different flow regimes

7.3.3 The effect of AE sensor location on AE Energy

In segregated flow regime, the results showed greatest AE energy levels acquired by AE sensor 1 located at the pipe bottom, whilst AE sensor 2 located on pipe top recorded a low sensitivity to the AE signals generated by sand particles. This was expected as the AE sensor 2 is the maximum distance from the source (sand particles at the pipe bottom). In addition to that, the collision between the sand particles and the pipe due to the lower V_{SL} and V_{SG} leads to weak AE signals captured by the AE sensor 1. Therefore, segregated flow regime shows low AE energy levels comparing to the intermittent flow regime, see Figure 7.18.

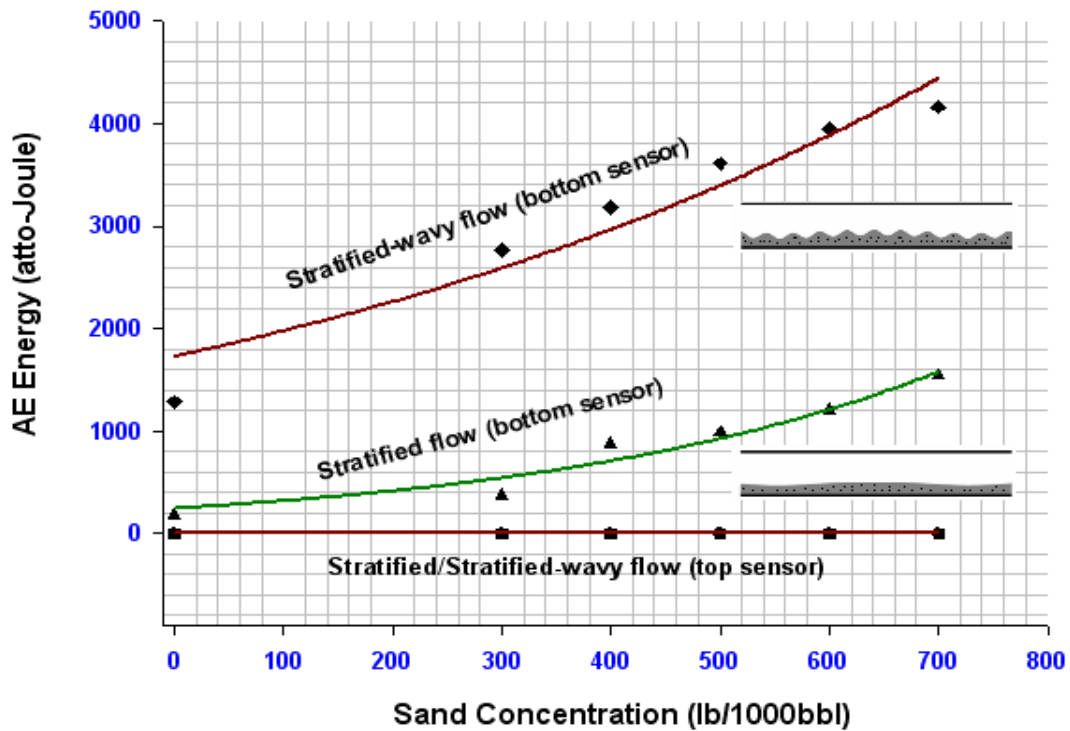


Figure 7-18: AE energy levels plotted against sand concentration for stratified & stratified-wavy flows (top & bottom sensors)

In intermittent flow regime, results presented in figure 7.17 indicated that movement of sand particles in the liquid plug body due to the increase in flow rates was enough to energetic sand particles to generate AE signals. AE sensor 1 located at the pipe bottom was showed greatest AE energy levels compared with AE sensor 2 located at the pipe top. This was expected as the AE sensor 2 is the maximum distance from the main source of the energy (sand particles) which tends to impact on the pipe bottom. In addition, the increase in energy levels is a result of the increase in intensity of sand concentration.

In slug flow regime, results presented in Figures 7.19 showed greatest AE energy levels acquired by AE sensor compared with the rest of the flow regime due to the reason of; high V_{SL} and V_{SG} causes sand particles were transported with the flow as they are left up by the turbulence generated at the front of slug, result in significantly energetic as heading to the pipe bottom.

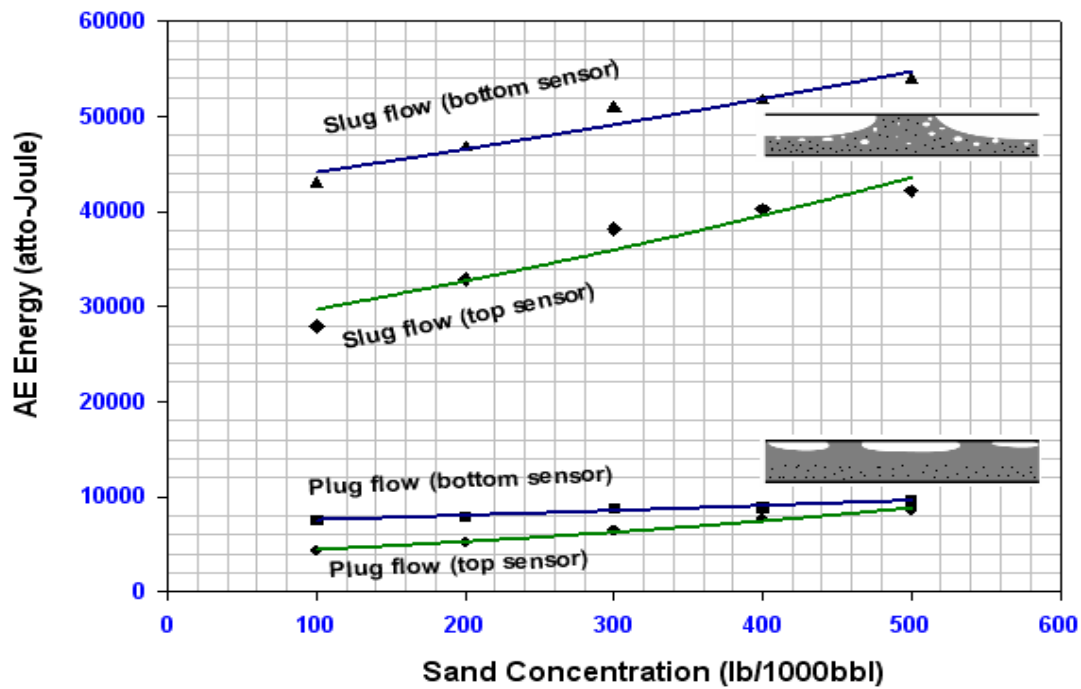


Figure 7-19: AE energy levels plotted against sand concentration for slug & plug flows (top & bottom sensors)

7.3.4 The effect of V_{SL} , V_{SG} and Sand Concentration on AE Energy

A summary of results from the numerous tests is presented in Appendix B and Table B-1, which reflect the general observations and of the effect of V_{SL} , V_{SG} and sand concentration on AE energy trend. The results revealed that, at constant V_{SL} an increase in AE energy was noted with increasing in V_{SG} values ranging from 0.2 ms^{-1} to 2.0 ms^{-1} and increasing in sand concentration ranging from $0 \text{ lb}/1000 \text{ bbl}$ to $700 \text{ lb}/1000 \text{ bbl}$, see Figure 7.20. The increase in V_{SG} significantly accelerates the velocity of sand particles in the stream. Therefore, the probability of the sand particles hitting the steel pipe will increase as the V_{SG} increases, resulting in an increase of AE energy levels. Also, the increase in sand concentration injected leads to an increase in the number of sand particles impacting on the pipe's walls. This results in an increase in number of elastic waves generated by the impact, which in turn increase in the AE energy levels.

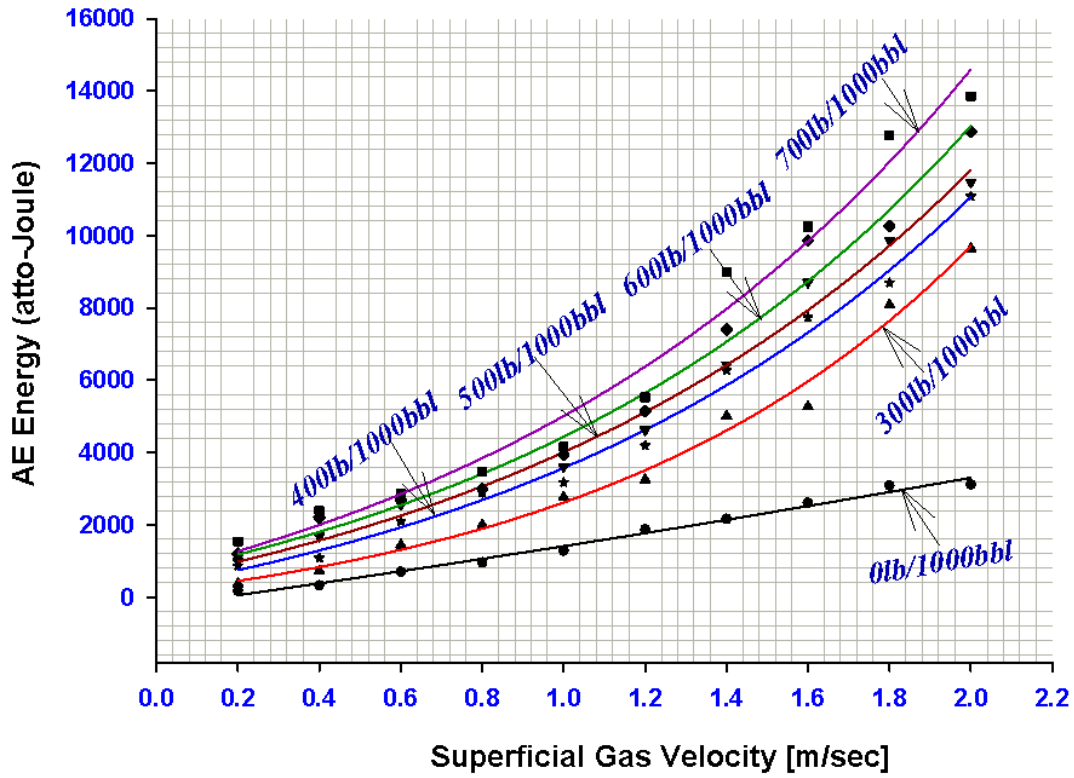


Figure 7-20: AE-Energy levels against a range of superficial gas velocity (Vsg) for different sand concentration and constant VSL of 0.2 m/s

Also, for a constant amount of sand concentration and varying values of Vsg and VSL were applied, the observations showed a correlation between AE energy levels, VSL and Vsg. AE energy levels increased with an increase in the VSL or Vsg or both of them, see Figure 7.21.

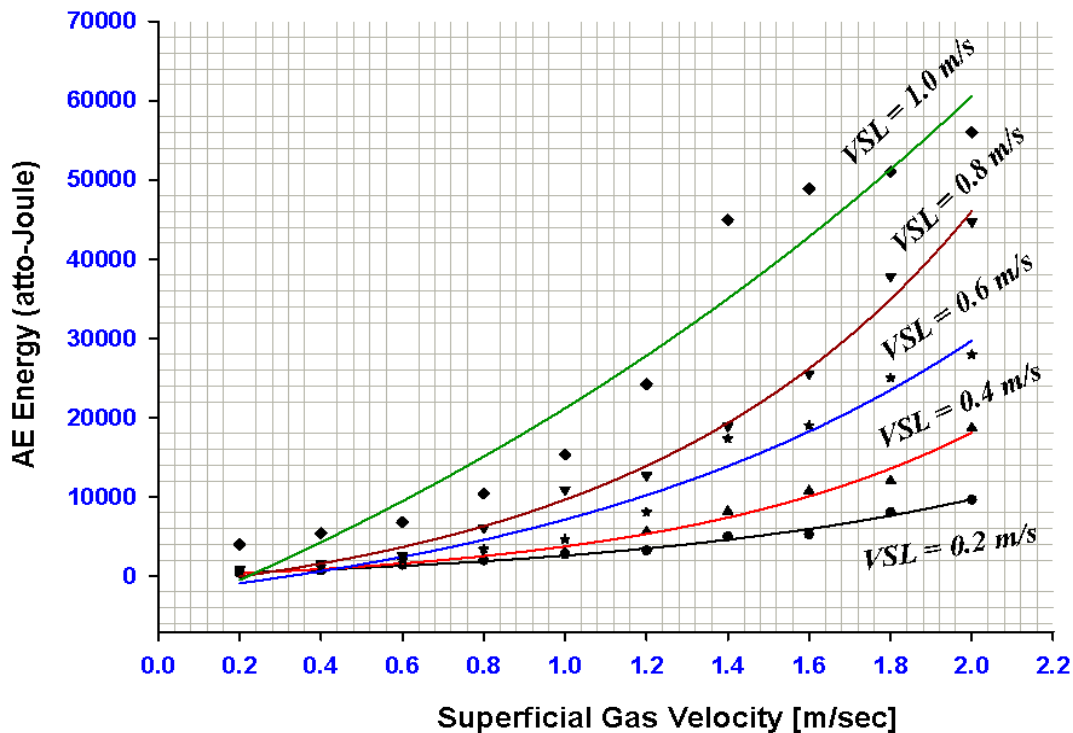


Figure 7-21: AE-Energy levels against a range of superficial gas velocity (V_{SG}) & superficial liquid velocity (V_{SL}) and constant sand concentration of 300lb/1000bbl

7.4 Identification of Minimum Transport Condition (MTC) for Sand in Two-Phase

Experiments undertaken were conducted with different sand concentrations (300 lb/1000bbl to 700lb/1000bbl at increments of 100lb/1000bbl, which equivalent to 0.856 kg/m³ to 1.997 kg/m³ at increments of 0.285 kg/m³). The concentration of sand was pumped into the pipe at speed of 0.128 m/s and V_{SL} values ranged from 0.1 ms⁻¹ to 1.2 ms⁻¹ at increments of 0.1 ms⁻¹, Table 6-5 in chapter 6, summarise the experimental measurements.

The forces controlling the motions of particles may be classified into three groups: (1) forces at the interface between the fluid and particles such as viscous forces; (2) forces due to the interactions between particles such as impingement; and (3) forces imposed by external fields such as gravity [86]. This implies that, there are three basic sources of Acoustic Emissions (AE); particle-particle collision, particle-wall collision, and, turbulent flow. The only AE source considered in this work is particle-

wall collision/impact, as signals generated from the other sources were assumed to be insignificant. For instance, AE generated from particle-particle collision/impact within the pipe will not be detectable by an AE sensor located on the pipe wall because of attenuation by the water between source and sensor on the pipe.

Sand flow patterns were recorded during the experiment, see Figure 7.22. At velocities of $V_{SL} > 1.0 \text{ ms}^{-1}$, homogenous flow was observed. At velocities between $0.6 \text{ ms}^{-1} < V_{SL} < 1.0 \text{ ms}^{-1}$, heterogeneous flow were noted. In this instance the concentration of particles across the pipe becomes non-uniform, and the particle velocity was slightly less than the V_{SL} . As a consequence, number of sand particles that impact the pipe wall increased. The increase in number of sand particles impacting on the pipe wall results in an increase in AE energy. At low fluid velocities saltation with a moving bed occurs (between $0.4 \text{ ms}^{-1} < V_{SL} < 0.5 \text{ ms}^{-1}$ see Figure 7.22). A small percentage of particles in the upper part of the pipe are in suspension and move with the liquid, but most particles are on the bottom of the pipe forming a bed of solids which moves at a slower, uniform rate. Here, low AE energy levels were measured. At very lower velocities a stationary bed occurs (between $0.1 \text{ ms}^{-1} < V_{SL} < 0.3 \text{ ms}^{-1}$ see Figure 7.22), the upper part of the pipe contains liquid only, while the lower part contains a deposit of sand. Almost no AE energy was measured.

It is known that, sand transport in horizontal pipelines has four main regimes, depending on the fluid flow rate and sand concentration. These flow regimes are shown on a plot of V_{SL} versus AE Energy for sand concentration of 600lb/1000bbl and C_V of 6.46E-04 see Figure 7.22.

Between $0.6 \text{ ms}^{-1} \leq V_{SL} \leq 0.9 \text{ ms}^{-1}$ below MTC, the sand particles suspended in the flow were subject to lift, drag and gravitational forces, the vertical distribution of the particles was not uniform. However, the sand particles were transported as heterogeneous flow. Between $0.4 \text{ ms}^{-1} \leq V_{SL} \leq 0.5 \text{ ms}^{-1}$, a sand bed build overtime and form scouring dunes (moving bed). At very low fluid flow rates $V_{SL} \leq 0.3$, stationary sand dunes (simple stationary bed) occurred, see Figure 7.22.

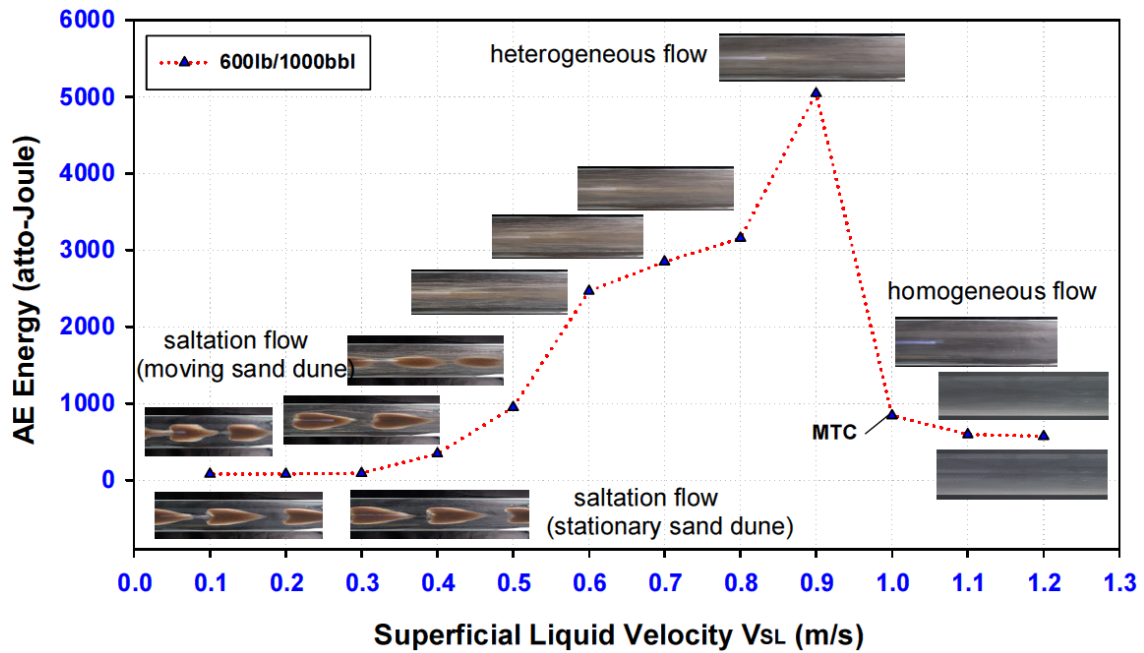


Figure 7-22: Sand flow pattern in water flow for sand concentration of 600lb/1000bbl and CV of 6.46E-04 at V_{SL} ranges of between 0.1 ms^{-1} to 1.2 ms^{-1}

A summary of results from the numerous tests is presented in Figure 7.23. For sand concentration of 600lb/1000bbl (1.712 kg/m^3 , $C_V = 6.46\text{E-}04$), it was noted that AE energy levels increased gradually as V_{SL} decreased from 1.2 ms^{-1} to 1.0 ms^{-1} . At $V_{SL} \geq 1.0 \text{ ms}^{-1}$, the sand particles were suspended in the liquid phase and the flow was homogeneous. At $V_{SL} = 0.9 \text{ ms}^{-1}$ the sand particles were observed to be no longer uniformly distributed across the pipe (heterogeneous flow regime) and consequently, AE energy levels increased. This was attributed to the increase in number of sand particles which impacted on the pipe wall, given the flow regime is no longer homogeneous. Thus, for $V_{SL} > 0.9 \text{ ms}^{-1}$ AE energy decreases rapidly with increase in flow, as can be seen in Figure 7.23. This drop in AE is the result of the sand particles within the stream having less contact with the pipe wall as V_{SL} increases. At flow conditions of $V_{SL} \geq 1.0 \text{ ms}^{-1}$ (homogeneous flow), the AE energy levels remain relatively level, see Figure 7.23. Table 6-3 in chapter 6, summarise the experimental measurements.

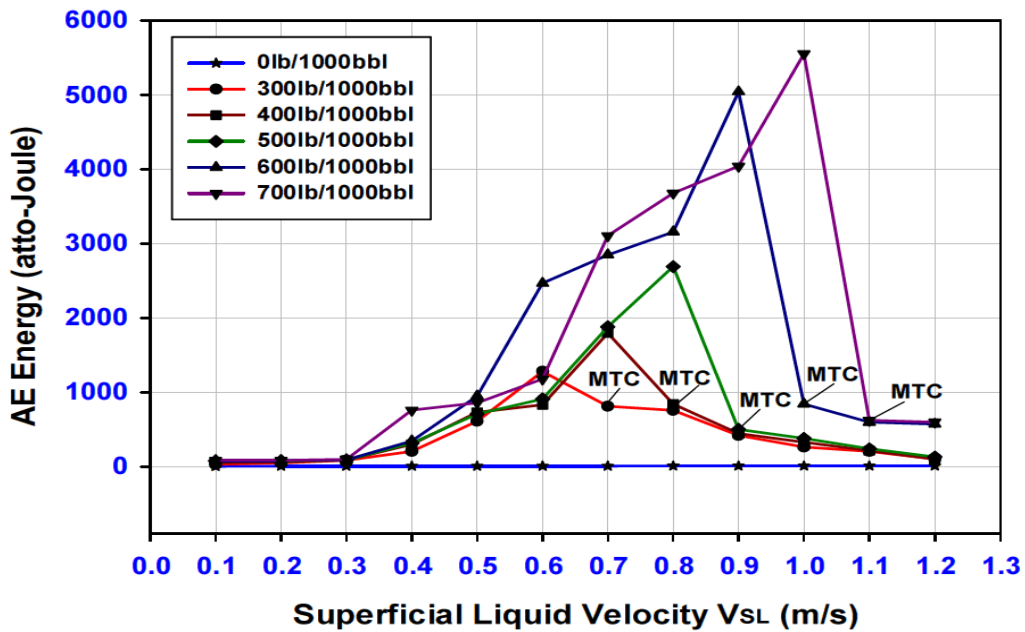


Figure 7-23: AE-Energy plotted against V_{SL} for a range of Sand Concentration

For V_{SL} from 0.9 ms⁻¹ to 0.1 ms⁻¹, there is a decrease in the AE. The decrease in AE energy below 0.9 ms⁻¹ is attributed to a reduction of impact energy of momentum on the pipe from the sand particles within the flow. At very low levels of V_{SL} (V_{SL} ≤ 0.5 ms⁻¹), sand dunes began to form and the generation of AE continually dropped. In this instance the generation in AE is attributed to the rolling of the particles over the pipe. These particles have less energy from those associated with higher V_{SL} levels and therefore it is not surprising that the generation of AE is reduced. Therefore, sand minimum transport velocity (V_{MTC}) in this case was identified at 1.0 ms⁻¹ and define as the condition at which the sand particles will remain suspend in the liquid (homogeneous flow) and are not deposited in the pipe.

Based on the experimental observations of sand-water flow in horizontal pipe, V_{MTC} was influenced by two main factors; superficial liquid velocity (V_{SL}) and sand concentration. This is a linear relationship as shown in Figure 7.24. Table 6-4 in chapter 6, summarise the experimental measurements.

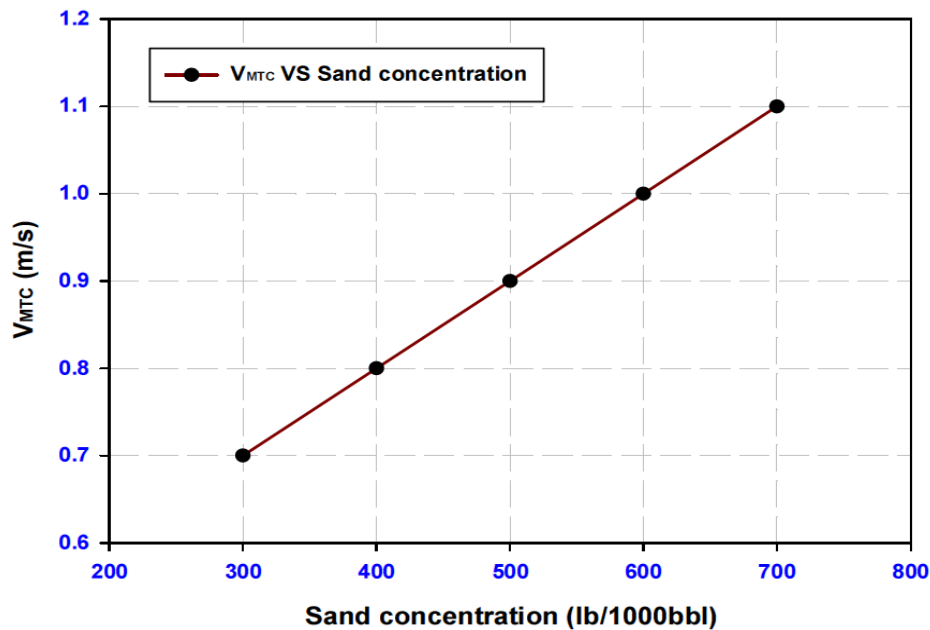


Figure 7-24: V_{MTC} (m/s) VS sand concentration (lb/1000bbl)

Reducing V_{SL} from 1.2 ms⁻¹ to 1.1 ms⁻¹, produced an increase in AE energy of only 4%. As the V_{SL} changed from 1.1 ms⁻¹ to 1.0 ms⁻¹, a greater change in the AE energy level, of 41% increase was measured. However, as V_{SL} approached V_{MTC} (0.9 ms⁻¹ heterogeneous flow) there was a substantial increase in AE energy by 499%. This was because the characteristics of the sand flow suddenly changed and particles started drop out of the carrier fluid and impact on the pipe. For further decrease in V_{SL} from 0.9 ms⁻¹ to 0.8 ms⁻¹, drop out of sand particles increases and a noticeable reduction from levels at 0.9 ms⁻¹ in AE energy by 60% occurs. This reduction in AE energy level continues with further decrease in V_{SL}, by 11% and 16% at 0.7 ms⁻¹ and 0.6 ms⁻¹ respectively. However, when V_{SL} is so low that the sand particles start to form a moving sand dune (V_{SL}= 0.5 ms⁻¹ and 0.4 ms⁻¹, saltation flow), there is a very large reduction in measured AE energy (161% to 160%). Finally, when moving sand dunes became stationary at very low V_{SL} (0.3 ms⁻¹, 0.2 ms⁻¹ and 0.1 ms⁻¹), the reduction AE energy was changed from 300%, 12% and 1%.

7.5 Monitoring the Presence of Droplet in a Horizontal Pipe

Several tests were undertaken using two different types of droplets (water and water/sand) with different volume injected ranging from 1 ml to 5 ml at increments of 1 ml. The droplets were injected into the pipe at VSG values of 9 ms^{-1} , 10 ms^{-1} and 11 ms^{-1} , Tables 6-6 and 6-7 in chapter 6, summarise the experimental measurements. Two basic sources of acoustic emissions were generated. These include droplet-droplet collision and droplet-wall collision. The only AE source considered in this work is droplet-wall collision/impact, as AE's generated from the other sources were found to be insignificant. For instance, AE generated from droplet-droplet collision within the pipe would not be detectable by an AE sensor located on the pipe wall was due to attenuation of the air medium between the source and the sensor on the pipe.

As the droplet travels from its release point through the horizontal pipe, it is subjected to many factors including the superficial gas velocity (VSG), gravitational force, drag force and lift force. The VSG is the most significant factor that affects the droplet motion. The gravitational force on the droplet downward and is a function of air density and droplet volume and the lift force is normal to the relative velocity due to the rotation of the fluid (the rotation causes pressure difference normal to the flow) [114]. The drag force is a function of air density, droplet size, and square of droplet velocity [115].

Figure 7.25 presents a summary of the results that were recorded by bottom sensor due to the collision of droplets (water-droplet and water-sand-droplet) with the pipe wall across a VSG of 9 ms^{-1} , 10 ms^{-1} and 11 ms^{-1} . The results demonstrated that AE energy levels increased with an increase in the volume of droplets injected for the same VSG. The increase in the volume of droplet injected leads to an increase in the number of collision on the pipe's walls. This results in an increase in number of elastic waves generated by the impact. Also observations showed an increase in the AE energy levels as the VSG increased from 9 ms^{-1} , 10 ms^{-1} and 11 ms^{-1} respectively for the same total volume of droplets injected. An increase in VSG significantly accelerates the velocity of diffused droplets in the flow through the pipe. Therefore, probability of droplets hitting the steel pipe will increase as the VSG increases, resulting in an increase of AE energy levels [112, 116].

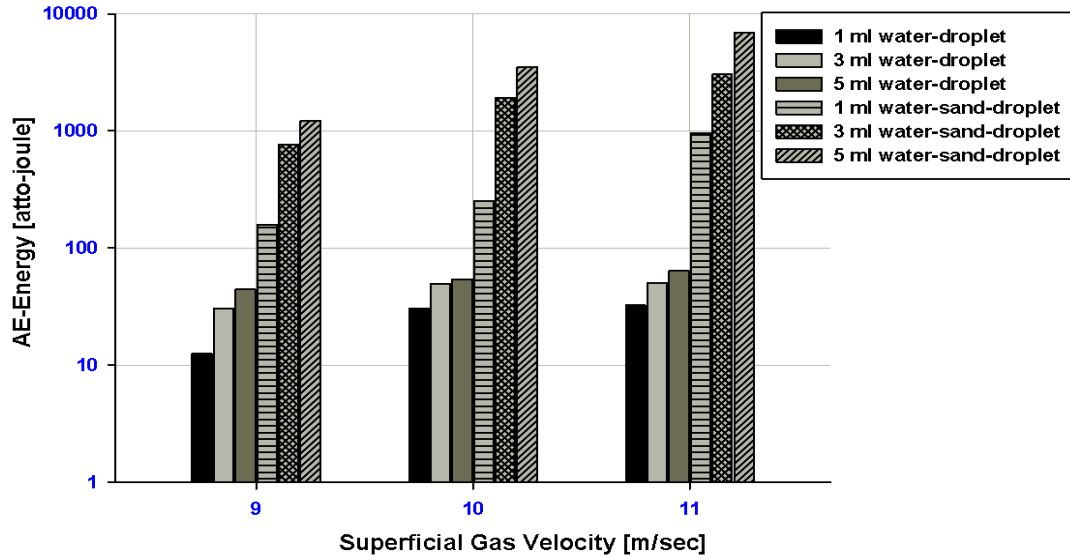


Figure 7-25: AE-Energy variation with increasing total droplet volume and Vsg captured by bottom sensor

Figure 7.26 presents a summary of the results that were recorded by the AE sensor located on the top of the pipe. The results demonstrated that AE levels measured by the top sensor were markedly different than had been noted with measurements recorded from the sensor located at the bottom of the pipe. The AE levels for water-sand droplets were on the same far as levels measured for water only droplets. Irrespective of this an increase in Vsg resulted in an increase in AE energy for all droplet size. For a fixed Vsg a 1ml incremental increase in water-droplet volume resulted in an average increase in AE energy depending on the specific Vsg values. Also, for a fixed droplet volume level an incremental increase in Vsg resulted in an increase in the AE energy levels.

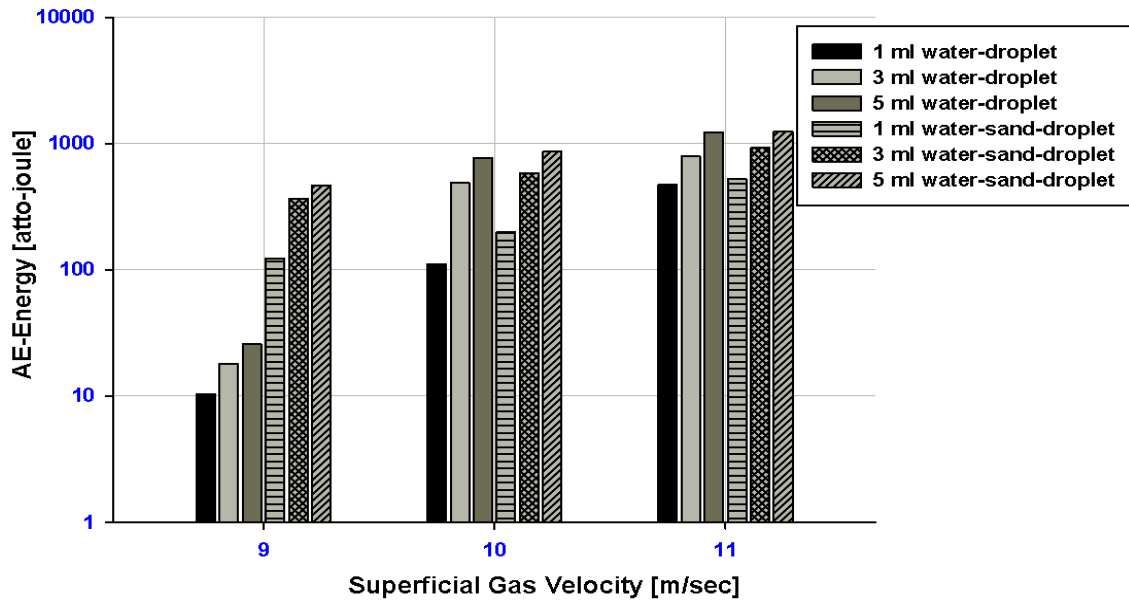


Figure 7-26: AE-Energy variation with increasing total droplet volume and Vsg captured by top sensor

In addition, AE-energy levels measured by bottom sensor were 22% to 82% higher than AE levels measured by top sensor. Moreover, AE energy levels generated by the impact of water-sand droplets were higher than the impact generated by water droplets. This was attributed to the increase in mass of the water-sand droplet, which in turn has a significantly increase in collision/impact force. Figure 7.27 shows the AE energy levels measured by both top and bottom sensors for water-sand droplets.

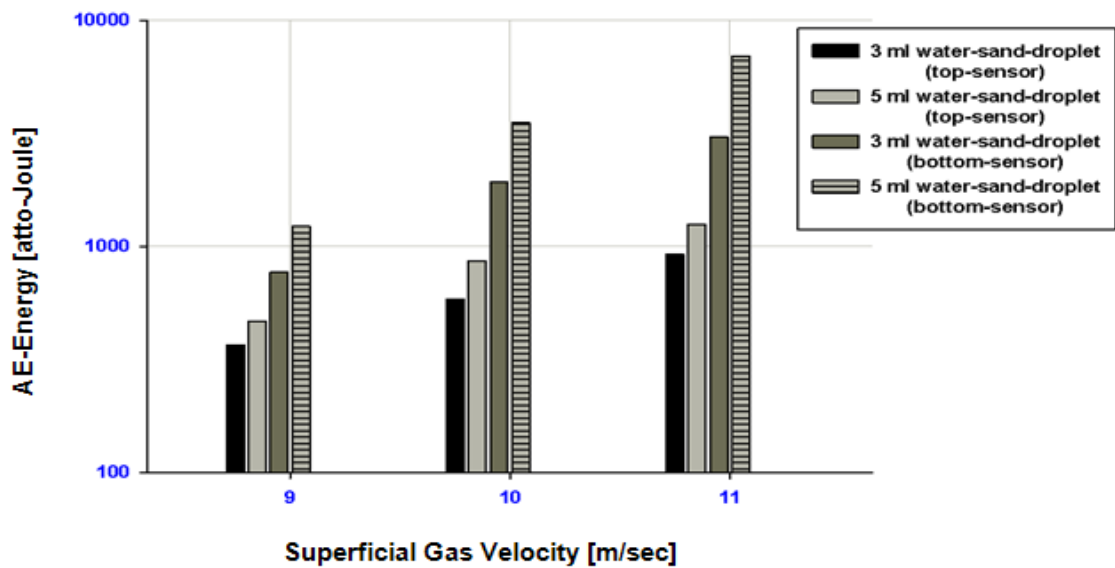


Figure 7-27: AE-Energy variation with increasing total droplet volume and Vsg captured by top & bottom sensors (water-sand droplets)

Results revealed that the energy captured by bottom sensor for both droplet volumes was higher than that captured by top sensor. This was attributed to the effect of gravitational force on the water-sand droplets causing impact of these droplets on the bottom of the pipe, closer to the sensor located at this position. Conversely the AE levels for the water only droplet was higher at the top sensor than the bottom sensor due to the lift force acting on the droplets, causing more impact with the top of the pipe, see Figure 7.28.

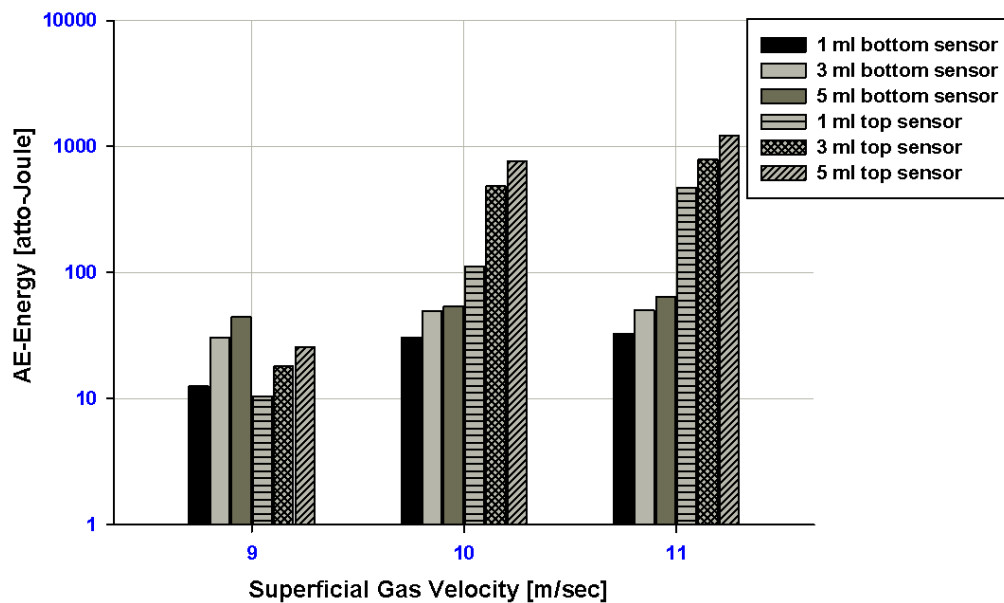


Figure 7-28: AE-Energy variation with increasing total droplet volume and V_{sg} captured by bottom & top sensors (water droplets)

Investigations in the time-frequency domain were undertaken with wavelet-analysis (AGU-Vallen Wavelet). Typical AE waveforms for a water-droplet and water-sand-droplet at V_{sg} of 9 ms^{-1} captured by bottom sensor are shown in Figures 7.29 and 7.30. These waveforms show that the AE transient events in the case of water-sand droplets were so closely coupled as to be of a continuous nature compared to water droplet. The authors attribute this to multiple impacts resulting in significantly more AE energy accumulated over a wider frequency range. The time-frequency plot (Figures 7.29 and 7.30) for droplet impacts on the pipe were different for the two cases both in terms of intensity and frequency range. From Figure 7.29 It was evident that the energy intensity levels between 450 kHz to 850 kHz were highest for water-only droplet impacts (220 to 240 μs). This level of intensity decreased significantly with time due to the attenuation; as can be seen from the decreased

energy levels at 330 μs . Figure 7.30 shows the maximum intensity of the AE energy for 5 ml water-sand droplet injection occurring at frequencies up to 1000 kHz (300 μs to 330 μs).

Figures 7.29 and 7.30, which are typical of all other test results, also demonstrate variations in the frequency content as a function of time. For instance, in Figure 7.29 the frequency between 220 μs and 240 μs had the highest energy intensity, because the initial part of the waveform contained the larger part of the energy of the impact signal. Reduction in frequency content was observed over 240 μs due to the dissipation in the energy of the impact signal. This would suggest that droplet impacts are responsible for the higher frequency content whilst the lower frequency, observed a few microseconds later, are attributed to attenuations and reflections. Figure 7.30 shows that the higher mass concentration of water-sand droplet had significantly greater impacts on steel pipe as evidenced by the presence of higher frequency content (up to 1000 kHz) across the recorded time frame in comparison to that recorded for water-only droplets. These results suggest that it may be feasible to investigate droplet characterisation by correlating particular high frequency bands over a time period with the total generated AE energy.

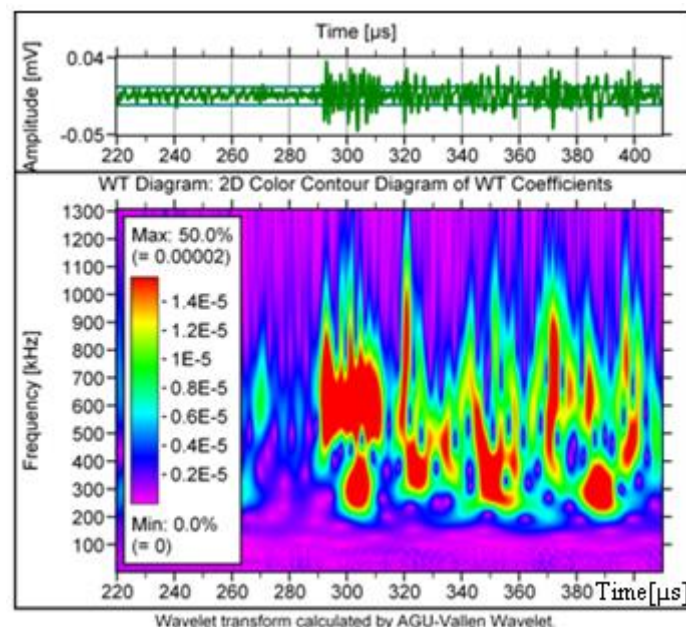


Figure 7-29: Wavelet analysis of AE signal for 5 ml of water-droplet at Vsg 9 ms^{-1} captured by bottom sensor

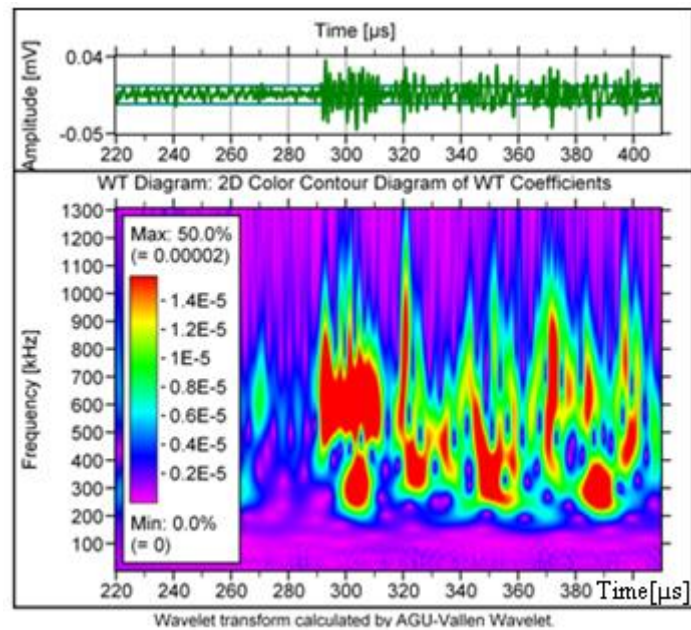


Figure 7-30: Wavelet analysis of AE signal for 5 ml of water-sand droplets at Vsg 9 ms⁻¹ captured by bottom sensor

It is known that the increase in gas flow rates leads to increase in AE energy levels, as seen in Figure 7.27 and 7.28. Wavelet transform can be used to depict the increase in AE energy levels, see Figures 7.29 and 7.30. At 9 ms⁻¹, the AE measured had frequency content up to 1000 kHz (Figures 7.30) whereas at 10 ms⁻¹, the frequency content reached 1300 kHz, see Figure 7.31.

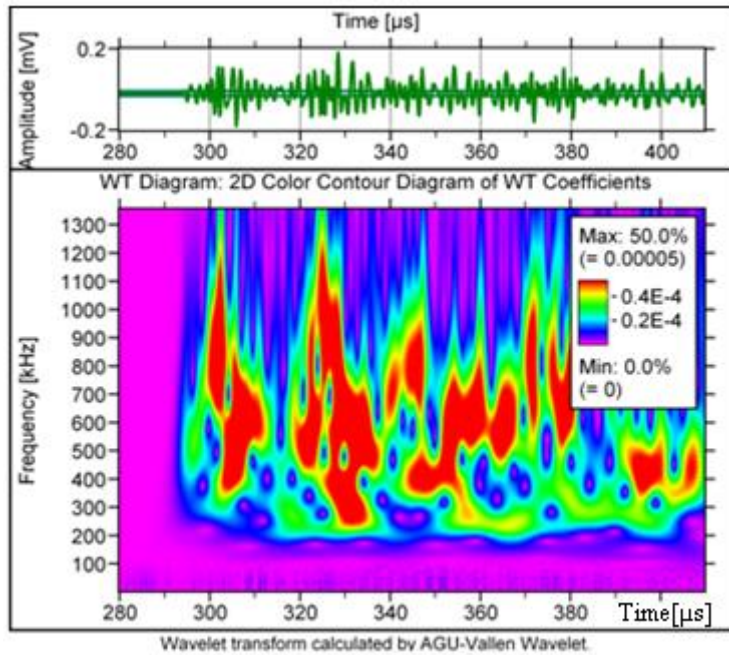


Figure 7-31: Wavelet analysis of AE signal for 5 ml of water-sand-droplets at $V_{sg} 10 \text{ ms}^{-1}$ captured by bottom sensor

Figure 7.32 and 7.33 illustrates a comparison between results that were recorded by the AE sensor located on top and bottom of the pipe for water only droplets. The results recorded at top AE sensor was analysed and showed that, the maximum intensity of AE energy at a frequency between 500 kHz and 900 kHz, see Figure 7.32. Whereas, the maximum frequency of the most intense AE energy captured from the bottom sensor was at approximately 600 kHz, see Figure 7.33. This was attributed to the impact of water droplet on the pipe top.

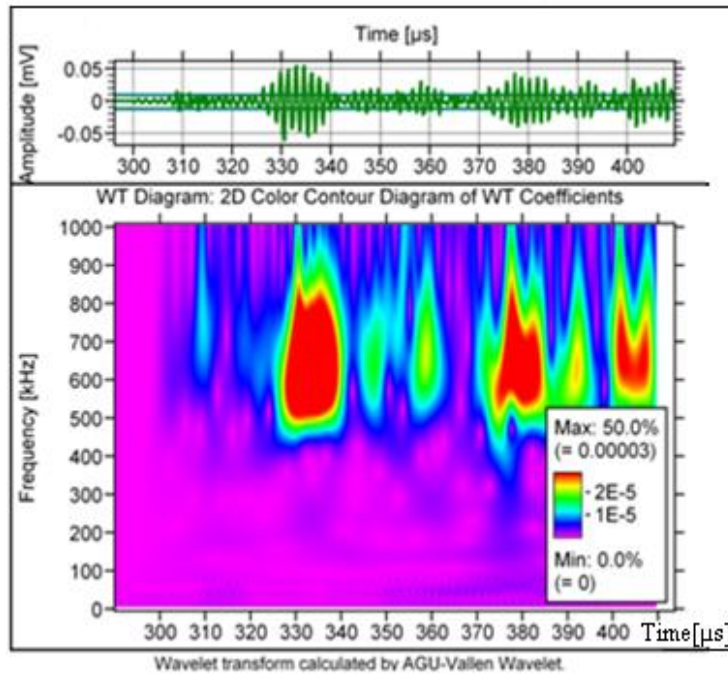


Figure 7-32: Wavelet analysis of AE signal for 5 ml of water-only at Vsg 11 ms⁻¹ captured by top sensor

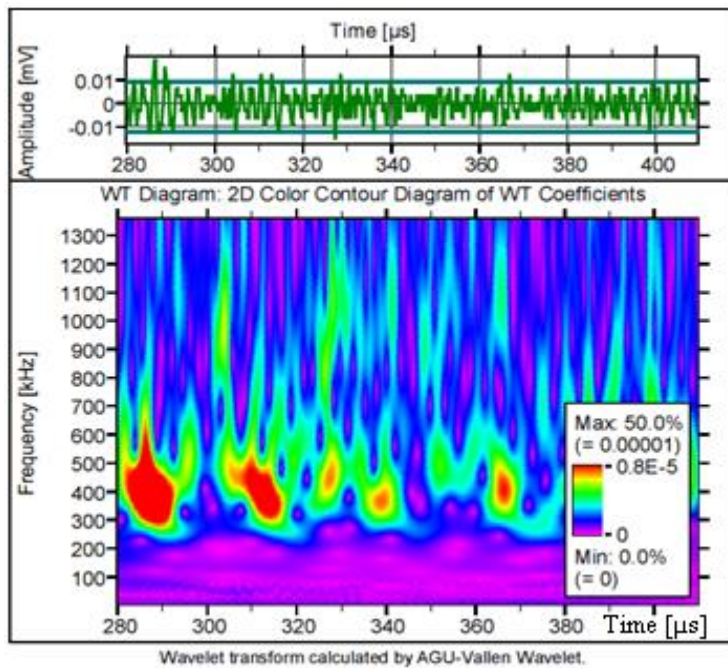


Figure 7-33: Wavelet analysis of AE signal for 5 ml of water-only droplets at Vsg 11 ms⁻¹ captured by bottom sensor (The red represents maximum energy)

8 Conclusion and Recommendations for Future Work

8.1 Conclusions

Prior to the multiphase flow experiments, impact tests using single particles of sand of diameters between 150 μm – 710 μm dropped from heights of 20 cm, 40 cm and 60 cm onto target plates (steel/ aluminium) were performed to assess the capability of AE sensors to detect the resulting sand impact. The results obtained show that a measurable AE signal was generated by the impacts and that the magnitude of the AE energy increased with particle size and drop height. The larger the mass and the greater the drop height the greater is the force of impact and thus the greater the resulting AE energy.

For monitoring sand particle concentration in air-sand two-phase flow, masses of sand from 0.1 g to 1.0 g in incremental steps of 0.1 g were injected into the horizontal pipe at superficial gas velocities (V_{SG}) of 8, 9, 10, 11 and 12 ms^{-1} . This test was to investigate the possible use of AE as a non-invasive technology for monitoring sand particle concentration levels in multi-phase flow conditions. The experimental findings clearly showed that the AE energy level increased with an increase in the quantity of sand injected for constant V_{SG} . It was also found that the AE energy level increased as the V_{SG} increased from 8 ms^{-1} to 12 ms^{-1} for the same quantity of sand injected. It is concluded that AE techniques can be used to assess the quantity of sand injected into a pipe for known flow rates. These findings provide the basis for the application of AE technology to monitoring three-phase flows in pipeline transportation.

For monitoring the presence of sand in air-water flow, the experimental investigation assessed concentrations of sand ranging from 300lb/1000bbl to 700lb/1000bbl in incremental steps of 100lb/1000bbl for superficial gas velocities (V_{SG}) between 0.2 ms^{-1} and 2.0 ms^{-1} and superficial liquid velocities (V_{SL}) between 0.2 ms^{-1} and 1.0 ms^{-1} . Both V_{SG} and V_{SL} were increased incrementally in steps of 0.1 ms^{-1} . The results of this investigation showed a correlation between AE energy levels, sand concentration, V_{SL} and V_{SG} . The results revealed that at constant V_{SL} an increase in

AE energy levels was noted with an increase in either V_{SG} or sand concentration. For a constant sand concentration AE energy levels increased with an increase in either the V_{SL} or V_{SG} , or both. The effects of sand concentration on AE energy levels for segregated flow regimes (stratified and stratified wavy) and intermittent flow regimes (plug and slug) in a horizontal pipe were also investigated experimentally.

Experimental observations reveal that stratified and stratified wavy flow (segregated flow regime) produced low AE energy levels due to the correspondingly lower values of V_{SL} and V_{SG} . Increase in V_{SL} caused a transition from stratified wavy flow to plug flow and led to an increase in AE energy levels. As V_{SG} was increased the plug flow became slug flow (intermittent flow regime) and there was a further increase in AE energy. The AE sensor recorded the highest values of AE energy under the slug flow regime due to the relatively high values of V_{SL} and V_{SG} . It was also found that AE energy levels increased with an increase in the quantity of sand injected.

To identify the minimum sand transport condition (MTC) in two-phase flow the experimental investigation involved assessing the sand concentration from 300lb/1000bbl to 700lb/1000bbl in incremental steps of 100lb/1000bbl. As previously the V_{SL} ranged from 0.1 ms^{-1} to 1.2 ms^{-1} . MTC represents the conditions at which the sand particles remain continuously suspended in the flow with minimal deposition. MTC was identified by monitoring AE energy levels. The results of the investigation showed that AE energy levels were influenced by variation of V_{SL} and sand concentration. The relation between the MTC and the sand concentration is a linear relationship.

To determine the AE energy levels produced by droplets within a flow in a horizontal pipe, several tests were undertaken using two different types of droplets (water and water/sand) were injected into the flow. The volume of the droplets ranged from 1 ml to 5 ml in incremental steps of 1 ml. The droplets were injected into the pipe at V_{SG} values of 9 ms^{-1} , 10 ms^{-1} and 11 ms^{-1} . The results clearly showed a correlation between AE energy levels, V_{SG} and volume of droplets injected. The results also demonstrated that AE energy levels increased with increase in the volume of droplets injected for the same V_{SG} . For the same droplet volume the AE energy levels also increased with an increase in V_{SG} . The results demonstrated that AE energy levels generated by the impact of water-sand droplets were higher than the

impact generated by water droplets, this is due to the greater mass of water-sand droplets for the same volume.

8.2 Recommendations for future work

This work has demonstrated that in principle AE technology can be used to monitor sand particle movement in a horizontal pipe. However, these responses only indicate that sand is present (detection) but do not provide a measure of how much damage the sand has caused. Thus, this research could be extended to cover the influence of impact angle and attenuation of the AE signal in the material forming the wall of the pipe.

This research work only investigated air-sand flow, air-water-flow and air-water-sand flow, further experimental tests should be conducted in order to investigate sand transport characteristics in air-oil and oil-water two-phase flows and air-oil-water three-phase flows. This research study was undertaken with horizontal pipes and so could be extended to vertical pipes.

Due to the limitations of the air compressor used in this project, only velocities up to 12 ms^{-1} were used. By increasing the capability of the air compressor, higher velocities and a greater range of flow regimes such as, annular and annular mist flows could be investigated.

REFERENCES

- [1] Al-Lababidi S., Mba D. and Addali A. (2012), Upstream multiphase flow assurance monitoring using acoustic emission, acoustic emission, Dr. Wojciech Sikorski (Ed.), ISBN:978-953-51-0056-0, *inTech*.
- [2] Goharzadeh A. and Rodgers P. (2008), Experimental characterization of solid particle transport by slug flow particle image velocimetry, *Journal of Physics: the 6th international symposium on measurement techniques for multiphase flows*, Conference Series 147 (2009) 012069, 15-17 December 2008, Naha, Okinawa, Japan.
- [3] Shirazi S. A., McLaury B.S. and Ali, M.M. (2000), Sand monitor evaluation in multiphase flow, *NACE International Conference*, Paper No. 00084.
- [4] Falcone G., Hewitt, G.F. and Alimonti, C. (2009), *Multiphase Flow Metering: Principles and Applications*, Elsevier, Developments of Petroleum Science Series, October 2009. ISBN-13: 978-0-444-52991-6, ISBN-10: 0-444-52991-8.
- [5] Tekna (ed.) (2005), *Handbook of Multiphase Flow Metering*, Rev. 2 ed.
- [6] Mark S., Zhi Y., Lynn G., Michael L. J., Derek L. and Benedict N. (2009), Sprite MRI of bubbly flow in a horizontal pipe, vol.199, pp. 126-135.
- [7] Hewitt G. F. (1982), Liquid-gas systems, In G. Hetsroni (Editor), *Handbook of Multiphase Flow Systems*, McGraw Hill book company, New York.
- [8] Schetz J. A. and Fuhs A. E. (1999), *Fundamentals of Fluid Mechanics*, John Wiley & sons.
- [9] Fan L.S. and Zhu C. (1998), *Principles of Gas-Solid Flows*, Cambridge University Press.
- [10] Vanoni V. A. (2006), *Sedimentation Engineering*, Library of Congress, USA.
- [11] Perez V. H. (2007), *Gas-liquid two-phase flow in inclined pipes* (PhD Thesis), University of Nottingham.

- [12] Beggs H. D. and Brill J. P. (1973), A study of two-phase flow in inclined pipes, Paper SPE 4007, *SPE-AIME 47th Annual Fall Meeting*, San Antonio, Tex.
- [13] Weber M. (1982), Vertical hydraulic conveying solids by air-lift, *Journal of pipelines*, Vol. 3, No. 2, 1982, pp. 137-152.
- [14] Heywood N. I. and Richardson J. F. (1978), Head loss reduction by gas injection for highly shear-thinning suspensions in horizontal pipe flow, *In: Proc Hydro-transport 5*, Paper C1, organised by BHRA Fluid Engineering, UK.
- [15] Acikgoz M., Franca F. and Laher R. T. (1992), An experimental study of three-phase flow regimes, *International Journal of Multiphase Flow* 18 (3): 327.
- [16] Bratland O. (2010): Pipe Flow 2, Multiphase Flow Assurance, available at <http://drbratland.com/PipeFlow2/>
- [17] Al-Lababidi S, Yan W. and Yeung H. (2007), Sand transportation in multiphase pipelines-minimum transport condition for water and two-phase air water flows in horizontal and inclined 2-inch pipe, Report No. 07/SA/S08.
- [18] Bird J. and Ross C. (2012), *Mechanical Engineering Principles*, second edition published 2012 by Routledge.
- [19] Omega (2001), *Flow & Level Measurement*, A Technical Reference Series brought by Omega, vol. 4.
- [20] Storck A., Latifi M. A., Barthole G., Laurent A. and Carpenter J. C. (1986), Electrochemical study of liquid-solid mass transfer in packed bed electrodes with upward and downward co-current gas-liquid flow, vol. 16, pp. 947-963.
- [21] Ahmed W. H. (2006), Capacitance sensors for void-fraction measurements and flow pattern identification in air-oil two-phase flow, vol. 6, pp. 1153-1163.
- [22] Tavoularis S. (2005), *Measurement in Fluid Mechanics*, Cambridge University Press 2005.

- [23] Klausner J. F. and Grove R. (2008), Solids composition measurements of phosphate slurry using impedance spectroscopy, Phase I: Feasibility study, Final report, University of Florida.
- [24] Hauptmann P., Hoppe N. and Puttmer A. (2002), Review Article Application of Ultrasonic Sensors in the Process Industry, vol. 13, pp. 73-83.
- [25] FlowMeters C. (2010), Ultrasonic Flowmeters, available at: <http://www.flowmeters.com/ufm/index.cfm?task=ultrasonic> (accessed December).
- [26] Sanderson M. L. and Yeung H. (2002), Guidelines for the use of ultrasonic non-invasive metering techniques, *Flow Measurement and Instrumentation*, vol. 13, No. 4, pp. 125-142.
- [27] Zuzunaga A. and Maron B. (2013), A survey of non-invasive and semi-invasive flow meters for mining applications: Understanding and selecting the right technology for the application, CiDRA Minerals Processing, Wallingford, USA.
- [28] Raffel, M., Willert, C. E., Wereley, S.T. and Kompenhans J. (2007), Particle Image Velocimetry, Second Edition Springer Berlin Heidelberg New York.
- [29] Shats, M., and Punzmann, H. (2006), Turbulence and Coherent Structures in Fluids, Plasmas and Nonlinear Media, World Scientific Publishing Co. Pte Ltd.
- [30] Adrian R. J. and Westerweel J. (2011), Particle Image Velocimetry, Cambridge University Press, 2011.
- [31] Jamaludin J., Zawahir M. Z., Abdul Rahim R., Yunus F. R. M., Nor Ayob N. M., Ridzuan Aw M. S., Fadzil N. S., Zakaria Z. and Fazalul Rahiman M. H. (2013), A review of tomography system, *Journal Technology (Science & Engineering)*, 64:5 (2013) 47-51.
- [32] Rasteiro M. G., Silva R., Garcia F. A. P. and Faia P. (2011), Electrical Tomography: a review of configurations and applications to particulate processes, *KONA Powder and Particle Journal* No. 29.

- [33] Williams, R.A. and Beck, M.S. (1995), *Process tomography: Principles, Techniques and Applications*, Butterworth-Heinemann, Oxford, 1995.
- [34] Liu Y., Wang X. and Takei S (2013), Solid-liquid two-phase flow image reconstruction based on ERT technique in microchannel, *TELKOMNIKA*, vol. 11, No. 1, pp. 173-180.
- [35] Mahmoud A., Fernandez A. and Arlabosse P. (2008), Analysis of electrical phenomena occurring in thermally assisted mechanical dewatering processes (TAMD)-a preliminary study, *INTECH*, ISBN 978-3-902613-25-7.
- [36] Miller R. K. and McIntire P. (1987), *Acoustic Emission Testing- Non-destructive Testing Handbook*, vol. 5 (*American Society for Non-destructive Testing*), 1987, ISBN 0-931403-02-2.
- [37] Elforjani M. A. (2010), *Condition monitoring of slow speed rotating machinery using acoustic emission technology (PhD Thesis)*, Cranfield University, Cranfield University Library.
- [38] Jones O. C and Delhaye J. M. (1976), Transient and statistical measurement techniques for two-phase flow, *Intl J of Multiphase Flow*, vol. 3, No. 2, pp. 89-116.
- [39] Cartellier A. and Achard J. L. (1990), Local phase detection probes in fluid-fluid two-phase flow, *Review of Scientific Instruments*, vol. 62, No. 2, pp. 279-303.
- [40] Werther J. (1999), Measurement techniques in fluidized beds, *Powder Technology*, vol. 102, No. 1, pp. 15-36.
- [41] Nicol, R. S. and Davidson, J. F. (1988), Gas holdup in circulating bubble columns, *Chemical Engineering Research and Design*, vol. 68, No. 2, pp. 152-158.
- [42] Nasr El-Din, H. A., Mac Taggart, R. S. and Masliyah J. H. (1996), Local solids concentration measurement in a slurry mixing tank, *Chemical Engineering Science*, vol. 51, No. 8, pp. 1209-1220.
- [43] Chaouki, J., Larachi, F. and Dudukovic, M. P. (1997), *Non-invasive monitoring of multiphase flows*, Elsevier Science B. V, ISBN: 0-444-82521-5.

- [44] MacKinnon, A., Brown, J. and Brown, G. K. (2011), Keeping acoustic sand monitoring simple, *NACE International Corrosion Conference & EXPO*, Paper No. 11396.
- [45] Deddis, C. (2008), Sand detection and monitoring position, (EPTG, BP), Aberdeen, Scotland, UK.
- [46] Nezhati, K., Roth, N. and Gaskin, R. (2000), On-line determination of particle size and concentration (solids and oil) using ViPA Analyser - A way forward to control subsea separators” presented at the IBC Production Separation Systems Conference, available at: <http://www.iceweb.com.au/Analyzer/Oil%20in%20Water/ViPA%20Tech%20Description.pdf> (accessed December).
- [47] Salama, M. M. (2000), Performance of sand monitors, *NACE International Corrosion Conference & EXPO*, Paper No. 85.
- [48] Bellarby, J. (2009), Well completion design, First Edition, 2009, Elsevier Science B. V., ISBN: 978-0-444-53210-7.
- [49] Wold, k., Stoen, R. and Rapone, M. (2012), Integration of intrusive and non-intrusive methods for corrosion and sand/erosion monitoring, *La Metallurgia Italiana* – No. 2/2012.
- [50] Wold, K. and Hopkins, S. (2009), Companies move toward integrated sand monitoring, *Sand Control E & P*, pp. 59-60.
- [51] Al-Lababidi, S., Yan, W. and Yeung, H. (2012), Sand transportation and deposition characteristics in multiphase flow in pipelines, *J. Energy Resources Technology*, vol. 134/34501-13, DOI: 10.1115/1.4006433.
- [52] Zhu, Z., Sand, K. W., and Teevens, P. J. (2010), Solids deposition in liquid petroleum (oil) and wet-gas pipelines for internal corrosion predictive modelling (ICPM), Proceeding of *Northern Area Western Conference (NACE)*, 2010, Calgary, Alberta.
- [53] Lynn, R. S., Wong, K. K. and Clark, H. M. (1991), On the particle size effect in slurry erosion, *Journal of Wear*, 149, pp. 55-71.
- [54] Buttle, D. J. and Scruby, C. B. (1990), Characterisation of Particle Impact

by Quantitative Acoustic Emission, *Journal of Wear*, vol. 137, pp. 63-90.

- [55] Shi, H., Cai, T. Y. and Jepson, W. P. (1999), Oil-water distributions in large diameter horizontal pipelines, Multiphase flow and heat transfer, *Proc, Fourth International Symposium*, Aug. 22-24, 1999, Xi'an China.
- [56] Singh, S. (2012), Experiments in Fluid Mechanics, Second edition, ISBN-978-81-203-4511-9, Printed by Mudrak, New Delhi.
- [57] Sumer, M. P. and Serife, S. H. (2008), Solid-Liquid Two-Phase Flow, Elsevier Science B. V., ISBN: 978-0-444-52237-5.
- [58] Richard, R. U. (2012), Sand transport by oil in tubing and pipelines, NTNU Faculty of Engineering, Norwegian University of Science and Technology, Faculty of Engineering, Science and Technology, Department of Petroleum Engineering and applied Geophysics. Available at: <http://www.ipt.ntnu.no/~jsg/studenter/prosjekt/2012RichardProject.pdf> (accessed December).
- [59] King, R. P. (2002), Introduction in Practical Fluid Flow, University of Utah, ISBN-0-7506-4885-6, www.itegra-india.com.
- [60] Chemloul, N. S., Chaib, K. and Mostefa, K. (2004), Simultaneous measurements of the solid particles velocity and concentration profiles in two phase flow by pulsed Ultrasonic Doppler Velocimetry, *J. of the Braz. Soc. of Mech. Sci. & Engineering*, Vol. XXXI, No. 4, pp.333- 343.
- [61] Goharzadeh, A. and Rodgers, P. (2009), Experimental characterisation of solid particle transport by slug flow using Particle Image Velocimetry, *Journal of Physics: Conference Series* 147 (2009) 012069.
- [62] Bello, O. O., Reinicke, K. M. and Teodoriu, C. (2005), Particle holdup profiles in horizontal gas-liquid-solid multiphase flow pipeline, *Journal of Chemical Engineering and Technology*, vol. 28, No. 12, pp. 1546-1553.
- [63] Duclos, J., Reuben, R. L. and Steel, J. A. (2004), Study of particle impacts in fluid flow using acoustic emission, *COMADEM 2004 International Congress & Exhibition on Machine Tool Performance Monitoring*, Heriot-Watt University, UK, pp. 566-575, ISBN 0-954-1307-1-5.

- [64] Albion, K., Briens, L., Briens, C. and Berruti, F. (2007), Flow regime determination in horizontal pneumatic transport of fine powders using non-intrusive acoustic probes, *Powder Technology*, vol. 172, Issue 3, 23 March 2007, pp. 157-166, ISSN 0032-5910.
- [65] Mazumder, Q. H., Santos G., Shirazi, S. A. and McLaury, B. S. (2003), Effect of sand distribution on erosion in annular three-phase flow, *Proceeding of ASME Fluids Engineering Division Meeting, FEDSM*, 2003-45498, Honolulu, July 6-10, 2003.
- [66] Drouillard, T. F. (1996), A history of acoustic emission, *Journal of AE* , vol. 14, No. 1, pp. 1-34.
- [67] Hellier, C. (2001), *Handbook of Non-destructive Evaluation*, McGraw-Hill, New York; London.
- [68] Holroyd, T. J. (2000). *The Acoustic Emission and Ultrasonic Monitoring*, Coxmoor Publishing Company, Oxford, UK.
- [69] Al-Lababidi, S., Addali A., Yeung H., Mba D., And Khan K. (2009), Gas void fraction measurement in two-phase gas-liquid slug flow using acoustic emission technology, *ASME*, 2009, vol. 131, No. 6, 064501, pp. 693-702.
- [70] Sikorska, J.Z., and Mba D. (2008), Truth, lies acoustic emission and process machines. *IMechE Part E*, 2008, vol. 222, No. 1), pp. 1-19.
- [71] Mohammadi, J. (2004), *NDT Methods Applied to Fatigue Reliability Assessment of Structures*, American Society of Civil Engineering, ISBN – 07844-0742-8.
- [72] Austin, R. K. and Coughlin, C. (2006), Distributed mode system for real time acoustic emission monitoring, Texas Research International, Inc., Invention – US-7080555-B2, Awarded by the U.S. Army.
- [73] Scruby, C. B. (1987), *Instrument science and technology*, An introduction to acoustic emission, *J. Phys. E: Sci. Instrum.* 20 (1987), pp. 946-953.
- [74] Miettinen, JPP. (1999), Acoustic emission in monitoring extremely slowly rotating rolling bearing, COMADEM 99, *Proceeding of The Twelfth International Congress on Condition Monitoring and Diagnostic Engineering*

Management, Oxford, UK, pp. 289-297.

- [75] Saches, W., Jmaes, R. and Yamaguchi, K. (1989), Acoustic Emission: current practice and future directions, *Paper presented at a symposium on world meeting on acoustic emission*, Charlotte, NC, on 20-23 March 1989, sponsored by AEWG.
- [76] Bendat, J. S. and Piersol, A. G. (2010), *Random data: analysis and measurement procedures*, 4th edition, Wiley, ISBN: 978-0-470-24877-5.
- [77] PAC (2007), *PCI-2 Based AE System User's Manual*, Physical Acoustics Corporation, Princeton Junction.
- [78] Vallen, S. (2012), *Acoustic Emission Sensors Specification*, Vallen Systeme GmbH.
- [79] Staszewski, W. J., Boller, C. and Tomlinson, G. R. (2004), *Health monitoring of aerospace structures: Smart sensor technologies and signal processing*, ISBN – 0-470-84340-3, John Wiley & sons Ltd, UK.
- [80] Grosse, C. U. and Ohtsu, M. (2008), *Acoustic Emission Testing: Basics for research applications in civil engineering*, ISBN 978-3-540-69972-9, Springer-Verlag BerlinHeidelberg.
- [81] NDT – ed. (210), *Modes of Sound Wave Propagation*, available at: www.ndt-ed.org/EducationResources/CommunityCollge/Ultrasonics/Physics/modeperopagation.htm (accessed December).
- [82] Calibration Principles, available at: http://www.isa.org/Template.cfm?Section=Find_Books1&template=Ecommerce/FileDisplay.cfm&ProductID=7577&file=ACFBA59.pdf (accessed December).
- [83] ASTM E 976 (1945), *Standard Guide for Determining the Reproducibility of Acoustic Emission Sensor Response*, American Society for Testing and Materials, West Conshohocken, USA.
- [84] Grosse, U. C. (2007), *Hsu-Nielsen Sources, Non-destructive Testing Encyclopaedia (NDT.net) Publications, Acoustic Emission (AE)*, available at:

www.ndt.net/ndtaz/ndtaz.php (accessed December).

- [85] Yan, T., Jones, B. E. (2000), Traceability of AE measurements using energy calibration methods, *Measurement Science and Technology*, doi:10.1088/0957-0233/11/11/101.
- [86] Johnson, R. W. (2000), Analyse Hazards - Not Just Risks, *Chemical Engineering Progress*, vol.96, No. 7, pp. 31 – 40.
- [87] Pumphrey, H. C. and Crum, L. A. (1989), Sources of ambient noise in the ocean and experimental investigation, Technical Report NCPA LC.011989, University of Mississippi.
- [88] Husin, S. (2011), Experimental investigation into the correlation between acoustic emission and bubble dynamic, (PhD Thesis), Cranfield University, Cranfield University Library.
- [89] Matula, T. J., Hallaj, I. M., Cleveland, R. O. and Crum, L. A. (1998), The acoustic emission from single-bubble sonoluminescence, *J. Acoust. Soc. Am*, vol. 103, No. 3, pp. 1377-1382.
- [90] Manasseh, R., Riboux, G. and Risso, F. (2008), Sound generation on bubble coalescence following detachment, *International Journal of Multiphase Flow*, vol. 34, pp. 938-949.
- [91] Kamp, A. M., Chesters A. K., Colin, C. and Fabre, J. (1999), Bubble coalescence in turbulent flows: a mechanistic model for turbulence-induced coalescence applied to microgravity bubbly pipe flow, *International Journal of Multiphase Flow*, vol. 27, pp. 1363-1396.
- [92] Yaacob, M. M., Alsaedi, M. A., Abdul Rahman, R., Bidin, N., Aqbool, W., Al-geelani, N. A. and Hosseinian, R. (2013), Detection and wavelet analysis of acoustic emission signal from partial discharge captured by multimode optical fiber and piezoelectric sensors in insulation oil, *Int. J. Phys. Sci.*, vol. 8, No. 21, pp. 1149-1160.
- [93] Derakhshan, O., Houghton, J.R., Jones, R.K. and March, P.A. (1989), Cavitation monitoring of hydro-turbines with RMS acoustic emission measurement, Symposium on Acoustic Emission: Current Practice and

Future Directions, Mar 20-23 1989 Published by ASTM, Philadelphia, PA, USA, Charlotte, NC, USA, pp. 305.

- [94] McNulty, P.J. (1985), Pump Hydraulic Noise: Its Uses and Cures, Marine Engineers Review, pp. 22-23.
- [95] Brennen, C. E., (1995) Cavitation Bubble Dynamics, Oxford University Press, ISBN: 0-19-509409-3.
- [96] Fahy, F. (2001), Foundations of Engineering Acoustics, Elsevier Academic Press, ISBN 0-12-247665-4.
- [97] Ziehl, P. H. (2008), Application of Acoustic Emission Evaluation for Civil Infrastructure, *Proc. of SPIE*, vol. 6934, No. 1.
- [98] Grosse, C.U. and Reinhardt, H.W. (2002), Signal conditioning in acoustic emission analysis using wavelets, *NDT.net* - September 2002, 7(9).
- [99] Maradei, C., Piotrkowski, R., Serrano, E. and Ruzzante, J.E. (2003), Acoustic emission signal analysis in machining process using wavelet packets, *Lat. Am. Res* [online], ISSN: 1851-8796, vol. 33, No. 4, pp. 443-448.
- [100] Piotrkowski, R., Gallego, A., Castro, E., Garcia-Hernandez, M. and Ruzzante, J. (2005), Ti and Cr nitride coating/steel adherence assessed by acoustic emission wavelet analysis, *NDT & E International*, 38, pp. 260-267.
- [101] Spasova, L.M. and Ojovan, M.I. (2008), Characterisation of Al corrosion and its impact on the mechanical performance of composite cement waste forms by the acoustic emission technique, *Journal of Nuclear Materials*, 375(3), pp. 347-358.
- [102] Parker, M. (2010), Digital Signal Processing, Elsevier Academic Press, ISBN 978-1-85617-921-8.
- [103] Havelock, D., Kuwano, S. and Vorlander, M. (2008), Handbook of Signal Processing in Acoustics - The FFT and Tone Identification, Springer, ISBN 978-0-387-30441-0.
- [104] Yoon, D.J., Weiss, W.J. and Shah, S.P, (2000), Assessing damage in

corroded reinforced concrete using Acoustic Emission. *Journal of Engineering Mechanics*, vol. 273, March, pp. 273-283.

- [105] Efi Foufoula, G. and Kumar, P. (1994), *Wavelet Analysis and its Applications*, Volume 4, Academic Press, INC., ISBN 0-12-262850-0.
- [106] Carmona, R., Hwang, W. L. and Torresani, B. (1998), *Wavelet Analysis and its Applications*, Volume 4, Academic Press, INC., ISBN 0-12-160170-6.
- [107] Chau, F. T., Liang, Y. Z., Gao, J. and Shao, X. G. (2004), *Chemometrics: From Basics to Wavelet Transform*, John Wiley & Sons, ISBN 0-471-20242-8.
- [108] Boulahbal, D., Farid Golnaraghi, M. and Ismail, F. (1999), Amplitude and phase wavelet maps for the detection of cracks in geared systems. *Mechanical and Signal Processing*, vol. 13, No. 3, pp. 423-436.
- [109] Ferlez, R.J. and Lang, D.C. (1998), Gear-Tooth Fault Detection and Tracking Using the Wavelet Transform, Prognosis of Residual Life Machinery and Structures, *Proceedings of the 52nd Meeting of the Society for Machinery Failure Prevention Technology*, pp. 451-460.
- [110] Loutas, T.H., Sotiriades, G. and Kostopoulos, V. (2004), On the application of wavelet transform of AE signals from composite materials. DGZfP-Proceedings BB 90-CD, Lecture 42, *EWGAE*.
- [111] Wang, W.J. and McFadden, P.D. (1996), Application of wavelets to gearbox vibration signals for fault detection. *Journal of Sound and Vibration*, vol. 192, No. 5, pp. 927-939.
- [112] El-Alej M, Mba D and Yan T, Investigation on sand particle impingement on steel pipe in two phase flow using acoustic emission technology, *The Journal of Applied Mechanics and Material*, ISSN 1660-9336, ISBN 978-3-03785-635-2.
- [113] Alssayh, M. A. (2013), Slug velocity measurement and flow regime recognition by using acoustic emission technology, (PhD Thesis), Cranfield University, Cranfield University Library.

- [114] Enwald, H. and Peirano, E. (1996), Almstedt A., and Eulerian (1996) Two-phase flow theory applied to fluidization, *International Journal of Multiphase Flow*, vol. 22 suppl., pp. 21-66.
- [115] Shi, H. and Kleinstreuer, C. (2007) Simulation and analysis of high-speed droplet spray dynamics, *Journal of Fluid Engineering*, vol. 129/621.
- [116] El-Alej, M, Mba, D, Yan t. and Alssayh, M. (2013) Identification of minimum transport condition for sand in two-phase flow using acoustic emission technology, *Journal of Applied Acoustics*, vol. 74, pp. 1266–1270.
- [117] Brennen, C. E., (2005), *Fundamentals of Multiphase Flow*, Cambridge University Press.
- [118] Aoda, Z. (2010), Visualization of flow pattern and measurement of liquid distribution in random packed column using electrical resistance tomography (ERT), Paper 665.
- [119] Breyse, D. (2012), *Non-Destructive Assessment of Concrete Structures: Reliability and Limits of Single and Combined Techniques*, Springer, ISBN 978-94-007-2735-9.
- [120] Wang, H. (2007), Signal processing for in-seam seismic based void detection technique, (PhD thesis), The Pennsylvania State University.
- [121] Balgobin, C. J. (2005), Sand Management of Ultra-High-Rate Gas Wells, *Latin American and Caribbean Petroleum Engineering Conference*, Rio de Janeiro, Brazil, 20-30, June, 2005.
- [122] Fernando, H. (2013), *Handbook of Environmental Fluid Dynamics*, CRC Press, USA, ISBN-13: 978-1-4665-5601-0.
- [123] Flake, C. (2012), *Phase diagrams, understanding the basics*, library of congress, ISBN-13: 978-1-61503-835-0, ASM International, USA.

Appendices

Appendix A

Table A-1: Experimental measurement method (1.5mm aluminium plate)

Drop Height (cm)	Particle Size (μm)	AE-Energy (atto-Joules)
20	150	809.11
	355	9253.66
	500	157310.67
	710	852961.25
40	150	2204.57
	355	42943.59
	500	346042.69
	710	4202738.50
60	150	2642.00
	355	80217.77
	500	988221.31
	710	6848772.00

Table A-2: Experimental measurement method (1.5mm steel plate)

Drop Height (cm)	Particle Size (μm)	AE Energy (atto-Joules)
20	150	1331.45
	355	16013.16
	500	382659.13
	710	1229647.50
40	150	2426.22
	355	85321.92
	500	956855.06
	710	5949023.50
60	150	4363.46
	355	89478.77
	500	2088509.75
	710	7322498.50

Appendix B

Table B-1: AE Energy VS Superficial Gas Velocity (V_{SG}) for Different Superficial Liquid Velocity (V_{SL}) and fixed Sand Concentration (SC)

Superficial Liquid Velocity (V_{SL}) m/s	Superficial Gas Velocity (V_{SG}) m/s	AE-Energy atto-Joules (SC = 0lb/1000bbl)	AE-Energy atto-Joules (SC = 300lb/1000bbl)	AE-Energy atto-Joules (SC = 400lb/1000bbl)	AE-Energy atto-Joules (SC = 500lb/1000bbl)	AE-Energy atto-Joules (SC = 600lb/1000bbl)	AE-Energy atto-Joules (SC = 700lb/1000bbl)
0.2	0.2	180.55	371.67	876.43	988.78	1201.46	1540.26
	0.4	324.64	731.44	1090.96	1685.38	2204.34	2392.43
	0.6	701.19	1450.23	2100.62	2571.75	2690.09	2855.83
	0.8	954.00	2000.28	2908.35	2929.04	2995.52	3480.35
	1.0	1283.06	2766.00	3180.17	3608.90	3946.34	4162.25
	1.2	2162.86	3254.07	4195.08	4624.07	5148.15	5530.10
	1.4	1871.90	5005.99	6275.88	6426.76	7396.79	8997.40
	1.6	2610.04	5265.33	7736.68	8710.51	9862.58	10245.90
	1.8	3086.47	8082.40	8698.57	9867.27	10264.00	12764.90
	2.0	3113.69	9642.91	11090.18	11473.54	12877.32	13849.97
0.4	0.2	207.32	454.77	1035.98	1552.62	2051.96	2116.28
	0.4	373.72	887.81	1407.85	3282.69	5260.90	5988.43
	0.6	740.79	1829.53	2492.61	4106.86	7322.36	7540.94
	0.8	1089.62	2339.67	3378.22	5580.36	9508.07	9595.83
	1.0	1870.70	2949.81	6403.83	9263.59	10374.91	10948.06
	1.2	2113.07	5606.27	7743.74	10281.83	14012.10	14351.28
	1.4	2189.25	8184.67	8794.99	11796.92	16904.04	17721.34
	1.6	2849.11	10771.67	11297.13	12548.36	19056.88	19183.02
	1.8	3404.73	12042.82	14317.81	16907.44	21434.42	22358.70
	2.0	3695.43	18679.41	20520.59	24131.44	24949.66	27071.79

Superficial Liquid Velocity (V_{SL}) m/s	Superficial Gas Velocity (V_{SG}) m/s	AE-Energy atto-Joules ($SC =$ 0lb/1000bbl)	AE-Energy atto-Joules ($SC =$ 300lb/1000bbl)	AE-Energy atto-Joules ($SC =$ 400lb/1000bbl)	AE-Energy atto-Joules ($SC =$ 500lb/1000bbl)	AE-Energy atto-Joules ($SC =$ 600lb/1000bbl)	AE-Energy atto-Joules ($SC =$ 700lb/1000bbl)
0.6	0.2	250.83	580.47	1471.16	2449.45	7798.31	7861.48
	0.4	375.59	1262.87	2360.43	4860.65	10149.58	10238.57
	0.6	855.57	2061.06	4203.92	4888.08	12257.24	13683.17
	0.8	1233.21	3434.59	4776.13	8114.67	16033.35	18878.50
	1.0	2061.06	4704.03	10299.36	13670.93	21466.13	22569.82
	1.2	2558.05	8110.36	18203.35	19477.26	33396.08	34826.90
	1.4	3364.80	17375.54	19704.75	23436.78	39668.59	41632.57
	1.6	3855.94	19047.87	24915.09	29842.71	41470.75	44231.16
	1.8	4009.82	25022.77	25123.61	35714.20	43036.37	48521.09
2.0	4328.82	27952.83	29044.88	37235.92	49950.06	53708.60	
0.8	0.2	284.95	905.54	1892.50	3745.85	8186.47	8483.07
	0.4	459.23	1582.38	3197.27	5396.52	12739.95	12989.35
	0.6	1087.50	2613.56	8105.27	8812.65	16911.55	16988.67
	0.8	1891.91	6085.10	10242.25	11267.24	18142.54	25933.15
	1.0	2352.64	10899.15	17912.30	28064.17	30501.04	33226.40
	1.2	3096.29	12700.20	30414.11	33382.75	37087.99	39722.62
	1.4	4167.95	18926.20	37763.06	45241.39	52477.13	55358.23
	1.6	4251.73	25521.86	39322.80	50922.36	61202.23	63013.02
	1.8	5274.08	37798.93	41025.09	57669.01	72382.05	74100.31
2.0	6293.71	50323.72	50323.72	67005.23	81545.09	85255.02	

Superficial Liquid Velocity (V_{SL}) m/s	Superficial Gas Velocity (V_{SG}) m/s	AE-Energy atto-Joules ($SC =$ 0lb/1000bbl)	AE-Energy atto-Joules ($SC =$ 300lb/1000bbl)	AE-Energy atto-Joules ($SC =$ 400lb/1000bbl)	AE-Energy atto-Joules ($SC =$ 500lb/1000bbl)	AE-Energy atto-Joules ($SC =$ 600lb/1000bbl)	AE-Energy atto-Joules ($SC =$ 700lb/1000bbl)
1.0	0.2	315.81	3981.46	4311.35	4459.36	8343.96	8532.02
	0.4	631.90	5437.70	5877.38	9735.43	14359.48	15838.43
	0.6	1379.66	6817.95	9326.66	11632.37	17939.04	19896.14
	0.8	2096.35	10447.59	15341.32	16087.08	21660.40	30025.89
	1.0	2682.14	15361.35	28320.90	35726.10	36772.73	39088.50
	1.2	3538.05	24229.53	40345.59	45214.62	58674.48	61813.98
	1.4	4309.56	44959.36	50016.82	53947.68	68203.44	70814.95
	1.6	6092.25	48875.36	51544.60	64861.70	70052.58	71775.53
	1.8	7675.67	50999.48	55154.54	65313.91	79036.61	80974.28
	2.0	9347.14	55970.91	58628.38	69734.91	83932.30	90561.56

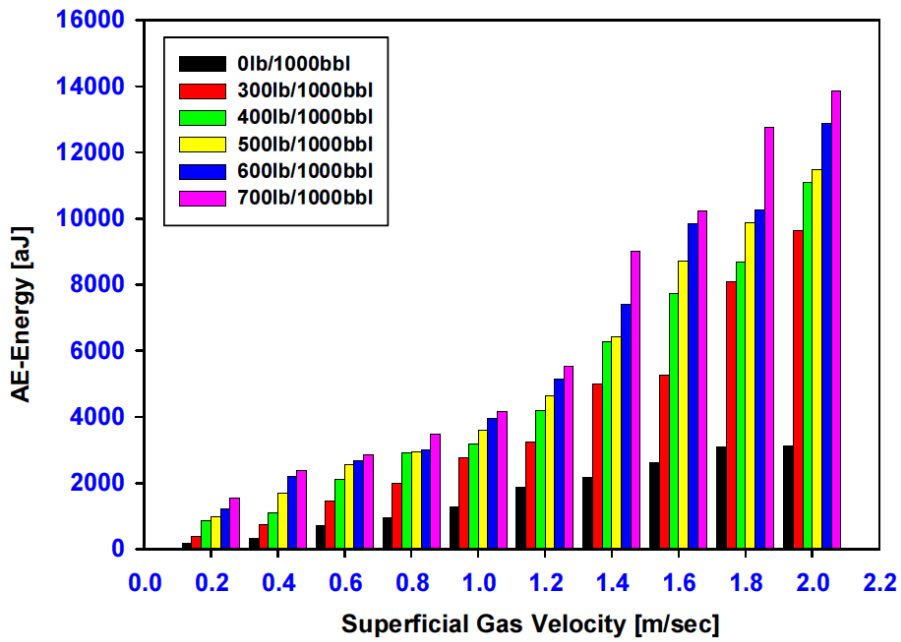


Figure B-1: AE Energy VS Superficial Gas Velocity (V_{SG}) for Different Sand Concentration and fixed Superficial Liquid Velocity (V_{SL}) of 0.2 ms⁻¹

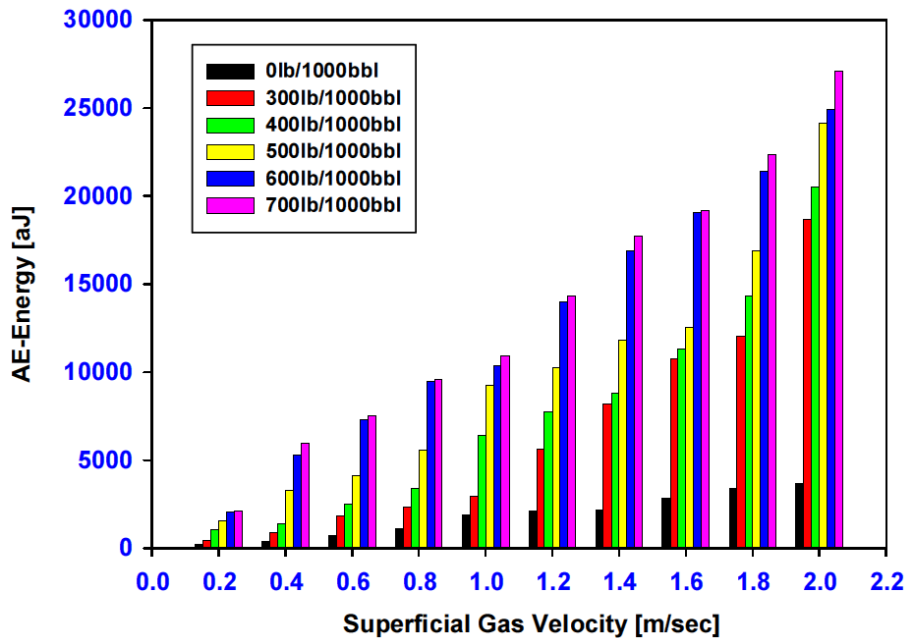


Figure B-2: AE Energy VS Superficial Gas Velocity (V_{SG}) for Different Sand Concentration and fixed Superficial Liquid Velocity (V_{SL}) of 0.4 ms⁻¹

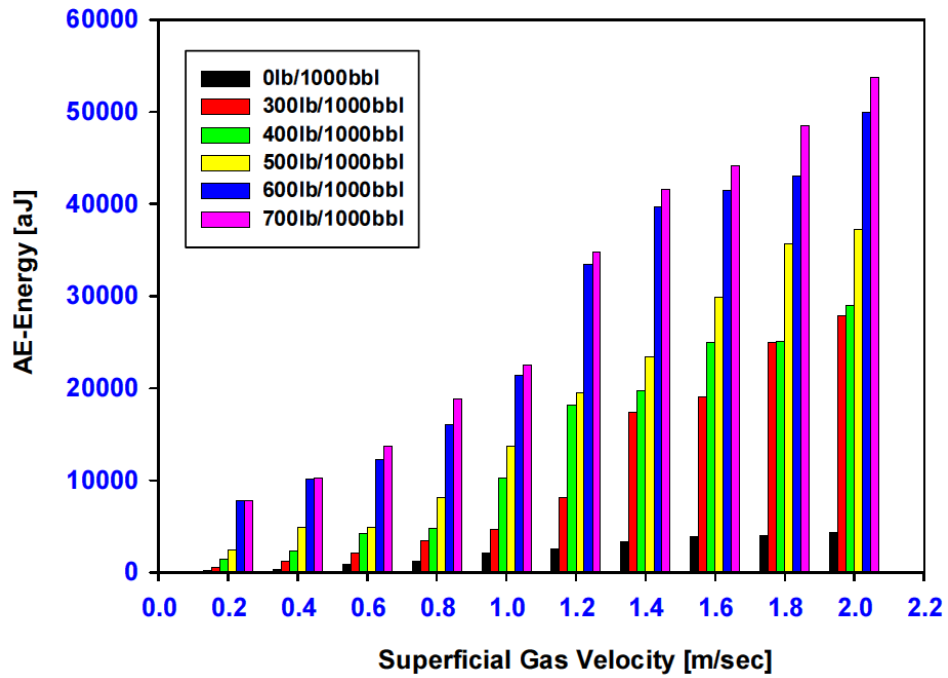


Figure B-3: AE Energy VS Superficial Gas Velocity (V_{SG}) for Different Sand Concentration and fixed Superficial Liquid Velocity (V_{SL}) of 0.6 ms⁻¹

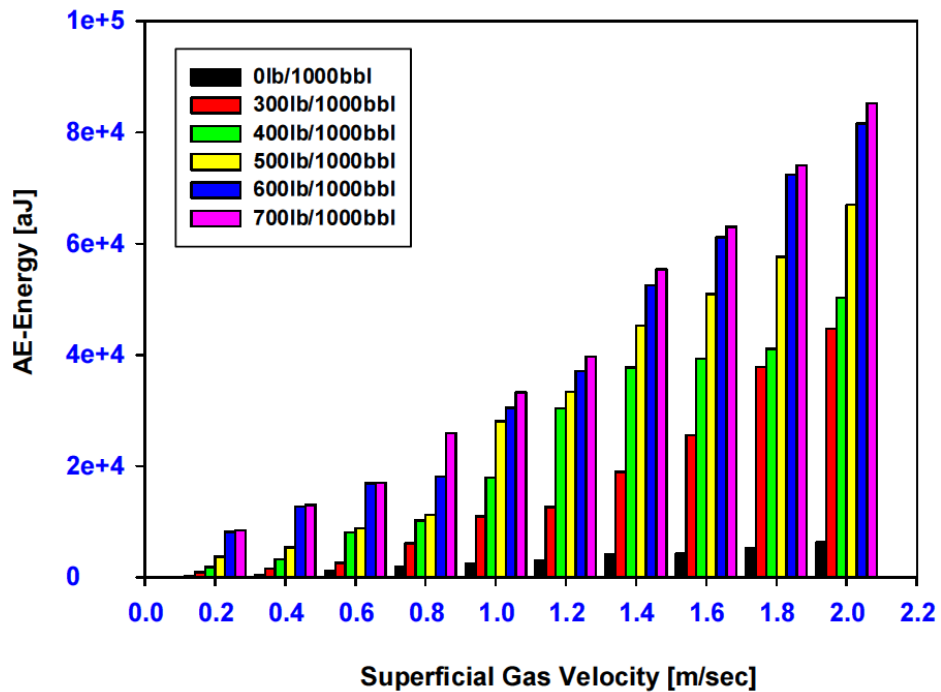


Figure B-4: AE Energy VS Superficial Gas Velocity (V_{SG}) for Different Sand Concentration and fixed Superficial Liquid Velocity (V_{SL}) of 0.8 ms⁻¹

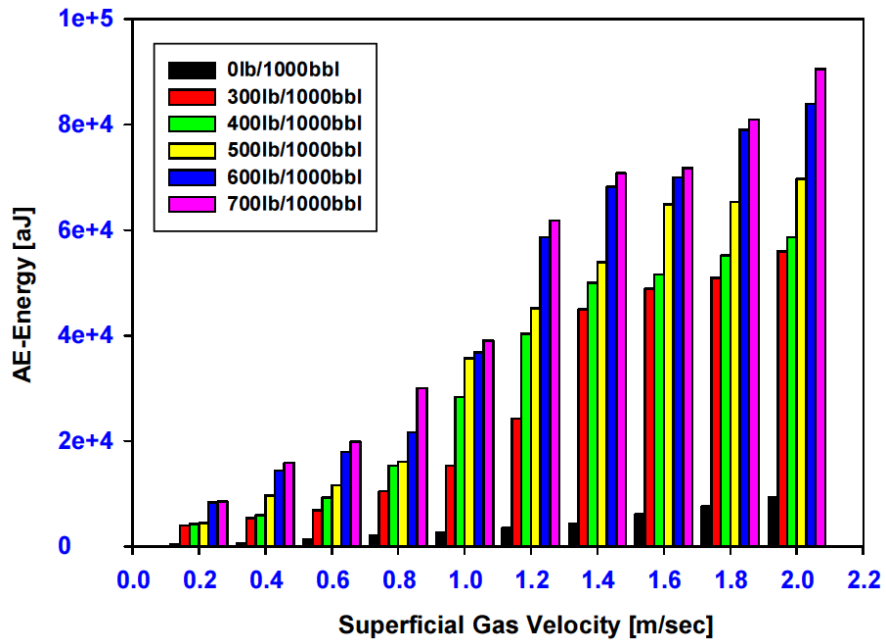


Figure B-5: AE Energy VS Superficial Gas Velocity (VSG) for Different Sand Concentration and fixed Superficial Liquid Velocity (VSL) of 1.0 ms⁻¹

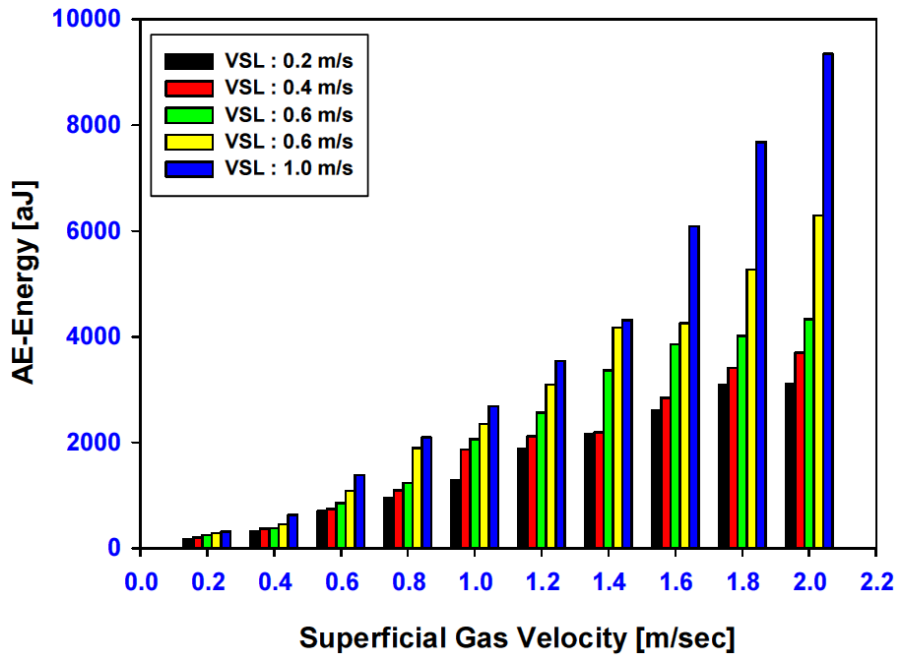


Figure B-6: AE Energy VS Superficial Gas Velocity (VSG) for Different Superficial Liquid Velocity (VSL) and fixed Sand Concentration of 0lb/1000bbl

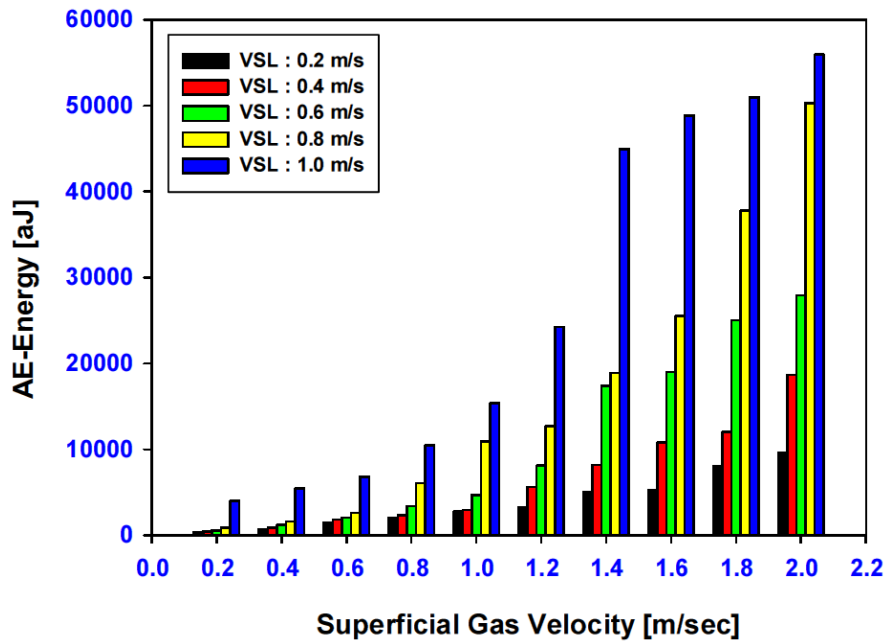


Figure B-7: AE Energy VS Superficial Gas Velocity (Vsg) for Different Superficial Liquid Velocity (VSL) and fixed Sand Concentration of 300lb/1000bbbl

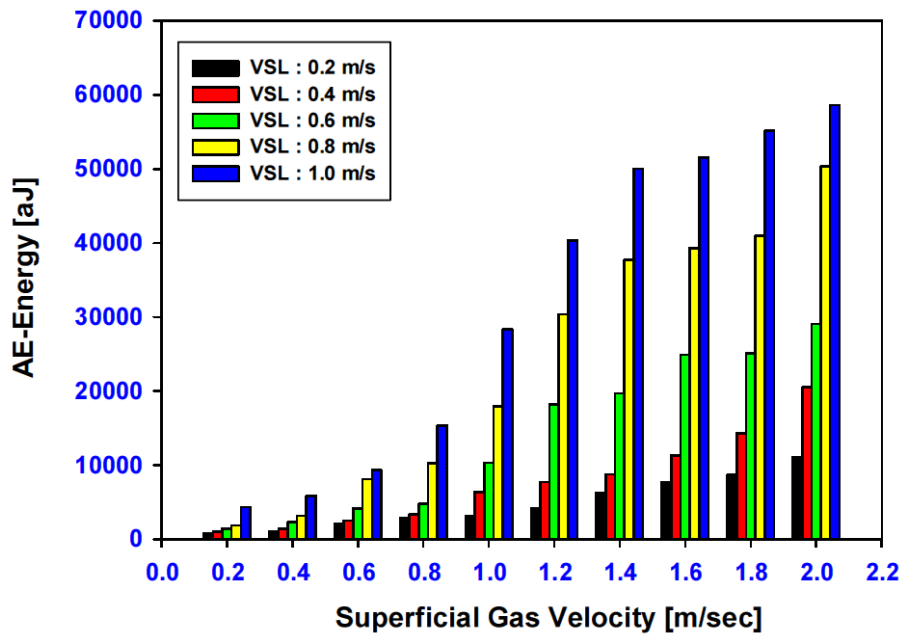


Figure B-7: AE Energy VS Superficial Gas Velocity (Vsg) for Different Superficial Liquid Velocity (VSL) and fixed Sand Concentration of 400lb/1000bbbl

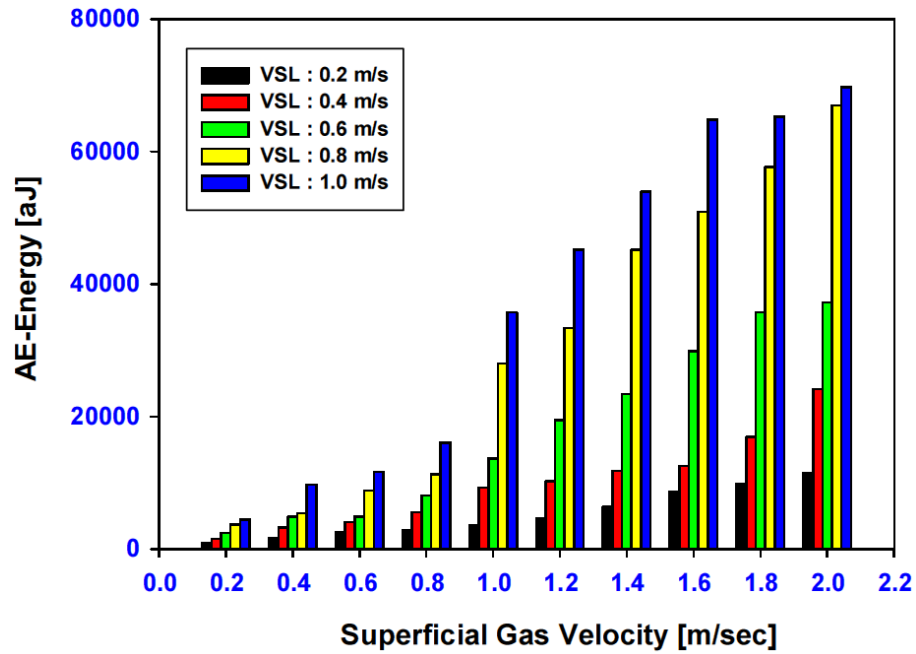


Figure B-8: AE Energy VS Superficial Gas Velocity (Vsg) for Different Superficial Liquid Velocity (Vsl) and fixed Sand Concentration of 500lb/1000bbi

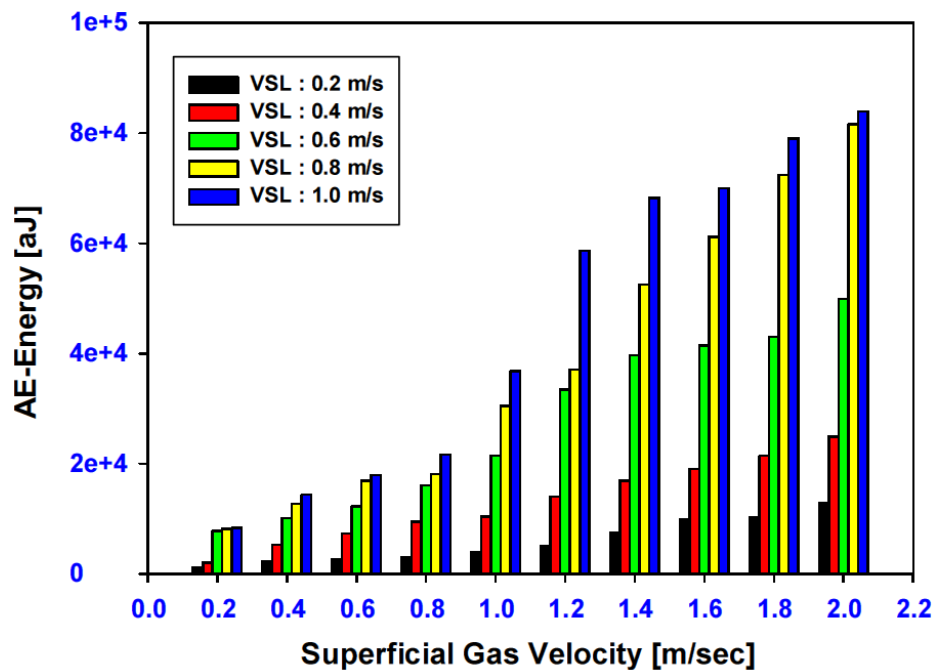


Figure B-9: AE Energy VS Superficial Gas Velocity (Vsg) for Different Superficial Liquid Velocity (Vsl) and fixed Sand Concentration of 600lb/1000bbi

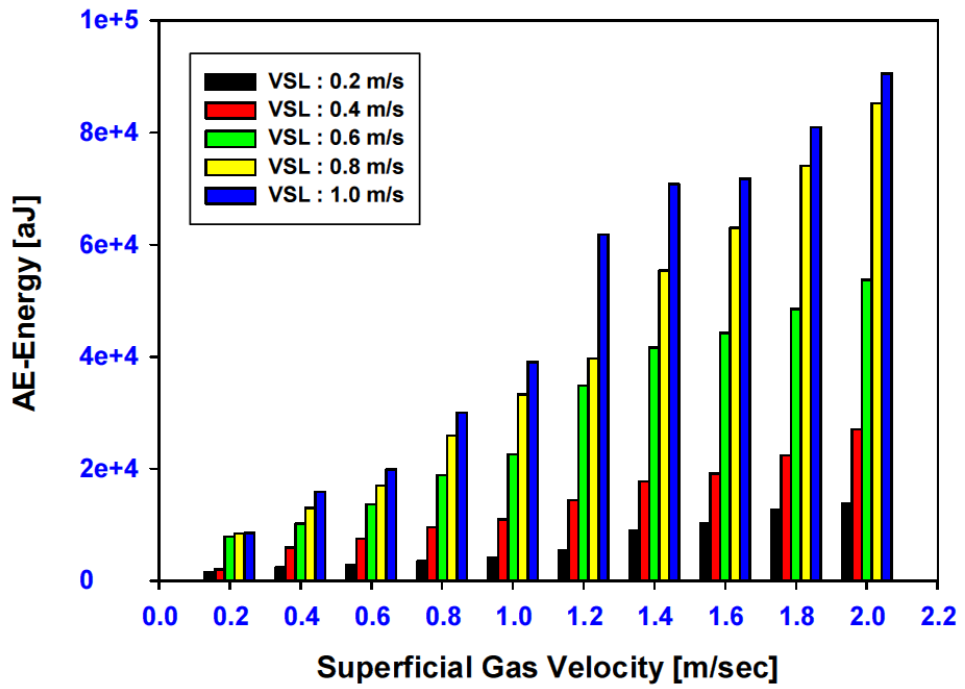



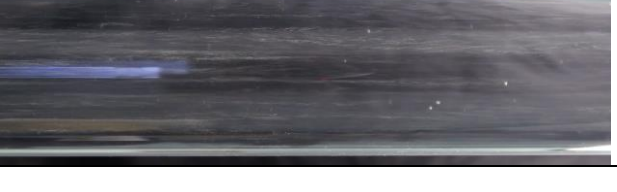



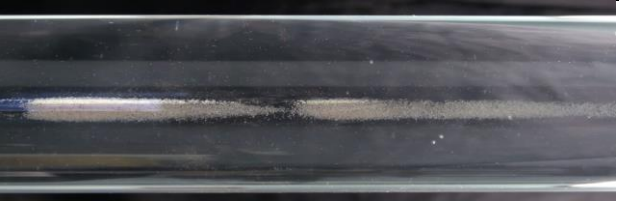


Figure B-10: AE Energy VS Superficial Gas Velocity (V_{SG}) for Different Superficial Liquid Velocity (V_{SL}) and fixed Sand Concentration of 700lb/1000bbl

Appendix C

Table C-1: Bottom view for sand-water characteristics in horizontal pipe for sand concentration 300lb/1000bbl

Superficial Liquid Velocity V_{SL} (ms^{-1})	Sand concentration	300lb/1000bbl	Sand behaviour in water flow
	Sand volume fraction	3.23E-04	
1.0	sand particles transport in the flow and was observed uniformly distributed across the pipe		
0.9	most sand particles transport in the flow with some sand streaks close to the pipe bottom		
0.8	higher intensity of sand concentration in streaks		
0.7	highest intensity of sand concentration in streaks and probably sand minimum transport condition		

Superficial Liquid Velocity V_{SL} (ms^{-1})	Sand concentration	300lb/1000bbl	Sand behaviour in water flow
	Sand volume fraction	3.23E-04	
0.6	highest intensity of sand concentration in streaks and sliding sand layer observed on the pipe bottom		
0.5	more sliding of sand layer and begin formation of sand dunes		
0.4	sand dunes continues to shape		
0.3	sand dunes continues to shape and moving slowly		

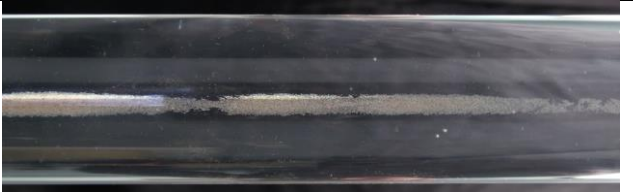
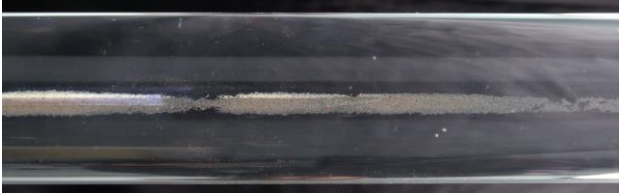



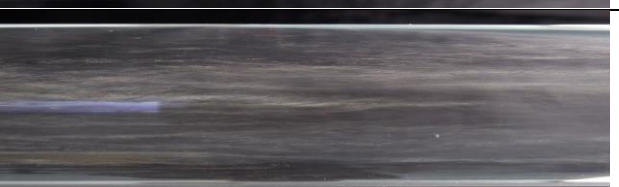
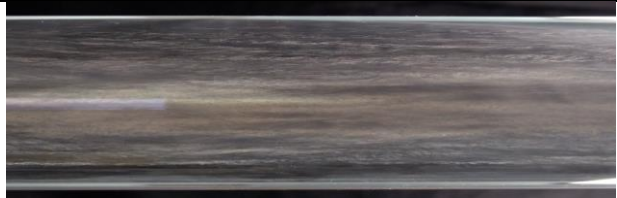



Superficial Liquid Velocity V_{SL} (ms^{-1})	Sand concentration	300lb/1000bbl	Sand behaviour in water flow
	Sand volume fraction	3.23E-04	
0.2	still some sand particles observed moving above the dunes		
0.1	stable sand dunes with few particles still moving above of them		

Table C-2: Bottom view for sand-water characteristics in horizontal pipe for sand concentration 400lb/1000bbl

Superficial Liquid Velocity V_{SL} (ms^{-1})	Sand concentration 400lb/1000bbl	Sand behaviour in water flow
	Sand volume fraction 4.31E-04	
1.0	most sand particles transport in the flow with some sand streaks close to the pipe bottom	
0.9	higher intensity of sand concentration in streaks	
0.8	highest intensity of sand concentration in streaks and probably sand minimum transport condition	
0.7	highest intensity of sand concentration in streaks and sliding sand layer observed on the pipe bottom	

Superficial Liquid Velocity V_{SL} (ms^{-1})	Sand concentration	400lb/1000bbl	Sand behaviour in water flow
	Sand volume fraction	4.31E-04	
0.6	more sliding of sand layer observed on the pipe bottom		
0.5	more sliding of sand layer and begin formation of sand dunes		
0.4	sand dunes continues to shape		
0.3	slowing moving sand dunes		


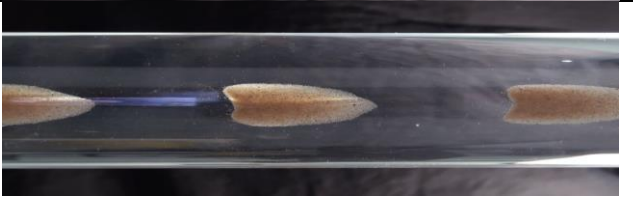









Superficial Liquid Velocity V_{SL} (ms^{-1})	Sand concentration	400lb/1000bbl	Sand behaviour in water flow
	Sand volume fraction	4.31E-04	
0.2	still some sand particles observed moving above the dunes		
0.1	stable sand dunes with few particles still moving above of them		

Table C-3: Bottom view for sand-water characteristics in horizontal pipe for sand concentration 500lb/1000bbl

Superficial Liquid Velocity V_{SL} (ms^{-1})	Sand concentration	500lb/1000bbl	Sand behaviour in water flow
	Sand volume fraction	5.38E-04	
1.0	higher intensity of sand concentration in streaks		
0.9	highest intensity of sand concentration in streaks and probably sand minimum transport condition		
0.8	sliding of sand layer observed on the pipe bottom		
0.7	more sliding of sand layer observed on the pipe bottom		

Superficial Liquid Velocity V_{SL} (ms^{-1})	Sand concentration	500lb/1000bbl	Sand behaviour in water flow
	Sand volume fraction	5.38E-04	
0.6	higher intensity of sand concentration in streaks		
0.5	sand dunes continues to shape		
0.4	slowing moving sand dunes		
0.3	still some sand particles observed moving above the dunes		

Superficial Liquid Velocity V_{SL} (ms^{-1})	Sand concentration	500lb/1000bbl	Sand behaviour in water flow
	Sand volume fraction	5.38E-04	
0.2	sand dunes started to close the gap between each other		
0.1	sand dunes started forming bridges between each other		